Form TH-4

National University of Sciences & Technology (NUST)

MASTER'S THESIS WORK

We hereby recommend that the dissertation prepared under our supervision by: Hassan Ahmed (00000321077)
Titled: Analytical Study of heat and mass transfer in the unsteady squeezing flow between parallel platesbe accepted in partial fulfillment of the requirements for the award of MS in Mechanical Engineering degree.

Examination Committee Members

1. Name: Riaz Ahmad Khan Signature:

2. Name: Hina Munir Dutt Signature:

3. Name: Adnan Munir Signature:

Supervisor: Muhammad Safdar Signature:

Date: 15 - Aug - 2023

15 - Aug - 2023

Head of Department Date

COUNTERSINGED

15 - Aug - 2023

Date Dean/Principal

Analytical Study of heat and mass transfer in the unsteady squeezing flow between parallel plates

Author

Hassan Ahmed

Regn Number

00000321077

Supervisor

Muhammad Safdar

DEPARTMENT OF MECHANICAL ENGINEERING

SCHOOL OF MECHANICAL & MANUFACTURING ENGINEERING

NATIONAL UNIVERSITY OF SCIENCES AND TECHNOLOGY

ISLAMABAD

AUGUST 2023

Analytical Study of heat and mass transfer in the unsteady squeezing flow between parallel plates

Author

Hassan Ahmed

Regn Number

321077

A thesis submitted in partial fulfillment of the requirements for the degree of

MS Mechanical Engineering

Thesis Supervisor:

Muhammad Safdar

Thesis Supervisor's Signature: _____ _____

DEPARTMENT OF MECHANICAL ENGINEERING

SCHOOL OF MECHANICAL & MANUFACTURING ENGINEERING

NATIONAL UNIVERSITY OF SCIENCES AND TECHNOLOGY

ISLAMABAD

AUGUST 2023

Thesis Acceptance Certificate

Certified that final copy of MS thesis written by **Hassan Ahmed Registration No. 321077**, of SMME has been vetted by undersigned, found complete in all respects as per NUST Statutes / Regulations, is free of plagiarism, errors, and mistakes and is accepted as partial fulfillment for award of MS degree. It is further certified that necessary amendments as pointed out by GEC members of the scholar have also been incorporated in the said thesis.

Signature:

Name of Supervisor: Dr. Muhammad Safdar

Date: 23-08-2023

Dr. Muhammad Safdar
Assistant Professor
School of Mechanical and Manufacturing Engineering (SMME) NUST, Islamabad

Signature (HOD): 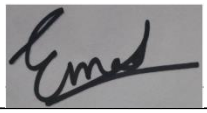

Date: 23-08-2023

Signature (Principal):

Date: 23-08-2023

Declaration

I certify that this research work titled "*Analytical Study of heat and mass transfer in the unsteady squeezing flow between parallel plates"* is my own work. The work has not been presented elsewhere for assessment. The material that has been used from other sources has been properly acknowledged / referred.

Signature of Student

Hassan Ahmed

2019-NUST-MS-Mech-321077

Language Correctness Certificate

This thesis has been read by an English expert and is free of typing, syntax, semantic, grammatical, and spelling mistakes. Thesis is also according to the format given by the university.

Signature of Student

Hassan Ahmed

2019-NUST-MS-Mech-321077

Signature of Supervisor

Dr. Muhammad Safdar

Certificate for Plagiarism

It is certified that MS Thesis Titled: Analytical Study of heat and mass transfer in the unsteady squeezing flow between parallel plates by Hassan Ahmed (321077) has been examined by me. I undertake the follows:

a. Thesis has significant new work/knowledge as compared already published or are under consideration to be published elsewhere. No sentence, equation, diagram, table, paragraph, or section has been copied verbatim from previous work unless it is placed under quotation marks and duly referenced.
b. The work presented is original and own work of the author (i.e., there is no plagiarism). No ideas, processes, results, or words of others have been presented as Author own work.
c. There is no fabrication of data or results which have been compiled/analyzed.
d. There is no falsification by manipulating research materials, equipment, or processes, or changing or omitting data or results such that the research is not accurately represented in the research record.
e. The thesis has been checked using TURNITIN (copy of originality report attached) and found within limits as per HEC plagiarism Policy and instructions issued from time to time.

Name & Signature of Supervisor

DR. MUHAMMAD SAFDAR

Signature:

Dr. Muhammad Safdar
Assistant Professor
School of Mechanical and Manufacturing
Engineering (SMME) NUST, Islamabad

Copyright Statement

- Copyright in text of this thesis rests with the student author. Copies (by any process) either in full, or of extracts, may be made only in accordance with instructions given by the author and lodged in the Library of NUST School of Mechanical & Manufacturing Engineering (SMME). Details may be obtained by the Librarian. This page must form part of any such copies made. Further copies (by any process) may not be made without the permission (in writing) of the author.
- The ownership of any intellectual property rights which may be described in this thesis is vested in NUST School of Mechanical & Manufacturing Engineering, subject to any prior agreement to the contrary, and may not be made available for use by third parties without the written permission of the SMME, which will prescribe the terms and conditions of any such agreement.
- Further information on the conditions under which disclosures and exploitation may take place is available from the Library of NUST School of Mechanical & Manufacturing Engineering, Islamabad.

Acknowledgements

I am thankful to my Creator Allah Subhana-Watala to have guided me throughout this work at every step and for every new thought which You setup in my mind to improve it. Indeed, I could have done nothing without Your priceless help and guidance. Whosoever helped me throughout the course of my thesis, whether my parents or any other individual, was Your will, so indeed none be worthy of praise but You.

I am profusely thankful to my beloved parents who raised me when I was not capable of walking and continued to support me throughout every department of my life.

I would also like to express special thanks to my supervisor Dr. Muhammad Safdar for his help throughout my thesis and also for Numerical and Analytical methods which he has taught me. I can safely say that I haven't learned any other engineering subject in such depth as the ones which he has taught.

I would also like to pay special thanks to Dr. Muhammad Safdar for his tremendous support and cooperation. Each time I got stuck in something; he came up with the solution. Without his help I wouldn’t have been able to complete my thesis. I appreciate his patience and guidance throughout the whole thesis.

I would also like to thank Dr. Riaz Ahmed Khan and Dr. Hina Munir Dutt for being on my thesis guidance and evaluation committee and express my special thanks to Dr. Adnan Munir for his help.

Finally, I would like to express my gratitude to all the individuals who have rendered valuable assistance to my study.

Dedicated to my special parents and my teachers whose tremendous support and cooperation led me to this wonderful accomplishment.

Abstract

This thesis investigates the unsteady flow of Non-Newtonian Fluid - Casson fluid between two squeezing/separating parallel plates under the presence of viscous dissipation, magnetohydrodynamic effect and joule dissipation. This investigation also involves the radiation and chemical reaction effects on Casson fluid. The fundamental governing equations for the Non-Newtonian Casson fluid flow problem is highly non-linear and coupled partial differential equation (PDEs) with time dependency. In order to reduce this highly nonlinear system of PDEs into Ordinary differential equations (ODEs), similarity transformations are used. The analytical and numerical solutions of the reduced ODEs are obtained using MAPLE through Homotopy Analysis Method (HAM) and Finite Difference Method (FDM), respectively. These results are validated with the previously published results derived by employing Shooting method along with results of bvp4c. Subsequently, the influence of prominent dimensionless flow parameters on velocity, heat transfer and mass flow are presented graphically with their physical aspects on engineering applications. The velocity field, heat transfer and mass flow contours are also plotted for each case in order to understand the effect of these flow parameters on flow, heat and mass distribution in the given Casson fluid flow.

A comprehensive analysis of the analytic procedure HAM and the approximate solution scheme FDM is carried out to compare the results provided by both for the considered flow model. This comparison encompasses performance of both the procedures on the basis of processing time, memory allocation (computational cost) and accuracy, through which effectiveness of these procedures is determined.

Key Words: *Casson Fluid, Magnetohydrodynamic, Viscous Dissipation, Radiation, Chemical Reaction, Similarity Transformation, Homotopy Analysis Method, Finite Difference Method, Analytic and approximate Solutions*

Table of Contents

Declaration ..... **i**

Language Correctness Certificate ..... **ii**

Copyright Statement ..... **iv**

Acknowledgements ..... **v**

Abstract ..... **vii**

Table of Contents ..... **viii**

List of Figures ..... **x**

List of Tables ..... **xiii**

CHAPTER 1. INTRODUCTION **1**

1.1 INTRODUCTION & APPLICATIONS: 1

1.2 LITERATURE REVIEW: 2

1.3 SCOPE & MOTIVATION: 6

CHAPTER 2. FLOW AND HEAT TRANSFER MODEL **7**

2.1 GOVERNING EQUATION 7

2.2 CASSON FLUID FLOW BETWEEN PARALLEL PLATES: 8

2.3 CONSTRUCTION OF SIMILARITY TRANSFORMATIONS 8

2.4 SOLUTION APPROACH 10

2.4.1 Homotopy Analysis Method (HAM): 10

2.4.2 Convergence of Solution 12

CHAPTER 3: VALIDATION AND COMPARISON **18**

3.1 VALIDATION OF RESULTS OF HAM: 18

3.2 COMPARISON OF RESULTS OF HAM WITH FINITE DIFFERENCE METHOD: 20

CHAPTER 4: RESULTS **21**

4.1 EFFECT OF FLOW PARAMETERS: 21

4.1.1 Effect of Casson Fluid Parameter (β): 21

4.1.2 Effect of Squeezing Number (S): 25

4.1.3 Effect of Hartmann Number (Ha): 29
4.1.4 Effect of Radiation Parameter (R): 33
4.1.5 Effect of heat Source/Sink parameter (Q): 35
4.1.6 Impact of Prandtl Number (Pr): 35
4.1.7 Effect of Eckert Number (Ec): 35
4.1.8 Impact of Dufour Number (Du): 35
4.1.9 Effect of Chemical Reaction Parameter (Kr): 36
4.1.10 Effect of Schmidt number (Sc): 36
4.1.11 Effect of Soret Number (Sr): 36
4.2 PHYSICAL AND ENGINEERING ASPECTS: 43
CHAPTER 4: CONCLUSION 50
APPENDIX A: PROGRAMMING CODE 52
APPENDIX A: VELOCITY FIELD AND CONTOURS OF TEMPERATURE AND CONCENTRATION 56
REFERENCES 61

List of Figures

Figure 1: Casson Fluid Flow Between Parallel Plates 8
Figure 2: h-curve for Influence of β at S=-4, Du=R=Q=Ec=Kr=0.1, Sr=0.5, Pr=0.7, Sc=0.7, δ =1.2, Ha=0.1, β=0.17 12
Figure 3: h-curve for Influence of Du at S=0.4, Du=Sr=Ha=Q=0.5, Kr=1.6, Sc=0.7, δ=0.01, R= Ec=0.1, Pr=1.2, β=0.2 13
Figure 4: h-curve for Ec at S=0.5, β =0.1, Du=0.5, Sr=0.5, Ha=0.5, Q=0.1, Kr=0.1, Pr=0.7, Sc=0.7, δ =0.1, R=0.1, Ec=0.5 13
Figure 5: h-curve for Pr at S=0.5, β=0.1, Du=0.5, Sr=0.5, Ha=0.5, Q=0.1, Kr=0.1, Sc=0.7, δ=0.1, R=0.1, Ec=0.1, Pr=1.3 14
Figure 6:h-curve for Influence of Ha at S=0.1, β=2.0, Du=0.5, Sr=0.5, R=0.1, Q=0.1, Ec=0.1, Kr=0.1, Pr=0.7, Sc=0.7, δ=0.5, Ha=2 14
Figure 7: h-curve for Influence of Q at S=0.4, β=0.2, Du=0.5, Sr=0.5, Ha=0.1, Q=0.1, Ec=1.0, Kr=0.1, Pr=0.7, Sc=0.7, δ=0.1, R=0.2 15
Figure 8: h-curve for Influence of at Kr S=0.1, β=0.5, Du=0.5, Sr=0.5, Ha=0.1, Q=0.1, Kr=0.3, Sc=0.7, δ=0.1, R=0.1, Ec=0.1, Pr=0.7 15
Figure 9: h-curve for Influence of R at S=0.4, β=0.2, Du=0.5, Sr=0.5, Ha=0.1, Q=0.1, Ec=1.0, Kr=0.1, Pr=0.7, Sc=0.7, δ=0.1, R=0.2 16
Figure 10: h-curve for Influence of Sc at S=0.1, β=0.5, Du=0.5, Sr=0.5, Ha=0.1, Q=0.1, Kr=0.1, Sc=1.4, δ=0.1, R=0.1, Ec=0.1, Pr=0.7 16
Figure 11: h-curve for Influence of S at β=0.8, Du=0.5, Sr=0.1, Ha=0.1, R=0.1, Ec=0.1, Kr=0.1, Pr=0.1, Sc=0.7, δ=5, Q=0.1, S=1.5 17
Figure 12: h-curve for Influence of Sr at S=0.1, β=0.5, Du=0.5, Sr=0.5, Ha=0.1, Q=0.1, Kr=0.1, Sc=0.5, δ=0.1, R=0.1, Ec=0.1, Pr=0.7 17
Figure 13: Effect of β on $f(\eta)$ at S=-4, Sr=0.5, R=0.1, Q=0.1, Ec=0.1, Kr=0.1, Pr=0.7, Sc=0.7, δ =1.2, Ha=0.1, Du=0.1 22
Figure 14: Effect of β on $f'(\eta)$ at S=-4, Sr=0.5, R=0.1, Q=0.1, Ec=0.1, Kr=0.1, Pr=0.7, Sc=0.7, δ =1.2, Ha=0.1, Du=0.1 22
Figure 15: Effect of β on $\theta(\eta)$ at S=-4, Sr=0.5, R=0.1, Q=0.1, Ec=0.1, Kr=0.1, Pr=0.7, Sc=0.7, δ =1.2, Ha=0.1, Du=0.1 23
Figure 16: Effect of β on $\phi(\eta)$ at S=-4, Sr=0.5, R=0.1, Q=0.1, Ec=0.1, Kr=0.1, Pr=0.7, Sc=0.7, δ =1.2, Ha=0.1, Du=0.1 23
Figure 15: (a) Temperature contours at wall temperature of 130 deg C at β = 0.17 (b) Temperature contours at wall temperature of 130 deg C at β = 0.9 24

Figure 16: (a) Concentration contours at concentration of 20 mol/m^3 at β = 0.17 (b) Concentration contours at concentration of 20 mol/m^3 at β = 0.9 24
Figure 17: (a) Velocity field/streamlines at β = 0.9 25
Figure 20: Influence of S on $f(\eta)$ at β=0.8, Du=0.5, Sr=0.1, Ha=0.1, R=0.1, Ec=0.1, Kr=0.1, Pr=0.1, Sc=0.7, δ=5, Q=0.1 26
Figure 21: Influence of S on $f'(\eta)$ at β=0.8, Du=0.5, Sr=0.1, Ha=0.1, R=0.1, Ec=0.1, Kr=0.1, Pr=0.1, Sc=0.7, δ=5, Q=0.1 27
Figure 22: Influence of S on $\theta(\eta)$ at β=0.8, Du=0.5, Sr=0.1, Ha=0.1, R=0.1, Ec=0.1, Kr=0.1, Pr=0.1, Sc=0.7, δ=5, Q=0.1 27
Figure 23: Influence of S on $\phi(\eta)$ at β=0.8, Du=0.5, Sr=0.1, Ha=0.1, R=0.1, Ec=0.1, Kr=0.1, Pr=0.1, Sc=0.7, δ=5, Q=0.1 28
Figure 24: (a) Temperature contours at wall temperature of 130 deg C at S = 0.5 (b) Temperature contours at wall temperature of 130 deg C at β = -7.5 29
Figure 25: (a) Concentration contours at concentration of 20 mol/m^3 at S=0.5 (b) Concentration contours at concentration of 20 mol/m^3 at S=-7.5 29
Figure 26: (a) Velocity field/streamlines at S = 0.5 (b) Velocity field/streamlines at S = 3.5 (c) Velocity field/streamlines at S = -7.5 29
Figure 27: Effect of Ha on $f(\eta)$ at S=R=Q=Ec=Kr=0.1, Du=Sr=0.5, Pr=Sc=0.7, δ=0.5, β=2.0 30
Figure 28: Effect of Ha on $f'(\eta)$ at S=R=Q=Ec=Kr=0.1, Du=Sr=0.5, Pr=Sc=0.7, δ=0.5, β=2.0 31
Figure 29: Effect of Ha on $\theta(\eta)$ at S=R=Q=Ec=Kr=0.1, Du=Sr=0.5, Pr=Sc=0.7, δ=0.5, β=2.0 31
Figure 30: Effect of Ha on $\phi(\eta)$ at S=R=Q=Ec=Kr=0.1, Du=Sr=0.5, Pr=Sc=0.7, δ=0.5, β=2.0 32
Figure 31: (a) Temperature contours at wall temperature of 130 deg C at Ha= 0.5 (b) Temperature contours at wall temperature of 130 deg C at Ha = 3.5 32
Figure 32: (a) Concentration contours at concentration of 20 mol/m^3 at Ha=0.5 (b) Concentration contours at concentration of 20 mol/m^3 at Ha=3.5 33
Figure 33: (a) Velocity field/streamlines at Ha = 0.5 33
Figure 34: Influence of R on $\theta(\eta)$ at S=0.1, Du=Sr=0.5, R=Q=Ec=Kr=0.1, Sc=Pr=0.7, δ=0.5, β=2.0 34
Figure 35: Influence of R on $\theta(\eta)$ at S=0.1, Du=Sr=0.5, R=Q=Ec=Kr=0.1, Sc=Pr=0.7, δ=0.5, β=2.0 34
Figure 36: Influence of Q on $\theta(\eta)$ at S=0.4, β=0.2, Du=0.5, Sr=0.5, Ha=0.1, Ec=1.0, Kr=0.1, Pr=0.7, Sc=0.7, δ=0.1, R=0.2 37
Figure 37: Influence of Q on $\phi(\eta)$ at S=0.4, β=0.2, Du=0.5, Sr=0.5, Ha=0.1, Ec=1.0, Kr=0.1, Pr=0.7, Sc=0.7, δ=0.1, R=0.25 37
Figure 38: Influence of Pr on $\theta(\eta)$ at S=0.5, β=0.1, Du=0.5, Sr=0.5, Ha=0.5, Q=0.1, Kr=0.1, Sc=0.7, δ=0.1, R=0.1, Ec=0.1 38
Figure 39: Influence of Pr on $\phi(\eta)$ at S=0.5, β=0.1, Du=0.5, Sr=0.5, Ha=0.5, Q=0.1, Kr=0.1, Sc=0.7, δ=0.1, R=0.1, Ec=0.1 38

Figure 40: Influence of Ec on $\theta(\eta)$ at S=0.5, β =0.1, Du=0.5, Sr=0.5, Ha=0.5, Q=0.1, Kr=0.1, Pr=0.7, Sc=0.7, δ =0.1, R=0.1 39
Figure 41: Influence of Ec on $\phi(\eta)$ at S=0.5, β =0.1, Du=0.5, Sr=0.5, Ha=0.5, Q=0.1, Kr=0.1, Pr=0.7, Sc=0.7, δ =0.1, R=0.1 39
Figure 42: Influence of Du on $\theta(\eta)$ at S=0.4, β=0.2, Sr=0.5, Ha=0.5, Q=0.5, Kr=1.6, Sc=0.7, δ=0.01, R=0.1, Ec=0.1, Pr=1.2 40
Figure 43: Influence of Kr on $\phi(\eta)$ at S=0.1, β=0.5, Du=0.5, Sr=0.5, Ha=0.1, Q=0.1, Sc=0.7, δ=0.1, R=0.1, Ec=0.1, Pr=0.7 40
Figure 44: Influence of Du on $\phi(\eta)$ at S=0.4, β=0.2, Sr=0.5, Ha=0.5, Q=0.5, Kr=1.6, Sc=0.7, δ=0.01, R=0.1, Ec=0.1, Pr=1.2 41
Figure 45: Influence of Sc on $\phi(\eta)$ at S=0.1, β=0.5, Du=0.5, Sr=0.5, Ha=0.1, Q=0.1, Kr=0.1, δ=0.1, R=0.1, Ec=0.1, Pr=0.7 41
Figure 46: Influence of Sr on $\theta(\eta)$ at S=0.1, β=0.5, Du=0.5, Ha=0.1, Q=0.1, Kr=0.1, Sc=0.5, δ=0.1, R=0.1, Ec=0.1, Pr=0.7 42
Figure 47: Influence of Sr on $\phi(\eta)$ at S=0.1, β=0.5, Du=0.5, Ha=0.1, Q=0.1, Kr=0.1, Sc=0.5, δ=0.1, R=0.1, Ec=0.1, Pr=0.7 42
Figure 48: Effect of S on Momentum Transport Coefficient at β=2.5, Du=0.5, Sr=0.5, Ha=0.3, Q=0.2, Kr=0.2, Sc=0.7, δ=0.5, R=0.2, Ec=0.2, Pr=0.7 44
Figure 49: Effect of Ha on Momentum Transport Coefficient at β=2.5,Du=0.5, Sr=0.5, S=2.5, Q=0.2, Kr=0.2, Sc=0.7, δ=0.5, R=0.2, Ec=0.2, Pr=0.7 45
Figure 50: Effect of β on Momentum Transport Coefficient at β=2.5, Du=0.5, Sr=0.5, Ha=0.3, Q=0.2, Kr=0.2, Sc=0.7, δ=0.5, R=0.2, Ec=0.2, Pr=0.7 45
Figure 51: Effect of Du on Heat Transfer Coefficient at S=2.5, β=0.5, Sr=0.5, Ha=1.5, Q=0.6, Kr=0.2, δ=0.1, R=0.6, Ec=0.2, Pr=0.7, Sc=0.7 46
Figure 52: Effect of S on Heat Transfer Coefficient at Du=0.2, β=0.5, Sr=0.5, Ha=1.5, Q=0.3, Kr=0.2, δ=0.1, R=0.6, Ec=0.2, Pr=0.7, Sc=0.7 46
Figure 53: Effect of R on Heat Transfer Coefficient at S=2.5, β=0.5, Sr=0.5, Ha=1.5, Q=0.3, Kr=0.2, δ=0.1, Du=0.2, Ec=0.2, Pr=0.7, Sc=0.7 47
Figure 54: Effect of Q on Heat Transfer Coefficient at Du=0.2, β=0.5, Sr=0.5, Ha=1.5, S=2.5, Kr=0.2, δ=0.1, R=0.6, Ec=0.2, Pr=0.7, Sc=0.7 47
Figure 55: Effect of S on Mass Transfer Coefficient at Du=0.5, β=0.5, Sr=0.2, Ha=0.5, Kr=0.1, Sr=0.2, δ=0.5, R=0.2, Ec=0.2, Pr=0.7, Sc=0.7 48
Figure 56: Effect of Sr on Mass Transfer Coefficient at Du=0.5, β=0.5, Sr=0.2, Ha=0.5, S=2.5, Kr=0.1, δ=0.5, R=0.2, Ec=0.2, Pr=0.7, Sc=0.7 48
Figure 57: Effect of Kr on Mass Transfer Coefficient at Du=0.5, β=0.5, Sr=0.2, Ha=0.5, S=2.5, Sr=0.2, δ=0.5, R=0.2, Ec=0.2, Pr=0.7, Sc=0.7 49

List of Tables

Table 1 Momentum, heat and mass transports with increasing order of approximation at Ha = Kr = S = δ = 0.5, Ec = Q = R = 0.3, Pr= Sc=1.5, β=0.3 18

Table 2 Momentum, heat and mass transports on different S at Ha = R = Q = Du = Sr = 0, Ec = Kr = Pr= Sc=1, β=∞, δ = 0.5 19

Table 3 Momentum, heat and mass transports at Ha = Kr = S = δ = 0.5, Ec = Q = R = 0.3, Pr= Sc=1.5, β=0.3 19

Table 4 CPU Time and Memory for Finite Difference Solution 20

Table 5 CPU Time and Memory for Homotopy Analysis Method 20

Table 6: Effect of Flow Parameters on Velocities, Temperature and Concentration 50

CHAPTER 1. INTRODUCTION

In this dissertation, heat and mass transfer for a Casson fluid between squeezing/separating parallel plates is studied. In this flow, the magnetohydrodynamic, radiation, chemical reaction and heat source/sink effects are also present to understand their combined effect on the behavior of fluid. In Chapter 1, brief introduction of Casson fluid and its application in the industries are discussed along with the literature review. In the second section, the governing PDEs are transformed into ODEs using Similarity Transformations and the same ODEs are solved using Homotopy Analysis Method. In the third section, the effectiveness of the Homotopy analysis method for Casson fluid flow applications is compared to the Finite Difference scheme and results are validated using previous published results. In the fourth section, in order to better understand the flow behavior, the effect of flow parameters on flow, heat, and mass distribution on the fluid flow between the parallel plates is investigated.

1.1 INTRODUCTION & APPLICATIONS:

Casson Fluid is a type of non-Newtonian fluid named after its discoverer British mathematician and rheologist, A. A. Casson. As the Newtonian fluid follows the newton law of viscosity in which shear stress and shear strain are linearly related. On contrary, shear stress has nonlinear relationship with shear strain in case of Casson fluid and Casson fluid has both elastic and viscous properties i.e., it acts as solid up to a particular shear rate while when the shear rates exceed the threshold value, Casson fluid starts to flow and behave as liquid. The following relations applies to it.

$$\tau = \tau_0 + \mu \sqrt{\dot{\gamma}}$$

where τ is the shear stress, τ_0 is the yield stress (a constant value representing the minimum stress required to initiate flow), μ is the consistency coefficient (a constant that determines resistance of a fluid to deformation) and $\dot{\gamma}$ is the shear rate.

Heat and mass transfer in squeezing/separating non-Newtonian Casson fluid between two parallel plates is an area of interest for scientists and engineers due to its widespread applications in a variety of industries. Fluid stretching sheets are used in a variety of sectors to optimize and improve productivity.

In Nuclear industry where safety is utmost priority, the Casson fluid has application in transportation and management of nuclear waste in the form of slurries and pastes. Also, the coolant of molten salt reactor in specific cases acts as Casson fluid and during the accident scenarios such as loss of Coolant Accident (LOCA), most of liquid coolant are vaporized and coolant act as non-Newtonian fluid whose behavior can be studied using Casson fluid equations.

In the food industry, sauces and dressings such as ketchup and mayonnaise are examples of non-Newtonian fluid. It also finds applications in Dairy products, Baked goods, Jams and Chocolate industries.

For the automobile industry, they are used to shape sheet metal into complex forms and geometries. They are used to produce paper goods and printing of a higher quality in the printing and paper industries. They are used to stretch fabric for curtains, rugs, and clothing in the textile industry. In the plastics business, they are utilized to make complex shapes for infusion forming. Liquid extending sheets can likewise be utilized in sheet metal manufacture, sheet metal framing, and wire shaping cycles. A useful instrument in medical research is a fluid film squeezing flow as it accurately measures the viscosity of fluids like blood and lymphatic fluid. It can also be used to evaluate and monitor the health of tissues and organs. Moreover, it enables a measurement of the extent of inflammation, assessment of the efficacy of treatments, or tracking of the progress of a healing process. Further, liquid film pressing stream is used to enhance drug conveyance, as it can precisely control the rate at which medications are conveyed to explicit region of the body. Lastly, it can be used to help develop targeted treatments and diagnose certain conditions like vascular diseases etc.

1.2 LITERATURE REVIEW:

In his paper, Stefan [1] initially looks into the squeezing flow and presents a basic mathematical model for it under thermodynamic conditions based on lubrication theory. Reynold's [2] modified the mathematical model for elliptical plates and used it in the application on Mr. Beauchamp Tower's Experiments. Additionally, Archibald [3] investigated a comparable issue for rectangular plates in Time Relations and Load Capacity for Squeeze Films. Domairry and Aziz [4] used homotopy perturbation approach to study the influence of viscous dissipation on flow and heat transfer in incompressible flow between parallel discs and Similar study for parallel plates using the homotopy perturbation approach was carried out by Siddiqui, Irum et al. [5]. Since many

scientists are working on the research and discovering solutions for different configurations. Wang used the Homotopy Analysis approach (HAM) to solve the governing equation for a liquid layer on an unstable stretching surface, whereas Anderson used the Shooting numerical approach to address the same issue. In his research, Wang emphasized the value of HAM in helping to better understand the flow mechanism for industrial use. Using HAM, Mustafa, Hayat et al. [6] examines heat and mass transport on an unstable squeeze flow between parallel plates. The impact of the Prandtl and Eckert numbers on the Nusselt number as well as the impact of the Schmidt number on the Sherwood number were presented in this work.

Weaver et al. [7] looked into interactions between species and how they influenced Natural convection heat and mass transfer in porous medium due to the combined effects of concentration and temperature gradients, as well as the thermal-diffusion and diffusion-thermo impacts. According to their analysis, the gradients in temperature and concentration within the flow regime cause the flow to occur. The concentration field and heat transfer properties of gyrotactic microorganisms floating in an Casson fluid flow close to a vertical rotating plate or cone retained in porous media in electromagnetic field were numerically studied by Raju and Sandeep [8]. (Sulochana, Payad et al.[8] investigated the Soret effect in the presence of a heat source or sink in the situation of three-dimensional Casson fluid flow across a stretching surface, taking into account heat and mass transfer characteristics. Nawaz, Hayat et al [9] investigated the role of Thermal diffusion and Mass diffusion effects on time independent MHD two-dimensional electrically conducting flow. Ojjela and Kumar [10] studied open channel flow of a two stress fluids with radiation and chemical reaction effects and the effect of the Soret as well as Dufour numbers on it. In addition, Khan, Qayyum et al.[11] investigated the effect of the thermal diffusion and mass diffusion effects in the situation of viscous MHD flow between non-parallel walls by taking the chemical reaction process into account. According to their findings, the temperature field grows as the Dufour number increases, while the concentration field decreases as the Soret number increases. Khan, Mohyud-Din et al.[12] have explored the thermal diffusion and mass diffusion effect on the viscous incompressible nano-fluid between two squeezing parallel disks under electromagnetic field. Their research shows that as the Schmidt and Soret numbers increase, the concentration field in the flow zone decreases. N B Naduvinamani and Usha Shankar [13] investigate heat and mass transfer in the presence of a chemical reaction by compressing an unsteady MHD Casson fluid between two parallel plates with joule and viscous dissipation. The

simplified governing equations of flow are solved using the RK-SM techniques, and the results describe the effect of different parameters on the non-Newtonian flow behavior of Casson Fluid. Further the same results are obtained using the bvp4c method.

Mustafa, Hayat et al. on The Unsteady Squeezing Flow Between Parallel Plates: Heat and Mass Transfer [6]:

In his paper, M. Mustafa analyzed the heat and mass transfer of two-dimensional, unsteady Newtonian fluid behavior between squeezing and separating parallel plates under the influence of viscous dissipation. The flow model or governing equation of mass, momentum, energy and concentration are non-linear and time dependent coupled partial differential equations. It is pertinent to mention that the governing equations are presenting the Newtonian fluid in absence of radiation, heat source/sink and MHD effects.

$$u_x + u_y = 0 \tag{1.1}$$

$$u_t + uu_x + vu_y = -\frac{1}{\rho}P_x + v\left(u_{xx} + u_{yy}\right) \tag{1.2}$$

$$v_t + uv_x + vv_y = -\frac{1}{\rho}P_y + v\left(v_{xx} + v_{yy}\right) \tag{1.3}$$

$$T_t + uT_x + vT_y = \frac{k}{\rho c_p}\left(T_{xx} + T_{yy}\right) + \frac{\mu}{\rho c_p}\left(4{u_x}^2 + \left(u_y + v_x\right)^2\right) \tag{1.4}$$

$$C_t + uC_x + vC_y = D_m\left(C_{xx} + C_{yy}\right) - k_l C \tag{1.5}$$

He converts the governing system of partial differential equations into ordinary differential equations using the similarity transformations represented by the similarity variables η, $\theta(\eta)$ and $\phi(\eta)$. Resultantly, the continuity equation is eliminated during this process and number of independent variables is reduce to one η.

Subsequently, he utilizes the Homotopy method to obtain the solution of the ODEs under the given boundary conditions. In this process, he obtained the solutions $f''(1)$, $\theta'(1)$ and $\phi'(1)$ at 1, 5, 8, 9, 10, 15, 20 and 30 order of approximation for particular case in order to converge the solution at 15^{th} order. Afterwards, he discusses the effect of Eckert number, Prandtl number and Squeezing number on temperature and effect of squeezing number, Schmidt number and chemical reaction parameter on concentration. Further, the effect of these parameters is also extended on Nusselt number and Sherwood number.

In the findings, he discussed that the velocity profile is inversely related to the squeezing

number, Prandtl and Eckert number is increasing the heat transfer rate as well as temperature. Also, Schmidt Number has an inverse relation with the concentration field and directly related to the Sherwood Number. Finally, the chemical reaction is increasing the Sherwood Number.

N B Naduvinamani and Usha Shankar Model on Thermal-Diffusion and Diffusion-Thermo Effects on Squeezing Flow of Unsteady Magneto-Hydrodynamic Casson Fluid between Two Parallel Plates With Thermal Radiation [13]:

In this paper, the study of non-Newtonian Casson fluid between squeezing/separating parallel plates is conducted. In this study the effect of electromagnetic field, radiation, chemical reaction and presence of heat source/sink in fluid are also included along with viscous and joule dissipation effects. The governing equation for the flow is:

$$u_x + u_y = 0 \tag{1.6}$$

$$u_t + uu_x + vu_y = -\frac{1}{\rho}P_x + v\left(1+\frac{1}{\beta}\right)\left(2u_{xx} + u_{yy} + v_{yx}\right) - \frac{\sigma B_o^2}{\rho(1-\alpha t)}u \tag{1.7}$$

$$v_t + uv_x + vv_y = -\frac{1}{\rho}P_y + v\left(1+\frac{1}{\beta}\right)\left(2v_{xx} + v_{yy} + u_{yx}\right) \tag{1.8}$$

$$T_t + uT_x + vT_y = \frac{k}{\rho c_p}\left(T_{xx} + T_{yy}\right) + \frac{\mu}{\rho c_p}\left(1+\frac{1}{\beta}\right)\left(2{u_x}^2 + \left(u_y + v_x\right)^2 + 2{v_y}^2\right) \tag{1.9}$$

$$+\frac{16\sigma^* T_o^3}{3\rho c_p k^*}T_{yy} + \frac{\sigma B_o^2}{\rho(1-\alpha t)}u^2 + \frac{Q^*}{\rho c_p}(T - T_\infty) + \frac{D_m k_T}{c_s c_p}C_{yy}$$

$$C_t + uC_x + vC_y = D_m\left(C_{xx} + C_{yy}\right) + \frac{D_m k_T}{T_m}T_{yy} - \frac{k_l}{(1-\alpha t)}(C - C_\infty) \tag{1.10}$$

The highly non-linear unsteady coupled system of partial differential equations is reduced using similarity transformations. The reduced ODEs are then solved using Runga Kutta Shooting method (RK-SM) and bvp4c method. They validate their results by comparing them with results of Mustafa [6].The convergence of the results for RK shooting method and bvp4c method are compared unlike Mustafa [6] model where the convergence is achieved by increasing the order of the equation . Afterwards, the effect of parameters i.e., Squeezing number, Casson fluid parameter, Hartmann number, Prandtl number, Schmidt number, Radiation parameter, Heat Source/sink number, Soret number and Dufour number on the flow field are plotted and their effect on heat and mass transfer are discussed. Like the previous model, they also studied the effect of these parameters on Nusselt number and Sherwood number to understand their physical aspects.

However, they obtained their solution through numerical method where these effects can only study in limited domain at limited points with limited accuracy which is restricted by processing cost and time i.e. If someone wants to investigate a larger domain, wants to increase the mesh size, or needs greater accuracy, the computing time and cost will rise. Further, these effects are not plotted as flow field or contours to fully understand their effects.

In his findings, he confirmed that the velocity profile is inversely related to the Squeezing number and temperature is also inversely related to Squeezing number Casson Fluid parameter and radiation parameter are also inverse function of temperature field. Dufour number is an increasing function of temperature. Soret number and Schmidt number are inversely related to Concentration field.

1.3 SCOPE & MOTIVATION:

Having the comprehensive literature survey, it is noted that the numerical methods provide results on discrete points and accuracy increases with increase in these discrete points, however, high computation cost and time restrict the results to finite number of points and on the other hand, analytical method like HAM can provide analytic solutions in the domain of interest without increasing the computation cost and time. Further, it claims to provide better understanding of the flow dynamics. So, it is worthwhile to understand the flow field, heat and mass transfer in the non-Newtonian flow of Casson fluid under effect of various forces using Homotopy Analysis method. For comparison the same problem is solved using the Finite Difference Method along with the previously presented published results to assess the accuracy, processing time and memory allocation. Additionally, a thorough explanation of the relationship between the flow control parameters for Casson fluid is provided, and to fully comprehend how the fluid would behave under the given conditions, flow field, temperature, and concentration contours must also be displayed.

CHAPTER 2. FLOW AND HEAT TRANSFER MODEL

In this section, the governing equations of Casson fluid between the parallel plates are shown along with the boundary conditions. These PDEs are transformed into ODEs using similarity transformation and the resulting ODEs are solved using Homotopy analysis method. Finally, the convergence control parameters are plotted. These parameters are used to determine at what value of these parameters the results are converging.

2.1 GOVERNING EQUATION

The analysis presented in this study considers unsteady two-dimensional flow model of MHD squeezing, viscous and incompressible Casson fluid between two parallel plates under the influence of radiation and chemical reaction process studied in [13] .Symmetrical flow is assumed across the center of the two plates to reduce the computation time. The equations of continuity, momentum, energy and concentration for this model are written as

$$u_x + u_y = 0 \tag{2.1}$$

$$u_t + uu_x + vu_y = -\frac{1}{\rho}P_x + v\left(1+\frac{1}{\beta}\right)\left(2u_{xx} + u_{yy} + v_{yx}\right) - \frac{\sigma B_o^2}{\rho(1-\alpha t)}u \tag{2.2}$$

$$v_t + uv_x + vv_y = -\frac{1}{\rho}P_y + v\left(1+\frac{1}{\beta}\right)\left(2v_{xx} + v_{yy} + u_{yx}\right) \tag{2.3}$$

$$T_t + uT_x + vT_y = \frac{k}{\rho c_p}\left(T_{xx} + T_{yy}\right) + \frac{\mu}{\rho c_p}\left(1+\frac{1}{\beta}\right)\left(2{u_x}^2 + \left(u_y + v_x\right)^2 + 2{v_y}^2\right) + \frac{16\sigma^* T_o^3}{3\rho c_p k^*}T_{yy} + \frac{\sigma B_o^2}{\rho(1-\alpha t)}u^2 + \frac{Q^*}{\rho c_p}(T - T_\infty) + \frac{D_m k_T}{c_s c_p}C_{yy} \tag{2.4}$$

$$C_t + uC_x + vC_y = D_m\left(C_{xx} + C_{yy}\right) + \frac{D_m k_T}{T_m}T_{yy} - \frac{k_l}{(1-\alpha t)}(C - C_\infty) \tag{2.5}$$

The following are the boundary conditions for Casson fluid squeezing flow.

$$y = \mathrm{h(t)} \rightarrow \ u = 0, \ v = v_w = \frac{dh}{dt}, \ T = T_w, C = C_w \tag{2.6}$$

$$y = 0 \rightarrow \ u_y = T_y = C_y = 0, \ v = 0 \tag{2.7}$$

The effect of chemical reaction is included in the concentration equation while the effects of joule dissipation and radiation are present in the energy equation.

2.2 CASSON FLUID FLOW BETWEEN PARALLEL PLATES:

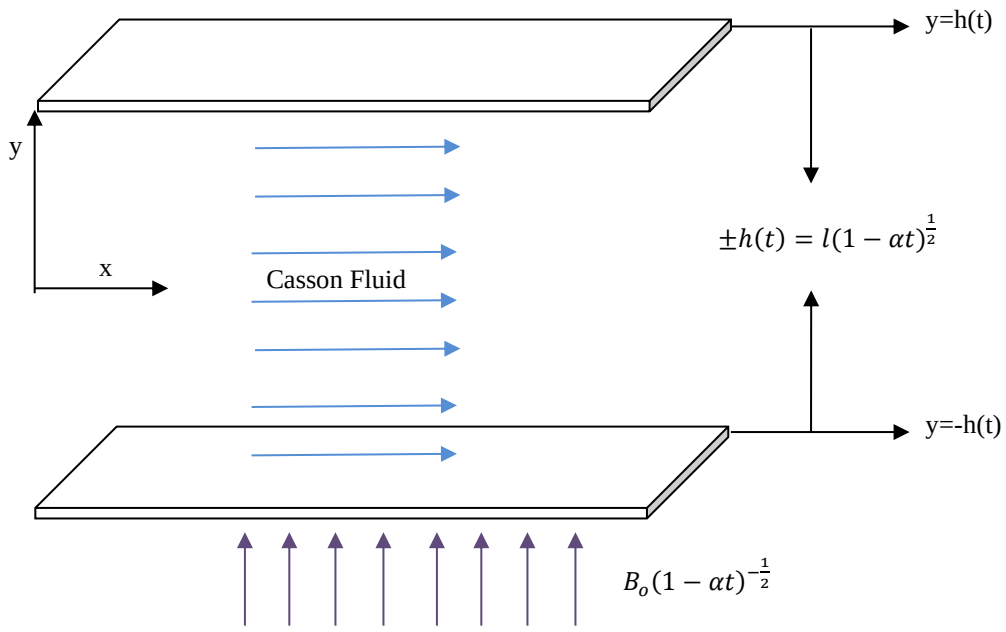

Figure 1: Casson Fluid Flow Between Parallel Plates

Figure 1 describes the flow configuration and geometry of the Casson fluid flow in which distance between the plates is expressed in direction of y and represented as $\pm h(t) = l(1-\alpha t)^{\frac{1}{2}}$ where l is the initial position of plates at t = 0 and α shows the speed and direction of the plates i.e. $\alpha > 0$ indicates that the plates are squeezing and $\alpha < 0$ shows that they are moving away. Further, the applicable boundary conditions are shown in (2.6) and (2.7)

$$y = h(t) \rightarrow \; u = 0, \; v = v_w = \frac{dh}{dt}, \; T = T_w, C = C_w \tag{2.6}$$

$$y = 0 \rightarrow \; u_y = T_y = C_y = 0, \; v = 0 \tag{2.7}$$

2.3 CONSTRUCTION OF SIMILARITY TRANSFORMATIONS

There is no current analytical and direct method to solve the equation (2.1), (2.2), (2.3), (2.4) and (2.5) with boundary conditions (2.6) and (2.7) because these equations are coupled and highly nonlinear in nature. Further, Homotopy Analysis Method requires ordinary differential equations as an input to provide the analytical solution. Therefore, Following Similarity transformations are used to convert these complex equations into non-linear ODEs [12, 14, 15]

$$u = \left(\frac{\alpha x}{2(1-\alpha x)}\right) f'(\eta), \qquad v = \left(\frac{-\alpha l}{2\sqrt{1-\alpha x}}\right) f(\eta) \tag{2.8}$$

$$\theta(\eta) = \frac{T - T_\infty}{T_w - T_\infty}, \qquad \phi(\eta) = \frac{C - C_\infty}{C_w - C_\infty}$$

Where $\eta = \frac{y}{l\sqrt{1-\alpha x}}$

By using the above similarity transformation on equation (2.1), (2.2), (2.3), (2.4) and (2.5) the following non dimensional equations are obtained:

$$\left(1 + \frac{1}{\beta}\right) f'''' - S(\eta f''' + 3f'' + f'f'' - ff''') - Ha^2 f'' = 0 \tag{2.9}$$

$$\left(1 + \frac{4}{3}\right) R\theta'' - \Pr S\,(f\theta' - \eta\theta' + Q\theta) + \Pr Ec\left(\left(1 + \frac{1}{\beta}\right)(f''^2 + 4\delta^2 f'^2) + Ha^2 f'^2\right)$$

$$+ DuPr\phi'' = 0 \tag{2.10}$$

$$\phi'' + ScS(f\phi' - \eta\phi') - ScKr\phi + SrSc\theta'' = 0 \tag{2.11}$$

Similarly, the boundary conditions (2.6) and (2.7) converted into the following form:

$$\begin{aligned} &\eta = 0 \rightarrow \ f = 0, \qquad f'' = 0, \qquad \theta = 0, \qquad \phi = 0 \\ &\eta = 1 \ \rightarrow \ f = 1, \qquad f' = 0, \qquad \theta = 1, \qquad \phi = 1 \end{aligned} \tag{2.12}$$

In equation (2.9), (2.10), (2.11) and (2.12), prime represents the derivative with respect to similarity variable η and the dimensionless numbers shown in the these equations are presented in the following table.

$$S = \frac{\alpha l^2}{2v} \qquad (Squeezing\ Number)$$

$$R = \frac{4\sigma^* T_\infty^3}{kk^*} \qquad (Radiation\ Parameter)$$

$$Ha = B_o l\sqrt{\frac{\sigma}{\mu}} \qquad (Hartmann\ Number)$$

$$Du = \frac{D_m k_t (C - C_\infty)}{c_p c_s v(T - T_\infty)} \qquad (Dufour\ Number)$$

$$Sr = \frac{D_m k_t (T - T_\infty)}{T_m v(C - C_\infty)} \qquad (Soret\ Number)$$

$$Sc = \frac{v}{D_m} \qquad (Schmidt\ Number)$$

$$Pr = \frac{\mu c_p}{k} \qquad (Prandtl\ Number),$$

$$\delta = \frac{h}{x} \qquad (Delta)$$

$$Kr = \frac{l^2 k_1}{v} \qquad (Chemical\ Reaction\ Parameter)$$

$$Q = \frac{2Q^*(1-\alpha t)}{\alpha \rho C_p} \qquad (heat\ source/Sink\ Parameter)$$

$$Ec = \frac{\alpha^2 x^2}{4C_p(T-T_\infty)(1-\alpha t)^2} \qquad (Eckert\ Number)$$

2.4 SOLUTION APPROACH

The equations (2.9), (2.10), (2.11) and (2.12) obtained from similarity transformation are analytically solved using HAM.

2.4.1 Homotopy Analysis Method (HAM):

In this method, we assume the solution can be expressed by:

$$(\eta^m | m = 0,1,2, \dots .)$$

In this step we assume the initial value of f_o, $\theta_o$and ϕ_o along with linear operators:

$$f_0(\eta) = \tfrac{1}{2}(3\eta + \eta^3), \qquad \theta_0(\eta) = 1, \qquad \phi_0(\eta) = 1\ .$$
$$L_f(f) = \frac{d^4 f}{d\eta^4}, \qquad L_\theta(\theta) = \frac{d^2\theta}{d\eta^2}, \qquad L_\phi(\phi) = \frac{d^2\phi}{d\eta^2} \tag{2.13}$$

The initial values mentioned above have been found out through the following:

$$L_f[C_1 + C_2\eta + C_3\eta^2 + C_4\eta^3] = 0$$
$$L_\theta[C_5 + C_6\eta] = 0, \qquad L_\phi[C_7 + C_8\eta] = 0 \tag{2.14}$$

We construct the zeroth order deformation equation which can be written as:

$$(1-q)L_f[F(\eta,q) - f_0(\eta)] = q h_f H_f N_f[F(\eta,q)]$$
$$(1-q)L_\theta[\theta(\eta,q) - \theta_0(\eta)] = q h_\theta H_\theta N_\theta[\theta(\eta,q)] \tag{2.15}$$
$$(1-q)L_\phi[\phi(\eta,q) - \phi_0(\eta)] = q h_\phi H_\phi N_\phi[\phi(\eta,q)]$$

$$F(0,q)=0, F(1,q)=1, F''(0,q)=0, F'(1,q)=0$$

$$\theta(0,q)=0, \theta(1,q)=1, \phi(0,q)=0, \phi(1,q)=1$$

In above equation, H_f, H_θ and H_ϕ are the auxiliary functions that are normally put equal to 1. Further, h_f , h_θ and $h_\phi$are non-zero auxiliary parameters and they must carry identical signs for a convergent solution. Also, q is an embedding parameter. For q=0 and q=1

$$\begin{aligned} &F(\eta,0)=f_0(\eta), \qquad F(\eta,1)=f(\eta)\\ &\theta(\eta,0)=\theta_0(\eta), \qquad \theta(\eta,1)=\theta(\eta)\\ &\phi(\eta,0)=\phi_0(\eta), \qquad \phi(\eta,1)=\phi(\eta) \end{aligned} \tag{2.16}$$

The second step is to construct the mth-order deformation equations and integrate them to find the solution that are built on the initial functions (2.16). In [4], one finds a detailed procedure to construct the mth-order deformation equations which, for example, for ODEs in case 1(a) of Table 1 are written as

$$\begin{aligned} &L_f[f_m(\eta)-x_m f_{m-1}(\eta)]=h_f H_f(\eta)R_{f,m}(\eta),\\ &L_\theta[\theta_m(\eta)-x_m\theta_{m-1}(\eta)]=h_\theta H_\theta(\eta)R_{\theta,m}(\eta),\\ &L_\phi[\phi_m(\eta)-x_m\phi_{m-1}(\eta)]=h_\phi H_\phi(\eta)R_{\phi,m}(\eta), \end{aligned} \tag{2.17}$$

where,

$$x_m=\begin{cases}1, & m>1\\ 0, & m=1\end{cases} \tag{2.18}$$

mth-order deformation equations for the given equations are:

$$\begin{aligned} &R_{f,m}(\eta)=\left(1+\frac{1}{\beta}\right)f'''''_{m-1}-S(\eta f'''_{m-1}+3f''_{m-1})+\sum_{k=0}^{m-1}S(f'_{m-1-k}f''_k-f_{m-1-k}f'''_k)\\ &-Ha^2f''_{m-1}\\ &R_{\theta,m}(\eta)=\left(1+\frac{4}{3}R\right)\theta''_{m-1}-PrS(\eta\theta'_{m-1}-Q\theta'_{m-1})+DuPr\phi''_{m-1}\\ &+\sum_{k=0}^{m-1}(PrSf_{m-1-k}\theta'_k+PrEc((1+\frac{1}{\beta})(f''_{m-1-k}f''_k+4\delta^2f'_{m-1-k}f'_k)-Ha^2f'_{m-1-k}f'_k)\\ &R_{\phi,m}(\eta)=\phi''_{m-1}-ScS\eta\phi'_{m-1}-ScKr\phi_{m-1}+SrSc\theta''_{m-1}+\sum_{k=0}^{m-1}ScSf_{m-1-k}\phi'_k \end{aligned} \tag{2.19}$$

Similarly, the boundary conditions become,

$$f_m(0) = 0, f_m(1) = 1, f_m''(0) = 0, f_m'(1) = 0$$
$$\theta_m(1) = 1, \theta_m'(0) = 0, \phi_m(1) = 1, \phi_m'(0) = 0 \quad (2.20)$$

Increasing the order of HAM can enhance the precision of such approximations. The m^{th}-order approximation of a function is obtained by adding up all the approximated values of that function, represented as $(f_0 + f_1 + f_2 + \cdots + f_m)$. The same method can be employed for the solutions of all cases written in Table 1.

2.4.2 Convergence of Solution

The system of equation (2.17) contains non-zero auxiliary parameters h_f, h_θ and h_ϕ also known as convergence control parameters. These parameters are determined by plotting the equation for f, θ and ϕ as function of h_f, h_θ and h_ϕ respectively at particular η and same plots are shown in figure 2 - 12. Each plot in figure 2 - 12 represents h-curves for each case of study for particular dimensionless numbers. By observing these graphs, it is evident that valid range of these parameters vary from case to case and can easily be extracted from graph. Further examining the behavior of these parameters by using 3D plot between f, θ and ϕ as functions of h_f, h_θ and h_ϕ, respectively, by varying η using 15^{th} −order HAM which lead to the fact that this system of equations converged at $h_f = h_\theta = h_\phi = -0.1 \sim -0.8$ depending on case under study.

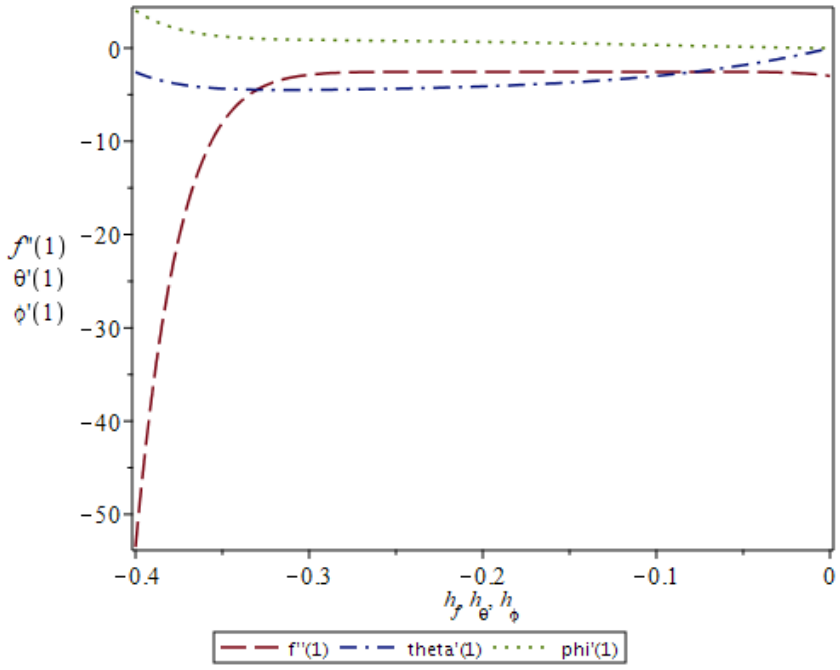

Figure 2: h-curve for Influence of β at S=-4, Du=R=Q=Ec=Kr=0.1, Sr=0.5,

Pr=0.7, Sc=0.7, δ =1.2, Ha=0.1, β=0.17

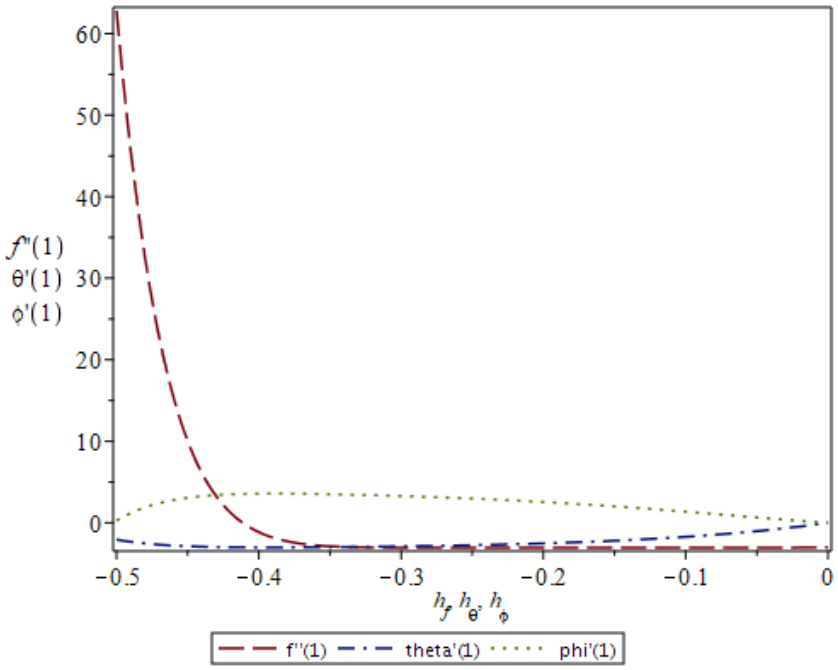

Figure 3: h-curve for Influence of Du at S=0.4, Du=Sr=Ha=Q=0.5, Kr=1.6, Sc=0.7, δ=0.01, R= Ec=0.1, Pr=1.2, β=0.2

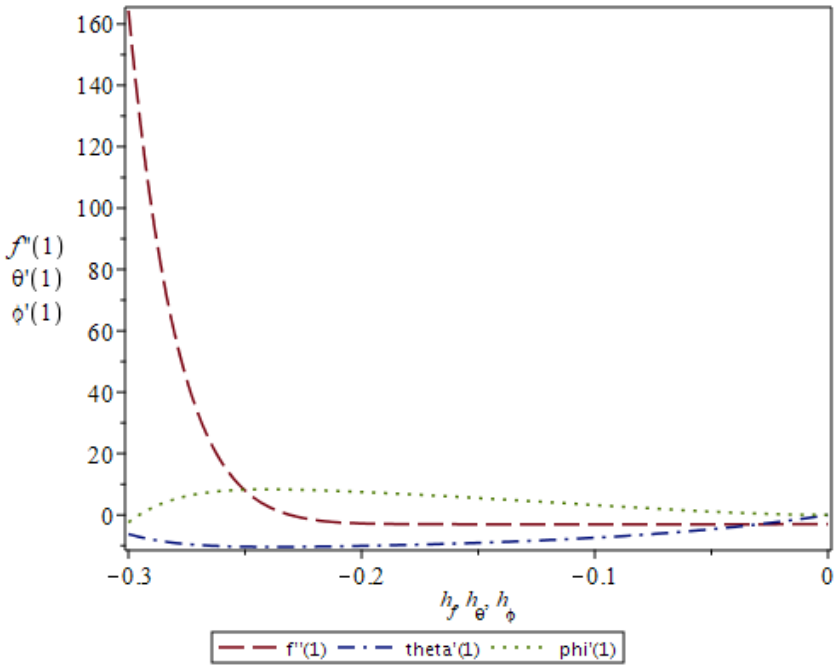

Figure 4: h-curve for Ec at S=0.5, β =0.1, Du=0.5, Sr=0.5, Ha=0.5, Q=0.1, Kr=0.1, Pr=0.7, Sc=0.7, δ =0.1, R=0.1, Ec=0.5

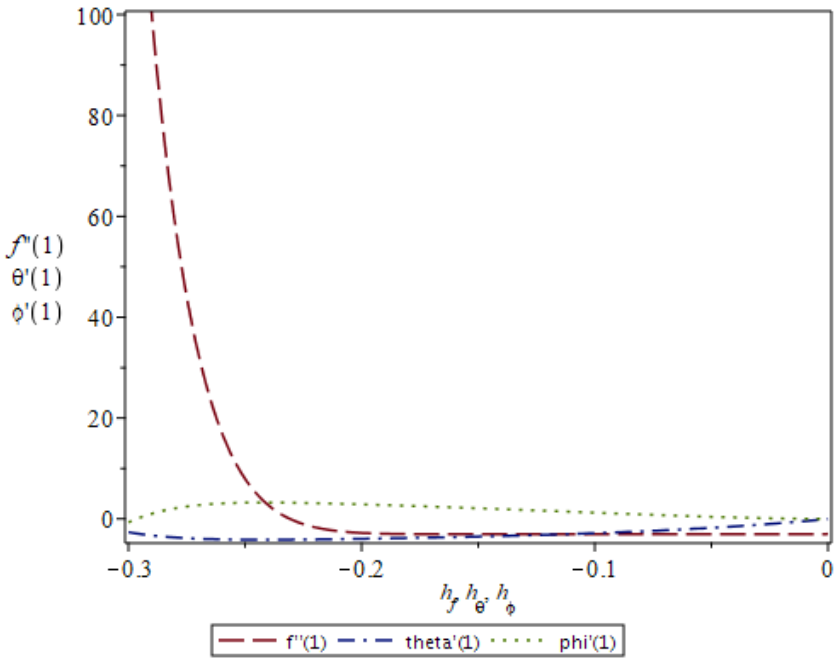

Figure 5: h-curve for Pr at S=0.5, β=0.1, Du=0.5, Sr=0.5, Ha=0.5, Q=0.1, Kr=0.1, Sc=0.7, δ=0.1, R=0.1, Ec=0.1, Pr=1.3

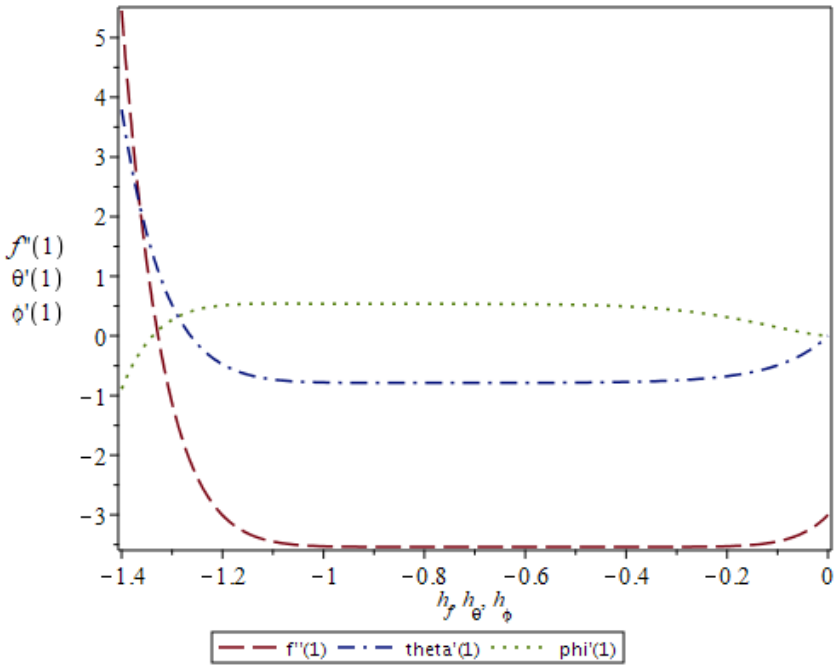

Figure 6:h-curve for Influence of Ha at S=0.1, β=2.0, Du=0.5, Sr=0.5, R=0.1, Q=0.1, Ec=0.1, Kr=0.1, Pr=0.7, Sc=0.7, δ=0.5, Ha=2

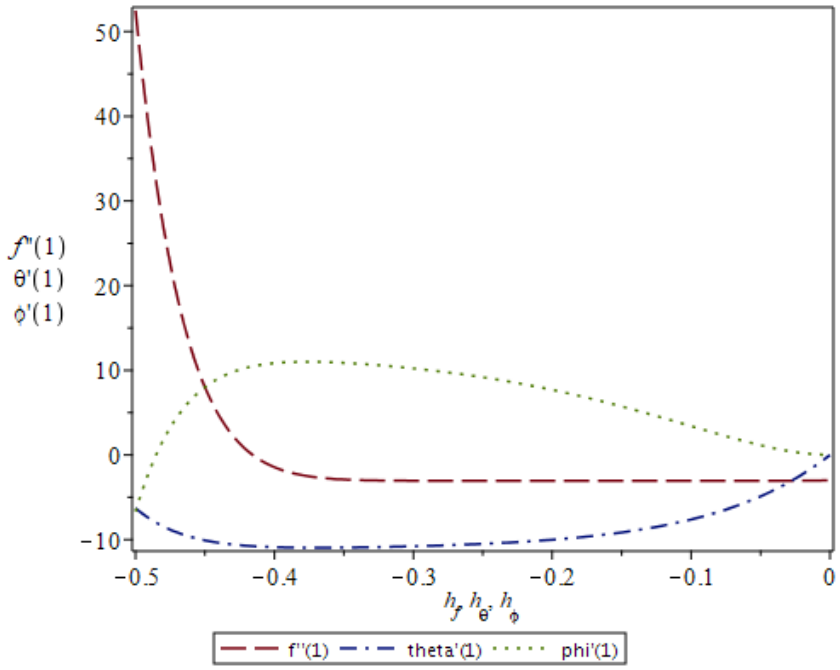

Figure 7: h-curve for Influence of Q at S=0.4, β=0.2, Du=0.5, Sr=0.5, Ha=0.1, Q=0.1, Ec=1.0, Kr=0.1, Pr=0.7, Sc=0.7, δ=0.1, R=0.2

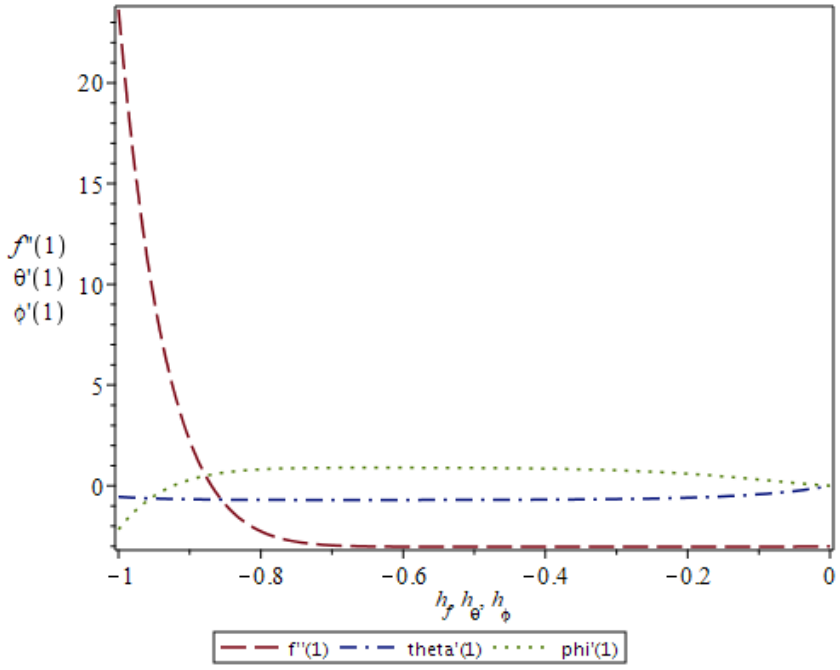

Figure 8: h-curve for Influence of at Kr S=0.1, β=0.5, Du=0.5, Sr=0.5, Ha=0.1, Q=0.1, Kr=0.3, Sc=0.7, δ=0.1, R=0.1, Ec=0.1, Pr=0.7

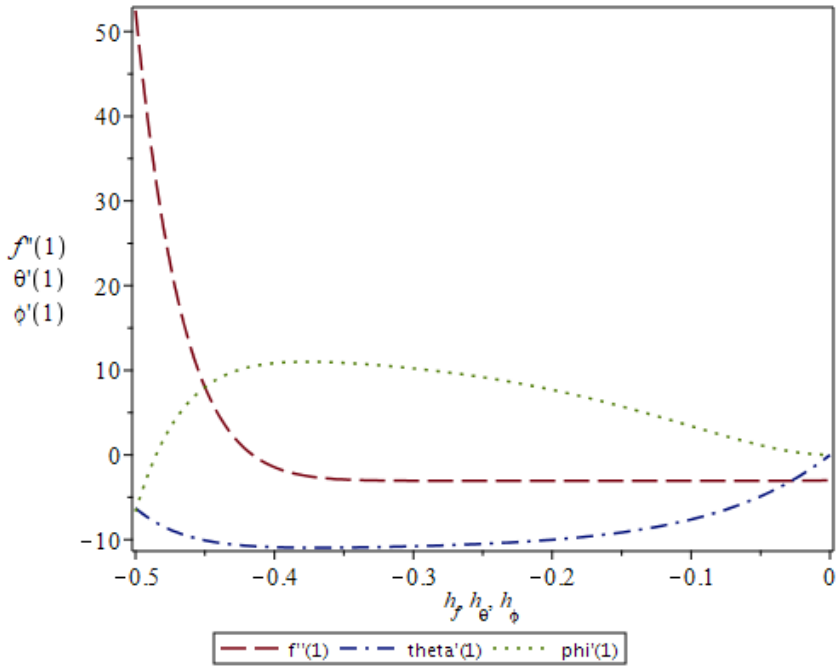

Figure 9: h-curve for Influence of R at S=0.4, β=0.2, Du=0.5, Sr=0.5, Ha=0.1, Q=0.1, Ec=1.0, Kr=0.1, Pr=0.7, Sc=0.7, δ=0.1, R=0.2

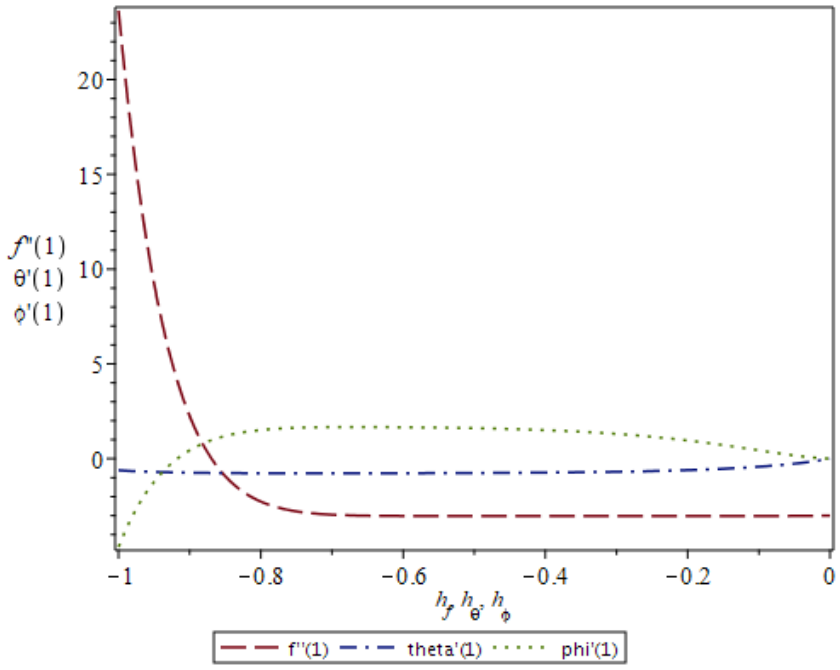

Figure 10: h-curve for Influence of Sc at S=0.1, β=0.5, Du=0.5, Sr=0.5, Ha=0.1, Q=0.1, Kr=0.1, Sc=1.4, δ=0.1, R=0.1, Ec=0.1, Pr=0.7

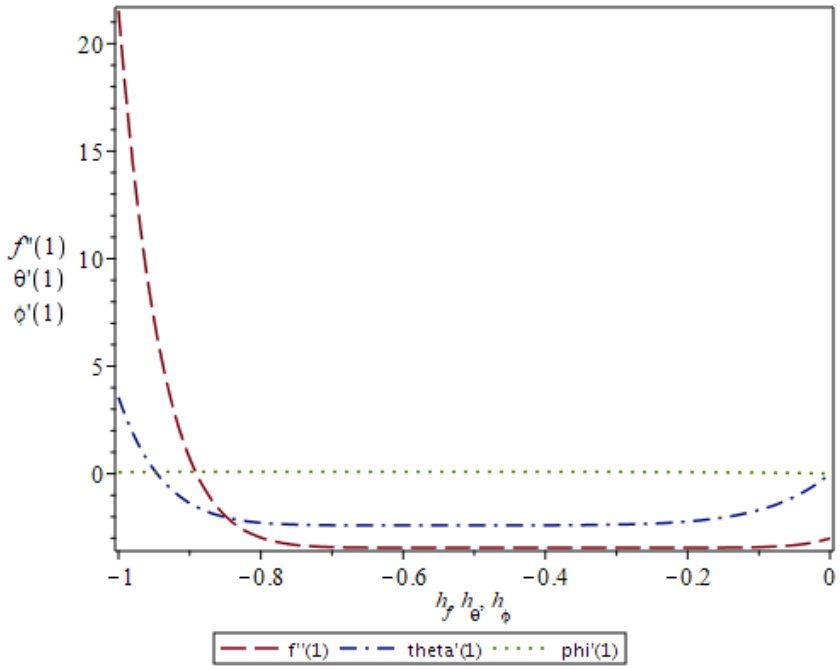

Figure 11: h-curve for Influence of S at β=0.8, Du=0.5, Sr=0.1, Ha=0.1, R=0.1, Ec=0.1, Kr=0.1, Pr=0.1, Sc=0.7, δ=5, Q=0.1, S=1.5

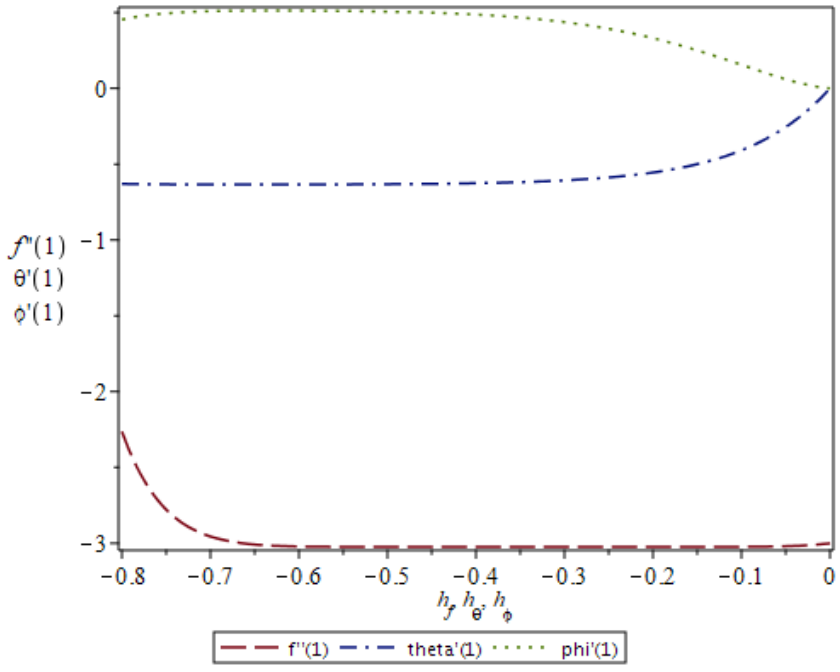

Figure 12: h-curve for Influence of Sr at S=0.1, β=0.5, Du=0.5, Sr=0.5, Ha=0.1, Q=0.1, Kr=0.1, Sc=0.5, δ=0.1, R=0.1, Ec=0.1, Pr=0.7

CHAPTER 3: VALIDATION AND COMPARISON

In this section, the results obtained from HAM are compared with previously published results in order to verify them, Further the effectiveness of HAM are investigated by comparing it with the results and performance of Finite difference scheme (Backward).

3.1 VALIDATION OF RESULTS OF HAM:

In this section, the systems of non-linear ODEs mentioned in equation (2.9), (2.10) and (2.11) that are subjected to boundary conditions (2.12) are solved using various order of approximation of HAM and results are shown in Table 1. This table indicates the convergence of analytical solution with an increase in the order of approximation, with the convergent results at 15^{th}-order of approximation with a precision up to 10^{-5}.

Table 1 Momentum, heat and mass transports with increasing order of approximation at Ha = Kr = S = δ = 0.5, Ec = Q = R = 0.3, Pr= Sc=1.5, β=0.3

Order	$f'''(1)$	$\theta'(1)$	$\phi'(1)$	*Order*	$f'''(1)$	$\theta'(1)$	$\phi'(1)$
5	-3.10687	-6.06438	0.56129	12	-3.09135	-6.20756	0.58256
8	-3.08768	-6.19218	0.57944	15	-3.09283	-6.20879	0.58285
9	-3.09577	-6.20225	0.58098	20	-3.09283	-6.20879	0.58285
10	-3.09016	-6.20461	0.58183	30	-3.09283	-6.20879	0.58285

Additionally, the same system of ODEs is solved using the Forward Difference Method, and the results are presented in Table 2. Also, the HAM and FDM results are validated by comparing them with those of the RK-shooting method and the bvp4c method derived by Naduvinamani [13]. The comparison of the HAM and FDM results with the shooting method and the bvp4c method demonstrates that the results are consistent. These findings illustrate the effectiveness of HAM analytical approach to effectively tackling complex non-linear problems [6]. For all the analytic and approximate solutions deduced using HAM and FDM respectively MAPLE codes are used here.

Table 2 Momentum, heat and mass transports on different S at Ha = R = Q = Du = Sr = 0, Ec = Kr = Pr= Sc=1, β=∞, δ = 0.5

S	$-f''(1)$				$-\theta'(1)$				$-\phi'(1)$			
	RK-SM	bvp4c	HAM	FDM	RK-SM	bvp4c	HAM	FDM	RK-SM	bvp4c	HAM	FDM
-1.0	2.170090	2.170090	2.170090	2.170090	3.319899	3.319899	3.319899	3.319899	0.8045587	0.8045587	0.8045587	0.8045587
-0.5	2.614038	2.614038	2.614038	2.614038	3.129491	3.129491	3.129491	3.129491	0.7814023	0.7814023	0.7814023	0.7814023
0.01	3.007134	3.007134	3.007134	3.007134	3.047092	3.047092	3.047092	3.047092	0.7612252	0.7612252	0.7612252	0.7612252
0.5	3.336449	3.336449	3.336449	3.336449	3.026324	3.026324	3.026324	3.026324	0.7442243	0.7442243	0.7442243	0.7442243
2.0	4.167389	4.167389	4.167389	4.167389	3.118551	3.118551	3.118551	3.118551	0.7018132	0.7018132	0.7018132	0.7018132

Table 3 Momentum, heat and mass transports at Ha = Kr = S = δ = 0.5, Ec = Q = R = 0.3, Pr= Sc=1.5, β=0.3

η	$f(\eta)$				$\theta(\eta)$				$\phi(\eta)$			
	RK-SM	bvp4c	HAM	FDM	RK-SM	bvp4c	HAM	FDM	RK-SM	bvp4c	HAM	FDM
0.0	0	0	0	0	3.4065	3.4065	3.4039	3.4039	0.7222	0.7222	0.7224	0.7224
0.1	0.1483	0.1483	0.1483	0.1483	3.3874	3.3874	3.3849	3.3849	0.7249	0.7249	0.7251	0.7251
0.2	0.2938	0.2938	0.2938	0.2938	3.3297	3.3297	3.3273	3.3273	0.7330	0.7330	0.7332	0.7332
0.3	0.4335	0.4335	0.4336	0.4336	3.2323	3.2323	3.2300	3.2300	0.7466	0.7466	0.7468	0.7467
0.4	0.5646	0.5646	0.5647	0.5647	3.0928	3.0928	3.0907	3.0907	0.7656	0.7656	0.7657	0.7657
0.5	0.6841	0.6841	0.6842	0.6842	2.9076	2.9076	2.9058	2.9058	0.7900	0.7900	0.7902	0.7902
0.6	0.7891	0.7891	0.7891	0.7892	2.6713	2.6713	2.6697	2.6697	0.8201	0.8201	0.8202	0.8202
0.7	0.8763	0.8763	0.8764	0.8765	2.3758	2.3758	2.3746	2.3747	0.8558	0.8558	0.8559	0.8559
0.8	0.9427	0.9427	0.9428	0.9429	2.0101	2.0101	2.0093	2.0093	0.8974	0.8974	0.8975	0.8975
0.9	0.9851	0.9851	0.9851	0.9851	1.5585	1.5585	1.5581	1.5581	0.9453	0.9453	0.9454	0.9454
1.0	1	1	1	1	1	1	1	1	1	1	1	1

3.2 COMPARISON OF RESULTS OF HAM WITH FINITE DIFFERENCE METHOD:

Nowadays, the effectiveness of method either analytical or numerical are not based on accuracy of the results of its solution but also the computational cost and time it consumed to achieve these solutions or in order words, is it feasible to achieve the required solution against its computational cost and time. In view of above, the computational cost of HAM is calculated and compared with the computational cost of finite difference scheme which is standard scheme used to solve differential problem. Table 4 represents the CPU time and memory of Numerical solution through Finite difference scheme (Backward difference) in which the solution is converging up to precision of 10^{-5} at 200 - 400 iterations depending upon different cases And Table 5 indicates the same data for the Homotopy Analysis method where the solution is converging at 10 to 15. By comparing both tables, it can be concluded that the CPU time and memory used for solution of HAM is definitely better than Numerical method of Finite difference scheme.

Table 4 CPU Time and Memory for Finite Difference Solution

S.No.	Number of Nodes	CPU Time	Memory Used
1	10	0.032 sec	1.765 MB
2	50	2.327 sec	111.28 MB
3	100	17.718 sec	826 MB
4	200	453.40 sec	20287 MB
5	400	23435.33 sec	907274 MB

Table 5 CPU Time and Memory for Homotopy Analysis Method

S.No.	Order of HAM	CPU Time	Memory Used
1	5	4.5	60.18
2	8	36.578	168
3	9	79.547	208.18
4	10	187.675	240
5	12	675	330
6	15	5364.297	437.835

CHAPTER 4: RESULTS

4.1 EFFECT OF FLOW PARAMETERS:

The influence of all the physical control parameters namely $Ha, Kr, S, \delta, Ec, Q, R, Pr, Sc, \beta$, Du and Sr on flow is analyzed here in order to develop a physical understanding of flow, heat, and mass transfer in regard to the present problem. All the computations are performed on MAPLE to determine the impact of each control parameter on flow rates, temperature, and concentration. The same data is presented graphically as well to help better understand the dynamics of the flow.

4.1.1 Effect of Casson Fluid Parameter (β):

In this subsection, the effect of Casson Fluid Parameter (β) on flow field, temperature and concentration is studied. The flow, temperature and concentration variables are plotted by varying Casson fluid parameter (β) using HAM and same is illustrated in Figure Figure 13, Figure 14, Figure 15 andFigure 16. Same results can be achieved using FDM. These results are in complete agreement with the results shown in Naduvinamani[13]. From these graphs it is evident that the slope of normal component of velocity increases with increasing Casson fluid parameter. This is caused by the reduced viscosity and the moving plates can transport its momentum more effectively than at lower values of Casson fluid parameter. Similarly, due to less resistance of the fluid and better momentum transport of the fluid the axial velocity also increases.

Moreover, the θ profile of the flow field decreases with increasing β as shown in Figure 15. However, the Figure 16 indicates that concentration field ϕ shows increment with increasing β.

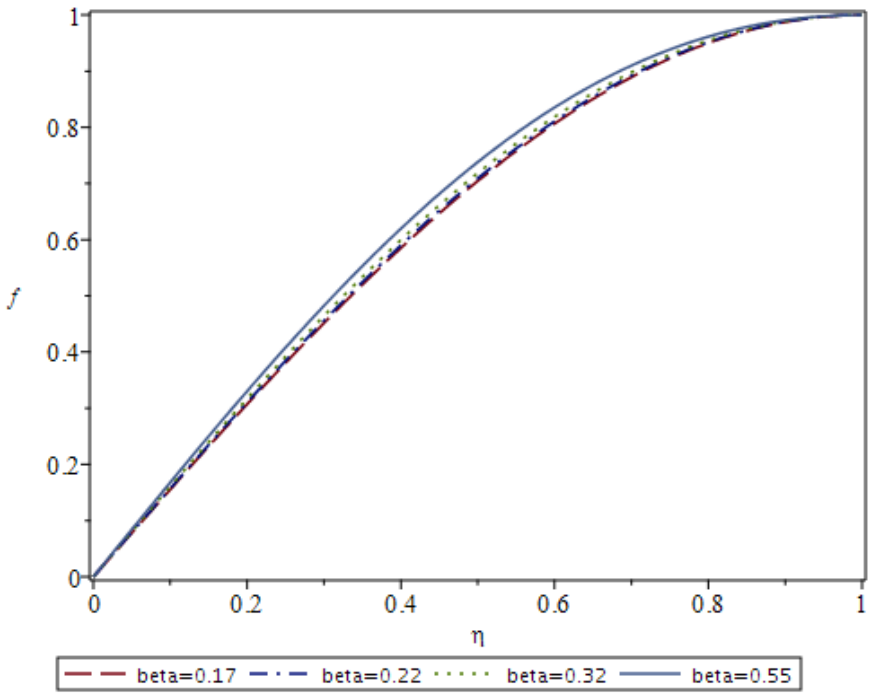

Figure 13: Effect of β on $f(\eta)$ at S=-4, Sr=0.5, R=0.1, Q=0.1, Ec=0.1, Kr=0.1, Pr=0.7, Sc=0.7, δ =1.2, Ha=0.1, Du=0.1

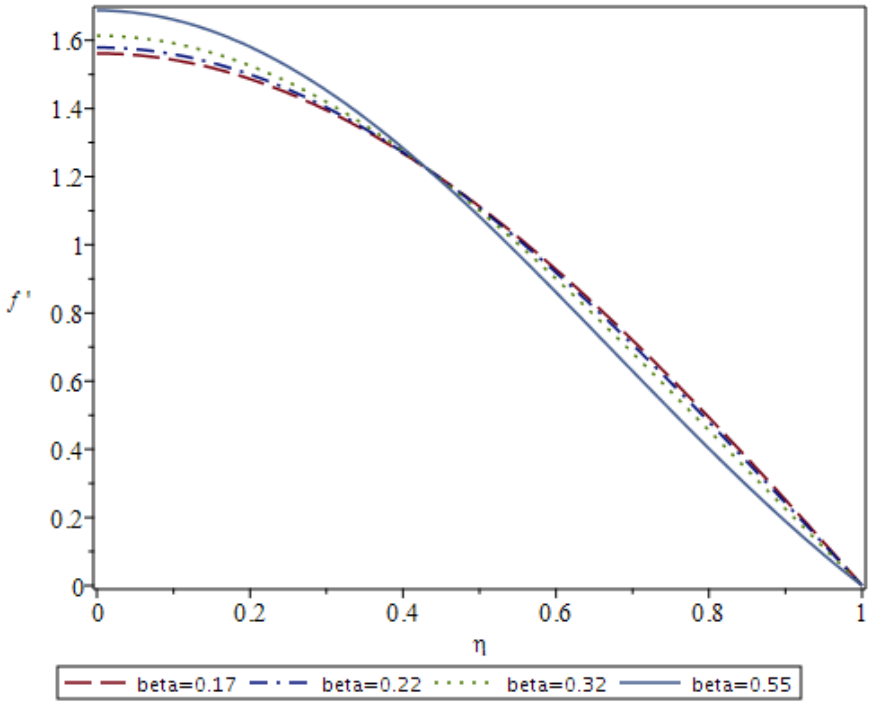

Figure 14: Effect of β on $f'(\eta)$ at S=-4, Sr=0.5, R=0.1, Q=0.1, Ec=0.1, Kr=0.1, Pr=0.7, Sc=0.7, δ =1.2, Ha=0.1, Du=0.1

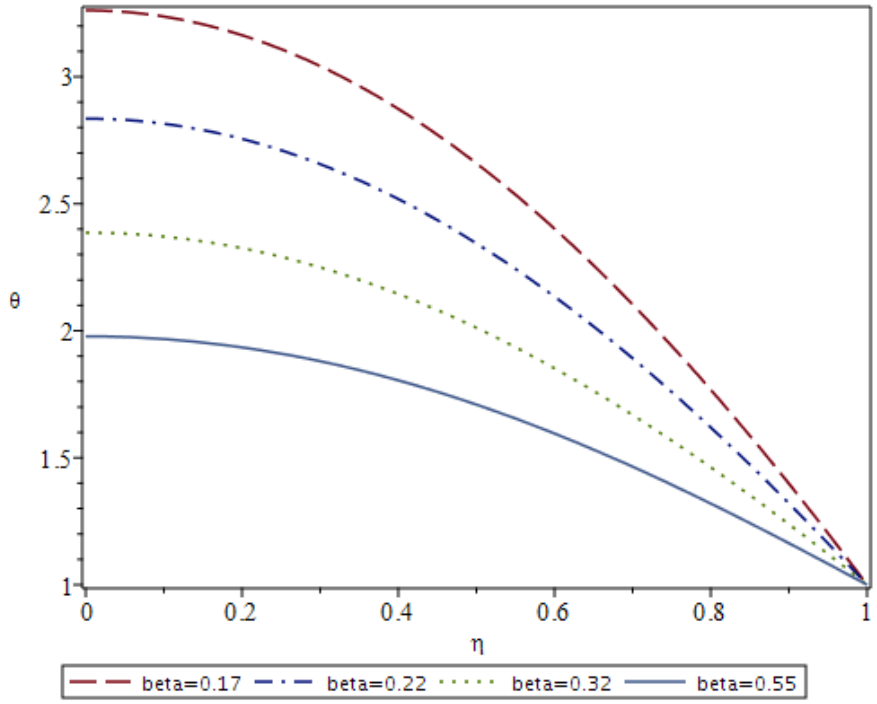

Figure 15: Effect of β on $\theta(\eta)$ at S=-4, Sr=0.5, R=0.1, Q=0.1, Ec=0.1, Kr=0.1, Pr=0.7, Sc=0.7, δ =1.2, Ha=0.1, Du=0.1

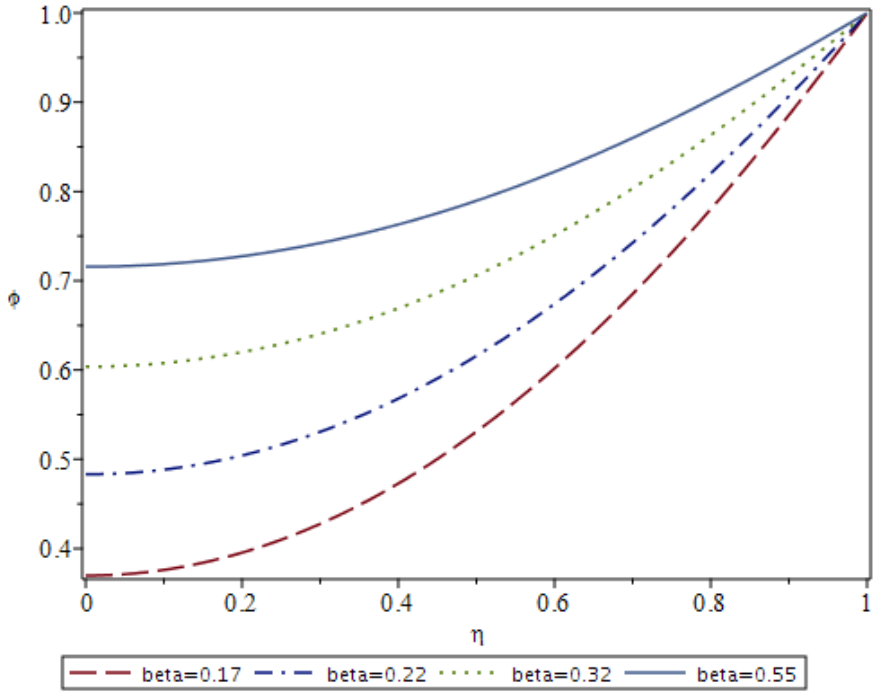

Figure 16: Effect of β on $\phi(\eta)$ at S=-4, Sr=0.5, R=0.1, Q=0.1, Ec=0.1, Kr=0.1, Pr=0.7, Sc=0.7, δ =1.2, Ha=0.1, Du=0.1

The dimensionless values η, $f(\eta)$, $\theta(\eta)$ and $\phi(\eta)$ are converted back to the velocities, temperature and concentration using equation (2.8) to better understand the behavior of flow field, temperature and concentration contours. By observing the Figure 13 to Figure 19, it is clear that trends of the graph of dimensionless parameters and contours of physical parameters are the same. In Figure 17, the temperature contours are plotted using MAPLE at β = 0.17 and β = 0.9. Also, the temperature at the plates wall is taken to be 130 deg Celsius and distance between plates L is taken to be 4m. The positive gradient is observed for both cases as we approached the center of fluid and also, at lower value of β the gradient and overall value of temperature of fluid is increasing. In Figure 18, the concentration contours are plotted using MAPLE at β = 0.17 and β = 0.9. Also, the concentration at the plates wall is taken to be 20 mol/m^3. The negative gradient is observed for both cases as we approached the center of fluid and also, at higher value of β the gradient and overall value of concentration of fluid is increasing slightly. Further, velocity field can be plotted by combining the values of $f(\eta)$ and $f\,'(\eta)$ as mentioned in Figure 19. In this case, β has no prominent effect on velocity field.

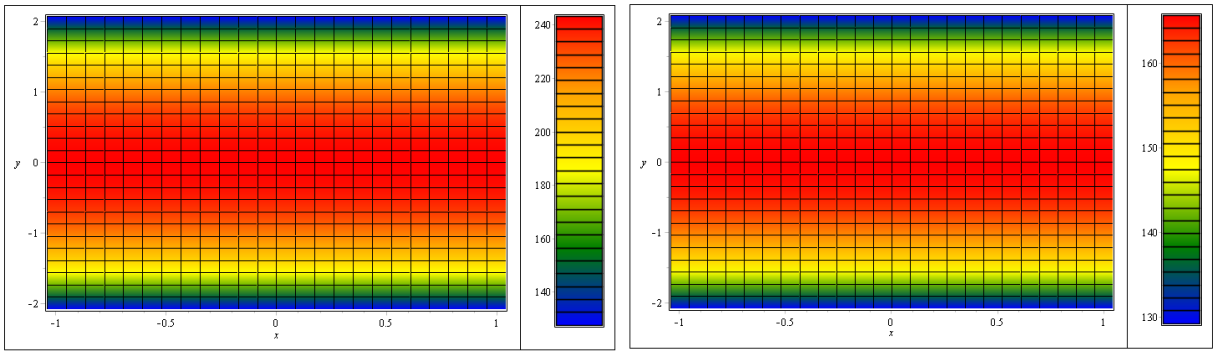

Figure 17: (a) Temperature contours at wall temperature of 130 deg C at β = 0.17 (b) Temperature contours at wall temperature of 130 deg C at β = 0.9

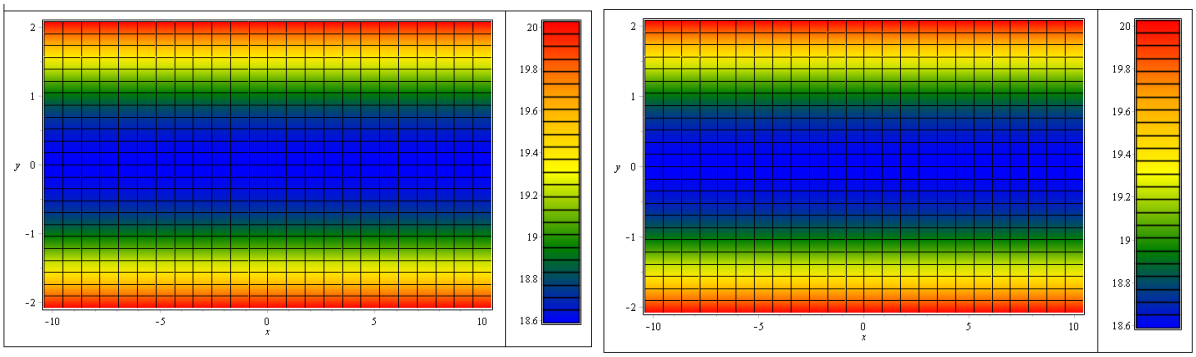

Figure 18: (a) Concentration contours at concentration of 20 mol/m^3 at β = 0.17 (b) Concentration contours at concentration of 20 mol/m^3 at β = 0.9

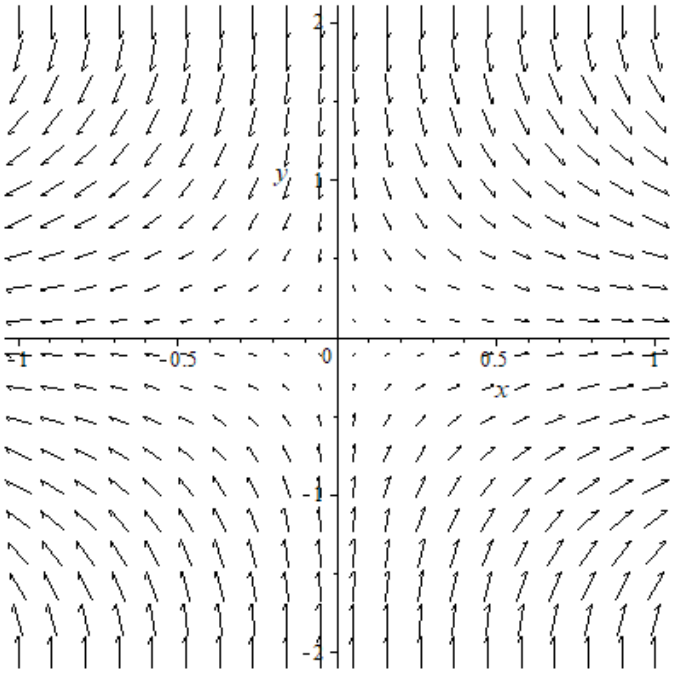

Figure 19: (a) Velocity field/streamlines at β = 0.9

4.1.2 Effect of Squeezing Number (S):

The effect of varying squeezing number (S) on flow field, temperature and concentration and same is depicted in Figure 20, Figure 21,Figure 22 and Figure 23. These results are also taken out using HAM that are found to perfectly align the results of Naduvinamani[13]. Subsequently, the squeezing number represents the movement of plates that is positive squeezing number shows that plates are moving away from each other, and negative Squeezing number (S) represents the plates are moving toward each other. For negative squeezing number, normal velocity shows rapid increase in magnitude at expanse of axial velocity near wall or η>0.65 as shown in Figure 20. This is caused by the movement of plates towards each other which creates a localized pressure gradient due to relatively high pressure near plate surface. However, the axial velocity increases rapidly after η=0.65 at expanse of normal velocity due to the fluid moving out of the system or release into surrounding similarly as, for example, cream moves out when the two biscuit are press towards each other. The same is illustrated in Figure 21. Furthermore, these effects increase with decreasing squeezing number for Squeezing number (S) <0.

However, for positive squeezing number the effect on flow field is similar to the Casson fluid parameter. The normal velocity which is shown as function $f(\eta)$ indicates that the normal velocity is zero at middle of plates and has same velocity as plates on the near to surface

of plate for all the value of Squeezing number, but the gradient of the function become steeper with increase in squeezing number as illustrated in Figure 21. Moreover, axial velocity which is shown as function f' is zero at plate surface and maximum in center of both plates. But the axial velocity increases with increasing Squeezing number for $\eta>0.45$ and decrease with increasing squeezing number for $\eta<0.45$.

The effect of Squeezing number (S) on temperature profile is depicted in Figure 22. This figure indicates that the temperature profile increases drastically with decreasing Squeezing number S at $S<0$ and these increases become more gradual for $S>0$.

Similarly, Figure 23 represents the effect of squeezing number on concentration field this figure shows that the concentration profile decreases rapidly with decreasing Squeezing number (S) at $S<0$ and these decreases become steadier for $S>0$.

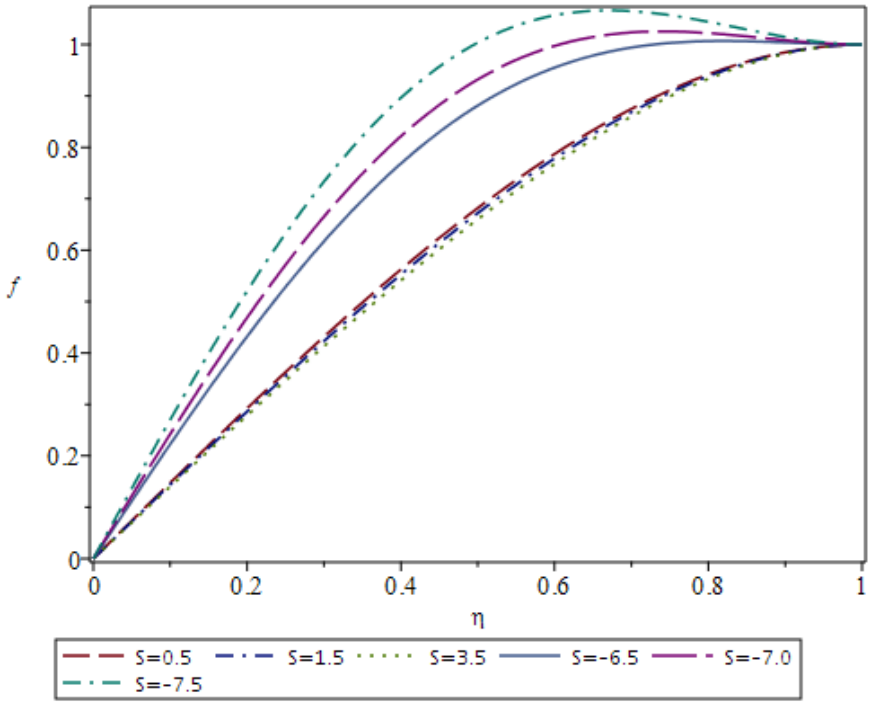

Figure 20: Influence of S on $f(\eta)$ at β=0.8, Du=0.5, Sr=0.1, Ha=0.1, R=0.1, Ec=0.1, Kr=0.1, Pr=0.1, Sc=0.7, δ=5, Q=0.1

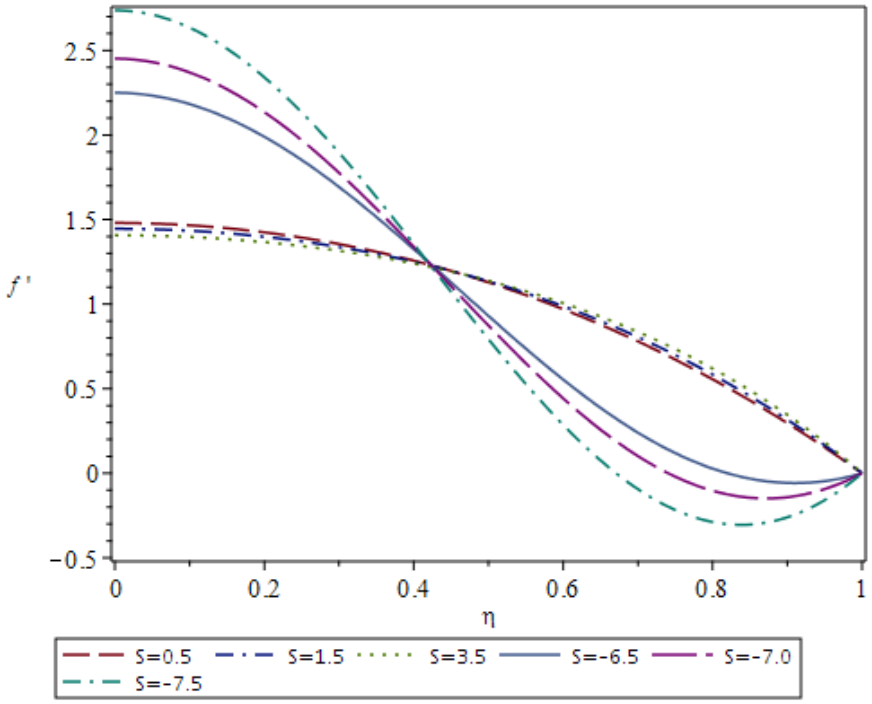

Figure 21: Influence of S on $f'(\eta)$ at β=0.8, Du=0.5, Sr=0.1, Ha=0.1, R=0.1, Ec=0.1, Kr=0.1, Pr=0.1, Sc=0.7, δ=5, Q=0.1

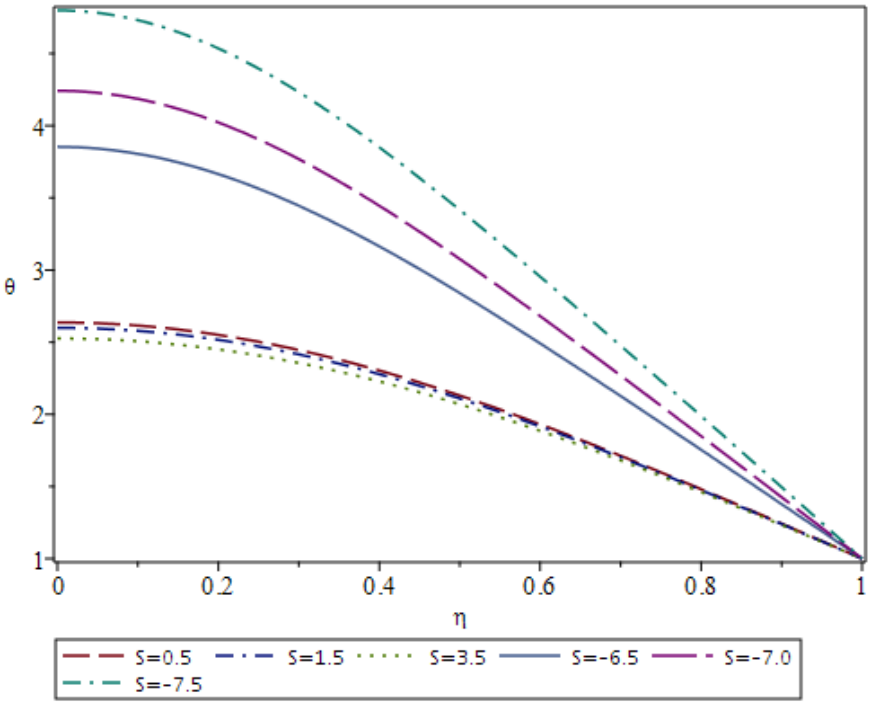

Figure 22: Influence of S on $\theta(\eta)$ at β=0.8, Du=0.5, Sr=0.1, Ha=0.1, R=0.1, Ec=0.1, Kr=0.1, Pr=0.1, Sc=0.7, δ=5, Q=0.1

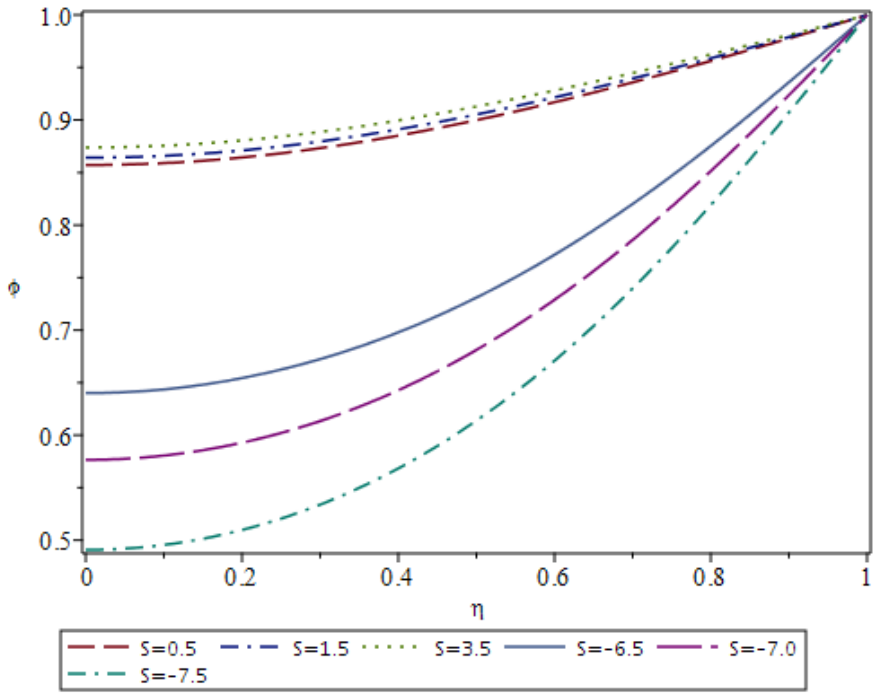

Figure 23: Influence of S on $\phi\ (\eta)$ at β=0.8, Du=0.5, Sr=0.1, Ha=0.1, R=0.1, Ec=0.1, Kr=0.1, Pr=0.1, Sc=0.7, δ=5, Q=0.1

The dimensionless values $\eta, f(\eta), \theta(\eta)$ and $\phi(\eta)$ are converted back to the velocities, temperature and concentration using the equation (2.8) to understand the behavior of flow field, temperature and concentration contours. By observing the Figure 20 to Figure 26, it is clear that trends of the graph of dimensionless parameters and contours of physical parameters are the same. In Figure 24, the temperature contours are plotted using MAPLE at S=0.5 and S=-7.5. Also, the temperature at the plates wall is taken to be 130 deg Celsius and distance between plates L is taken to be 4m. The positive gradient is observed for both cases as we approached the center of fluid and also, at lower value of S the gradient and overall value of temperature of fluid is increasing. In Figure 25, the concentration contours are plotted using MAPLE at S=0.5 and S=-7.5. Also, the concentration at the plates wall is taken to be 20 mol/m^3. The negative gradient is observed for both cases as we approach the center of fluid and also, at the higher value of S the gradient and overall value of concentration of fluid is increasing. Further, velocity field can be plotted by combining the values of $f(\eta)$ and $f'(\eta)$ as mentioned in Figure 26. In this case, squeezing number S significantly affects the velocity field of the flow and reversing the flow at negative S.

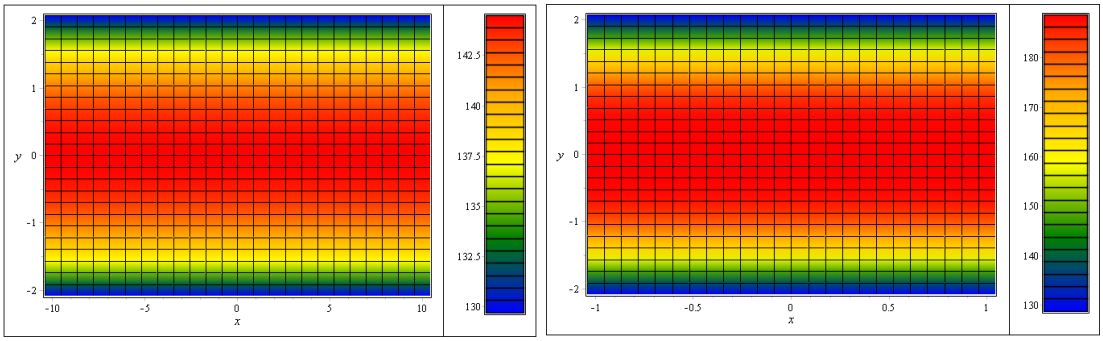

Figure 24: (a) Temperature contours at wall temperature of 130 deg C at S = 0.5 (b) Temperature contours at wall temperature of 130 deg C at β = -7.5

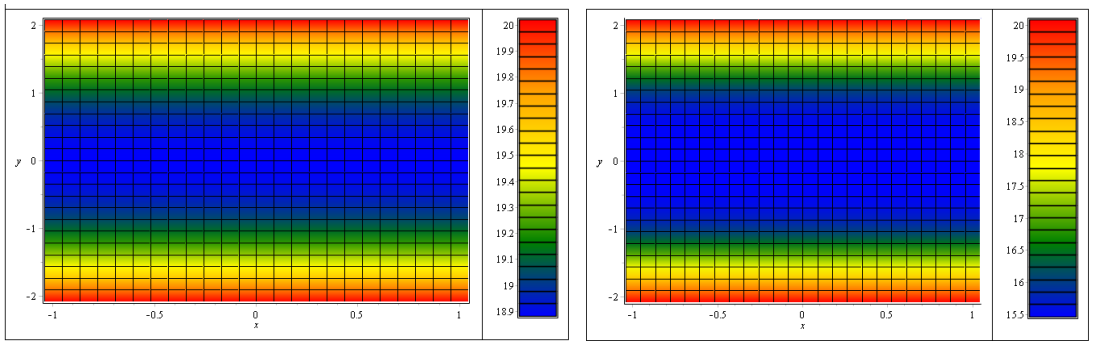

Figure 25: (a) Concentration contours at concentration of 20 mol/m^3 at S=0.5 (b) Concentration contours at concentration of 20 mol/m^3 at S=-7.5

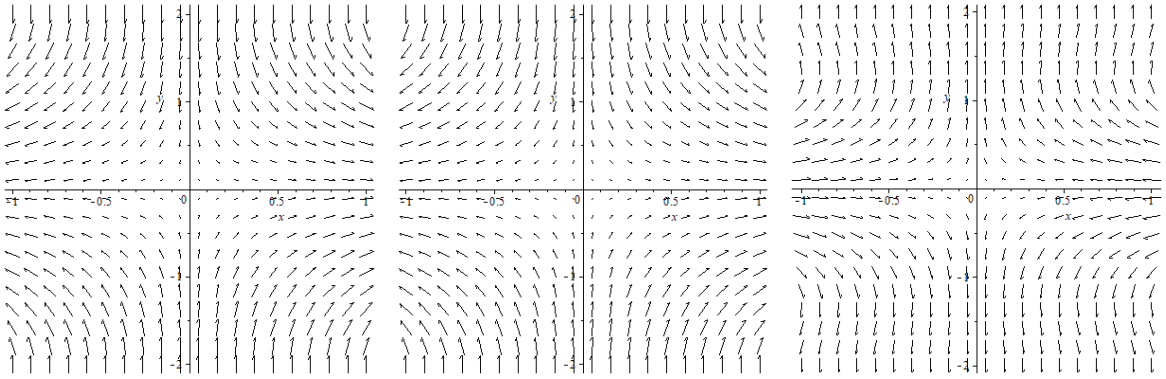

Figure 26: (a) Velocity field/streamlines at S = 0.5 (b) Velocity field/streamlines at S = 3.5 (c) Velocity field/streamlines at S = -7.5

4.1.3 Effect of Hartmann Number (Ha):

Impact of Hartmann Number on flow, temperature and concentration fields are shown in Figure 27 to Figure 30. Ha signifies the ratio of electromagnetic force to viscous force. So, with increasing Hartmann number, the slope of the normal velocity is flattened out, but the effect is not significant as shown in Figure 27. However, the increasing Ha Number is significant on axial

velocity as depicted in Figure 28. This is due to force generated by electromagnetic force in perpendicular direction or axial direction due to Lorentz Effect. Subsequently, the axial velocity has a direct relationship with Ha at η>0.45 and inverse relation with Ha when η<0.45. But Ha has no effect on axial velocities at η=0.45

The effect of Ha number on temperature field is illustrated in Figure 29 and it signifies that temperature field θ increases with increasing Hartmann Number due to increasing electromagnetic forces which dissipates more energy and heat to the fluid.

Similarly, the effect of Ha on concentration field ϕ is depicted in Figure 30, however, the Hartmann number holds inverse relationship with Concentration field and concentration effect reduces with increasing Hartmann number.

The dimensionless values $\eta, f(\eta), \theta(\eta)$ and $\phi(\eta)$ are converted back to the velocities, temperature and concentration using the equation (2.8) to understand the behavior of flow field, temperature and concentration contours. By observing the Figure 27 to Figure 33, it is clear that trends of the graph of dimensionless parameters and contours of physical parameters are the same. In Figure 31, the temperature contours are plotted using MAPLE at Ha=0.5 and Ha=3.5. Also, the temperature at the plates wall is taken to be 130 deg Celsius and distance between plates L is taken.

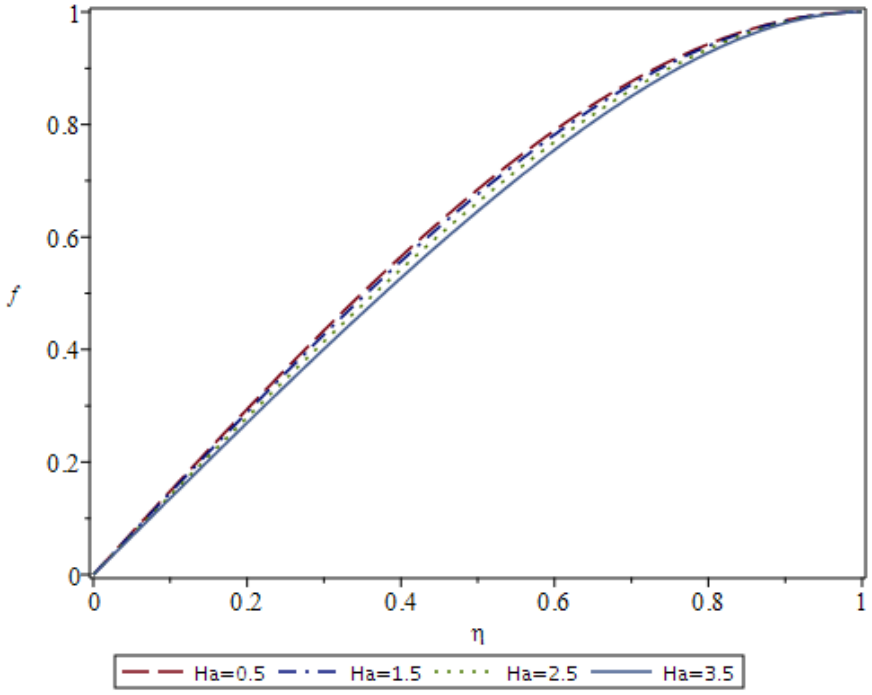

Figure 27: Effect of Ha on $f(\eta)$ at S=R=Q=Ec=Kr=0.1, Du=Sr=0.5, Pr=Sc=0.7, δ=0.5, β=2.0

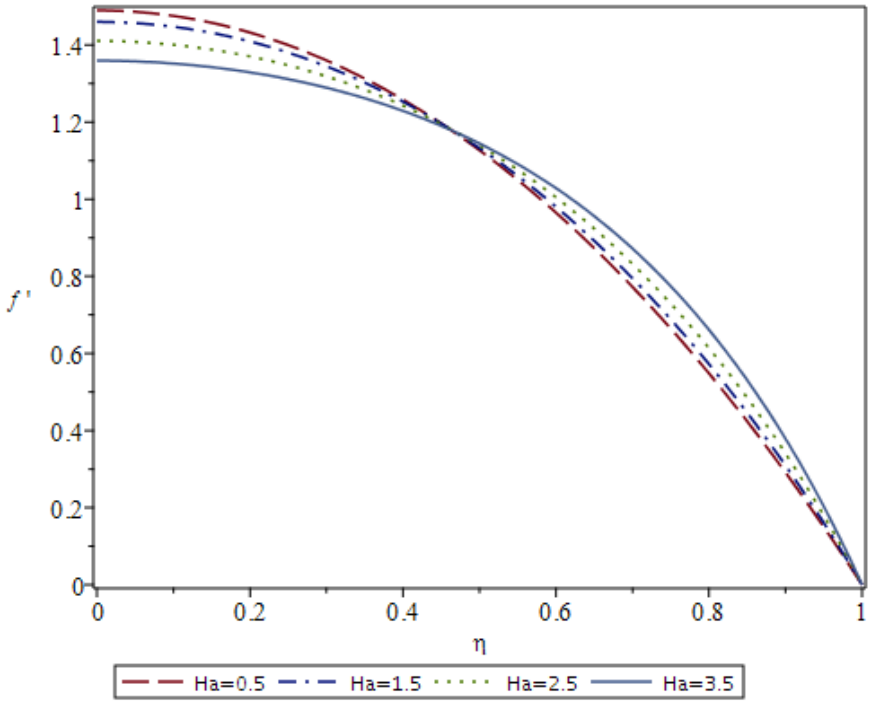

Figure 28: Effect of Ha on $f'(\eta)$ at S=R=Q=Ec=Kr=0.1, Du=Sr=0.5, Pr=Sc=0.7, δ=0.5, β=2.0

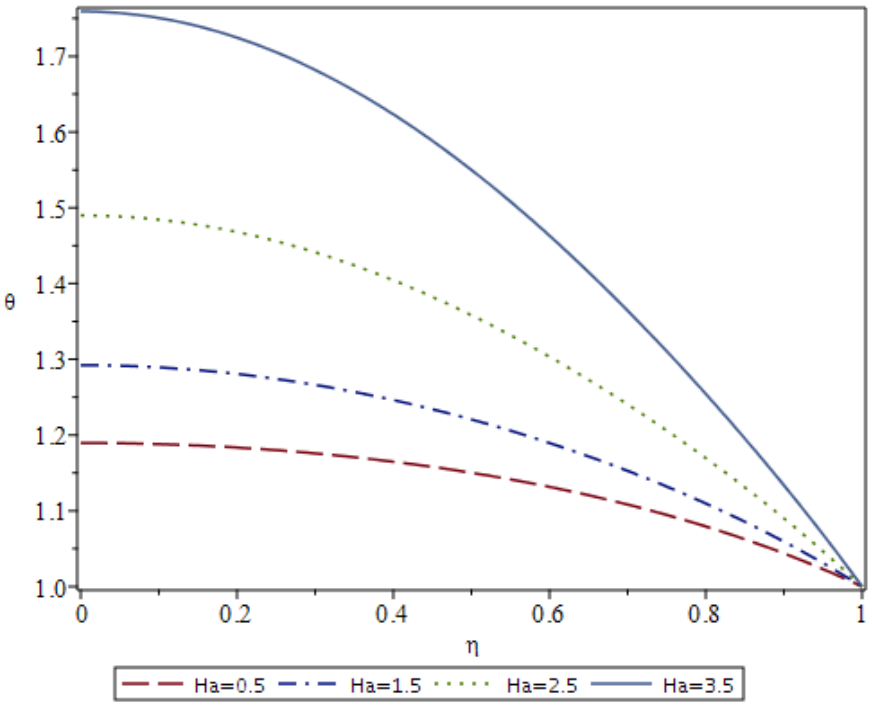

Figure 29: Effect of Ha on $\theta(\eta)$ at S=R=Q=Ec=Kr=0.1, Du=Sr=0.5, Pr=Sc=0.7, δ=0.5, β=2.0

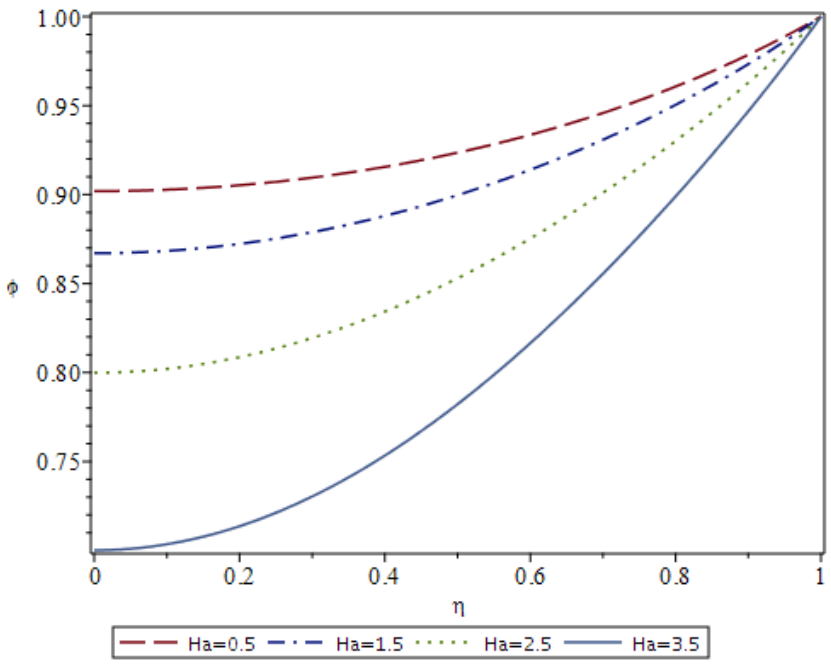

Figure 30: Effect of Ha on $\phi\ (\eta)$ at S=R=Q=Ec=Kr=0.1, Du=Sr=0.5, Pr=Sc=0.7, δ=0.5, β=2.0

to be 4m. The positive gradient is observed for both cases as approached to the center of fluid and also, at higher value of Ha the gradient and overall value of temperature of fluid is increasing. In Figure 32, the concentration contours are plotted using MAPLE at Ha=0.5 and Ha=3.5. Also, the concentration at the plates wall is taken to be 20 mol/m^3. The negative gradient is observed for both cases as approached to the center of fluid and also, at higher value of Ha, the overall value of concentration of fluid is decreasing. Further, velocity field can be plotted by combining the values of $f(\eta)$ and $f'(\eta)$ as mentioned in Figure 33. In this case, variation in the Hartmann number makes insignificant difference in velocity field.

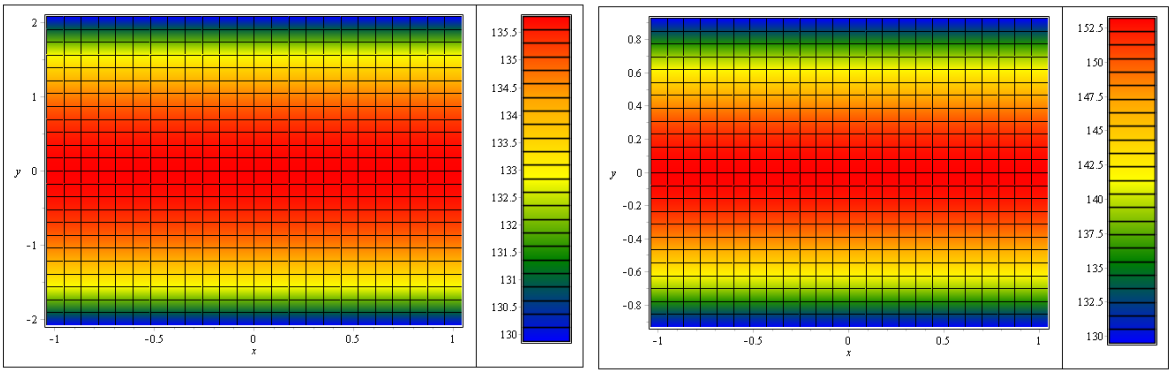

Figure 31: (a) Temperature contours at wall temperature of 130 deg C at Ha= 0.5 (b) Temperature contours at wall temperature of 130 deg C at Ha = 3.5

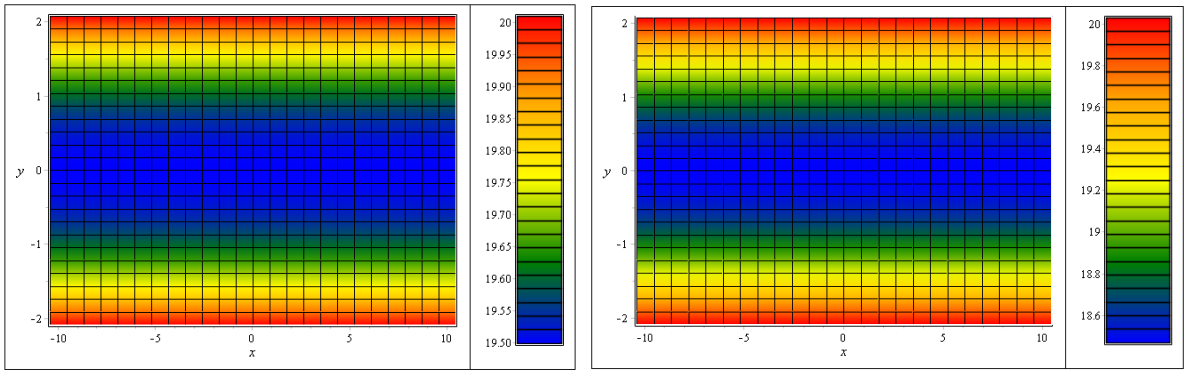

Figure 32: (a) Concentration contours at concentration of 20 mol/m^3 at Ha=0.5 (b) Concentration contours at concentration of 20 mol/m^3 at Ha=3.5

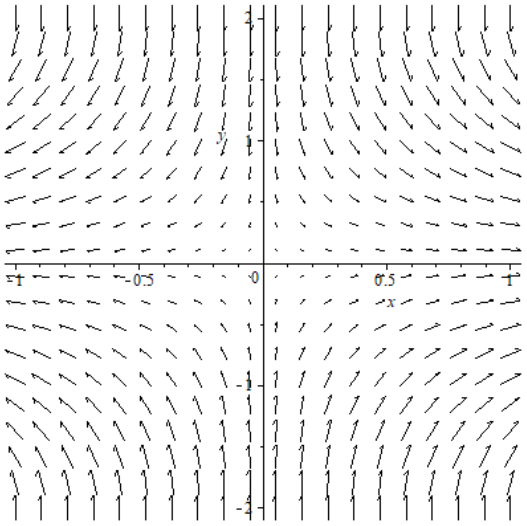

Figure 33: (a) Velocity field/streamlines at Ha = 0.5

4.1.4 Effect of Radiation Parameter (R):

This section shows the effect of radiation parameter on flow temperature and concentration and same is illustrated in Figure 34 to Figure 35. The radiation parameter R specifies the effect of conduction heat transfer to thermal radiation transfer. The radiation parameter has no effect on velocity profiles of flow field. However, the temperature field decreases with increase of radiation parameters. This is because higher radiation parameter implies reduced conduction effect, and less heat is transferred to center of the fluid and same is illustrated in Figure 34. Subsequently, there is reduced mass transfer at higher radiation parameter which is clearly portrayed in Figure 35. This reduction is produced by the overall low temperature of fluid at higher radiation parameter.

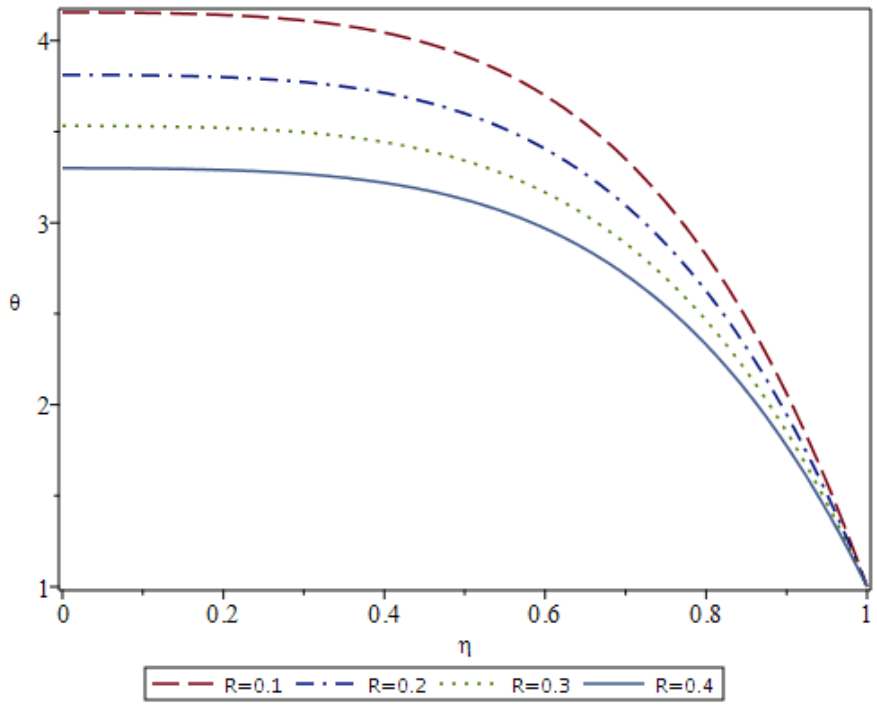

Figure 34: Influence of R on $\theta(\eta)$ at S=0.1, Du=Sr=0.5, R=Q=Ec=Kr=0.1, Sc=Pr=0.7, δ=0.5, β=2.0

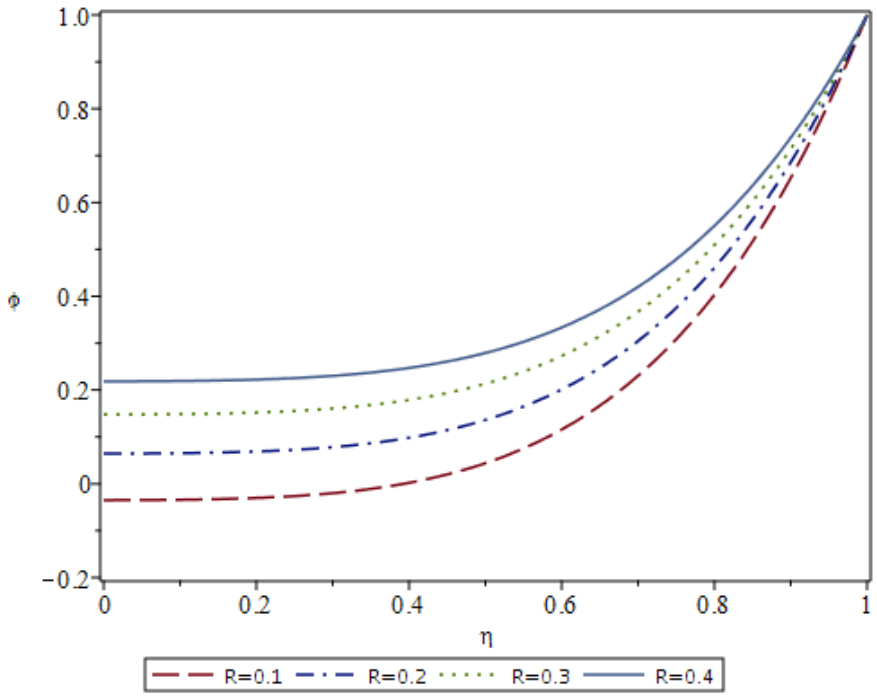

Figure 35: Influence of R on $\theta(\eta)$ at S=0.1, Du=Sr=0.5, R=Q=Ec=Kr=0.1, Sc=Pr=0.7, δ=0.5, β=2.0

4.1.5 Effect of heat Source/Sink parameter (Q):

The influence of heat generation or absorption parameter Q on flow behavior is illustrated in Figure 36 and Figure 37. Since, positive value of Q indicates the heat generation in the system while negative value represents heat absorption. Hence, the temperature profiles hold a direct relation with heat source/sink parameter and the temperature increases with increase in heat source/sink parameter because during heat generation the fluid has higher temperature and vice versa. Same behavior is clearly indicated in Figure 36. Consequently, the concentration field has inverse effect of change in source/sink parameter and the heat generation $Q>0$ in fluid decreases the concentration field and heat absorption $Q<0$ in fluid increases the concentration field and this effect is illustrated in Figure 37. While Q has no effect on velocity field of flow.

4.1.6 Impact of Prandtl Number (Pr):

The effect of Prandtl Number on temperature and concentration field is discussed in this section and same is shown in Figure 38 and Figure 39. Since, Prandtl number signifies the momentum diffusivity over thermal diffusivity and the higher Prandtl number indicates less effective heat conduction or smaller thermal boundary layer that is why the thermal gradient increases with increasing Prandtl number as illustrated in Figure 38. However, the concentration field reduces with an increase in the Prandtl number emphasizing the inverse relation among them that is highlighted in Figure 39. The overall temperature reduction is the cause of this reduced concentration field. While the Prandtl number has no significant effect on velocity field of flow.

4.1.7 Effect of Eckert Number (Ec):

This section underlines the effect of Eckert number on thermodynamics and concentration of flow field that is portrayed in Figure 40 and Figure 41 respectively. Eckert number is used to characterize the heat dissipation in flow field. A higher Eckert number means lower heat dissipation and higher temperature gradient. Figure 40 is pointing out the same behavior in which temperature profile increases with increase in Eckert number. Subsequently, the concentration field is declining with increasing Eckert number due to overall reduction in temperature of fluid and this behavior is shown in Figure 41.

4.1.8 Impact of Dufour Number (Du):

The effect of Dufour number on flow behavior is discussed in this section and same is illustrated in Figure 42 and Figure 44. Dufour number signifies the effect of concentration gradient

on the thermal influx in fluid and holds inverse relation with thermal influx. So, Dufour number hold inverse relation with heat transfer and therefore, it holds direct relation with temperature profile and temperature gradient and the same behavior is highlighted in Figure 42 where temperature gradient increases with increasing Dufour number. Since thermal flux seems to be varying with Dufour Number, therefore, the concentration field doesn't have significant effect and the concentration field decreases slightly with increase in Du as shown in Figure 44. Furthermore, the velocity field seems to be independent of Du.

4.1.9 Effect of Chemical Reaction Parameter (Kr):

The effect of varying Chemical Reaction Parameter (Kr) on concentration and same is depicted in Figure 43. For Kr>0 or positive value, the increasing value of Kr is enhancing the concentration field. However, the inverse behavior is observed for Kr<0 where concentration field is diminishing with increasing value of Kr. This highlights that whether the reaction is constructive or destructive, both cases will increase the concentration gradient. Furthermore, Kr doesn't produce considerable effect on temperature and velocity field.

4.1.10 Effect of Schmidt number (Sc):

Impact of Schmidt number (Sc) on flow, concentration fields is shown in Figure 45. Since, Sc represents the ratio of viscous diffusion to mass diffusion rate and hold inverse relation with the mass diffusion rate, therefore, the growing Schmidt number will decrease the concentration of the fluid cause by reduced mass diffusion rate. Further, it is pertinent to note that the field is a monotonically diminishing function of Sc.

4.1.11 Effect of Soret Number (Sr):

The effect of Soret number (Sr) on flow behavior is discussed in this section and same is illustrated in Figure 46 and Figure 47. Since, Soret Number (Sr) is inverse of Dufour Number (Du), and it implies the effect of temperature gradient on mass flux. The temperature field experiences no considerable effect of varying Sr and increases slightly with increasing of Soret Number as illustrated in Figure 46. Conversely, the concentration field experience significant effect of Soret number and decreases with increasing value of Sr because the Soret Number has inverse relation with mass transfer as mentioned in Figure 47. Furthermore, velocity field is independent of Soret number.

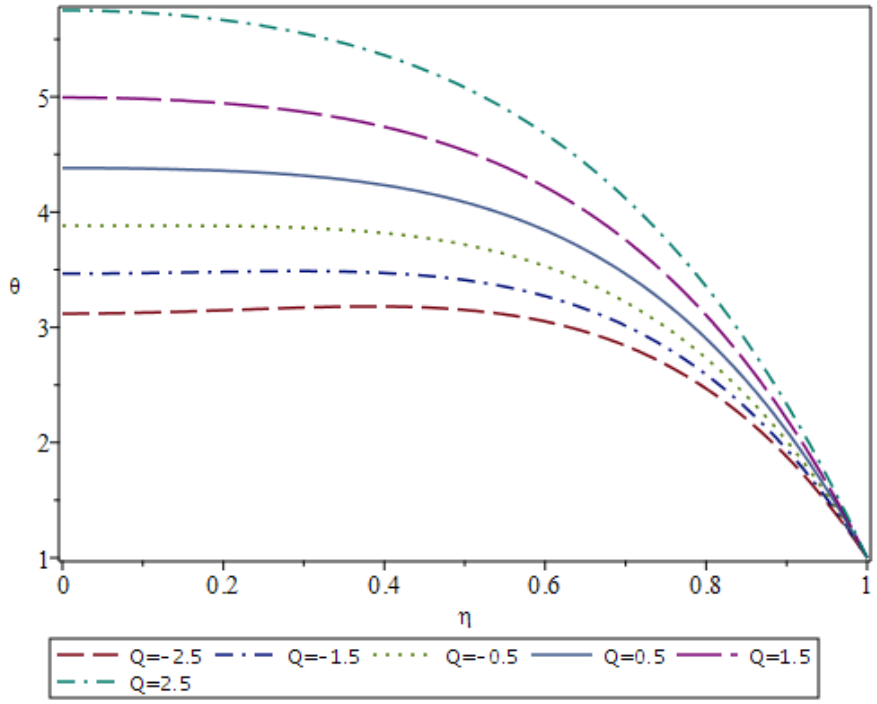

Figure 36: Influence of Q on $\theta(\eta)$ at S=0.4, β=0.2, Du=0.5, Sr=0.5, Ha=0.1, Ec=1.0, Kr=0.1, Pr=0.7, Sc=0.7, δ=0.1, R=0.2

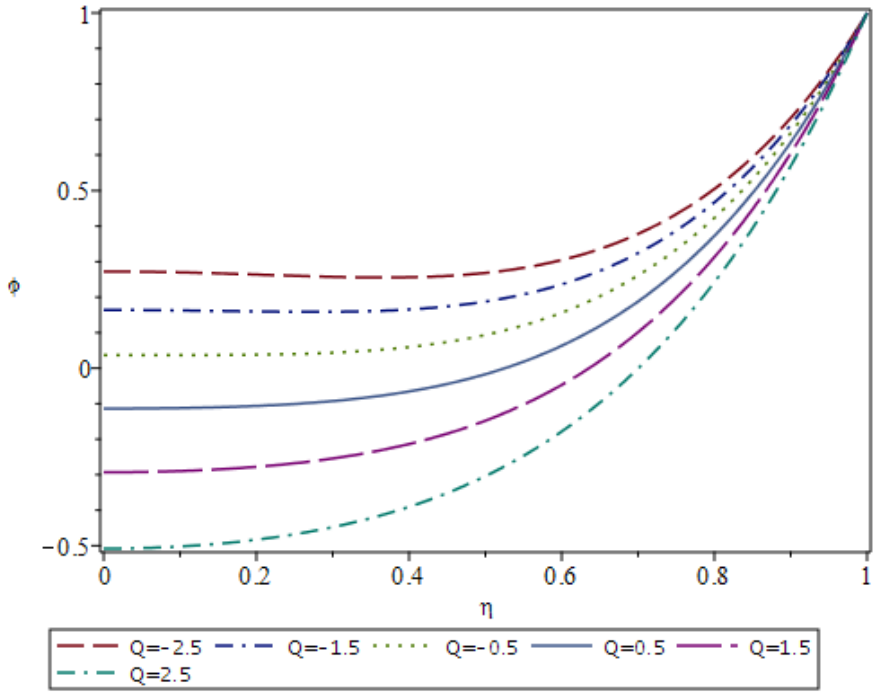

Figure 37: Influence of Q on $\phi(\eta)$ at S=0.4, β=0.2, Du=0.5, Sr=0.5, Ha=0.1, Ec=1.0, Kr=0.1, Pr=0.7, Sc=0.7, δ=0.1, R=0.25

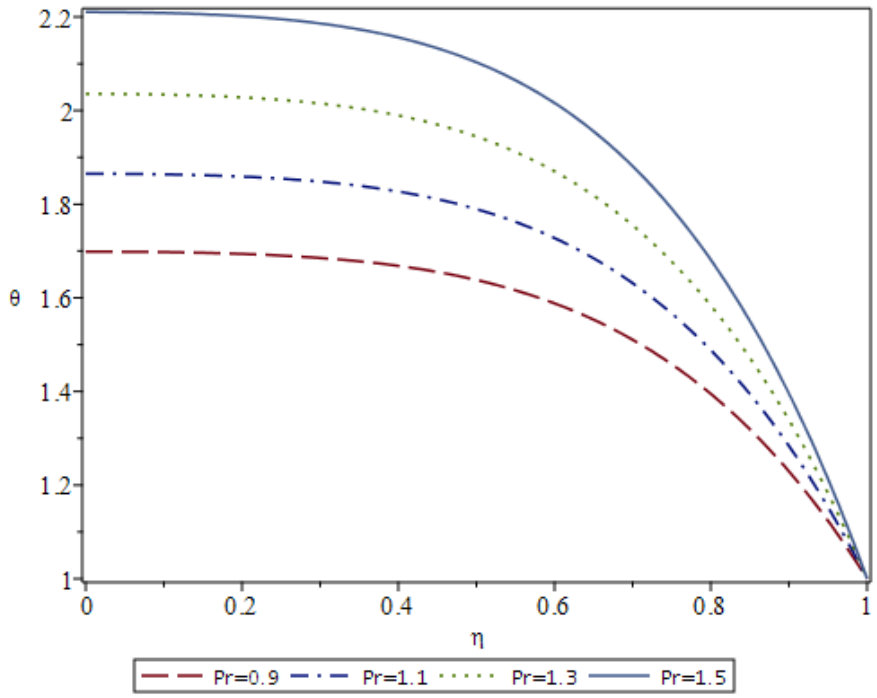

Figure 38: Influence of Pr on $\theta(\eta)$ at S=0.5, β=0.1, Du=0.5, Sr=0.5, Ha=0.5, Q=0.1, Kr=0.1, Sc=0.7, δ=0.1, R=0.1, Ec=0.1

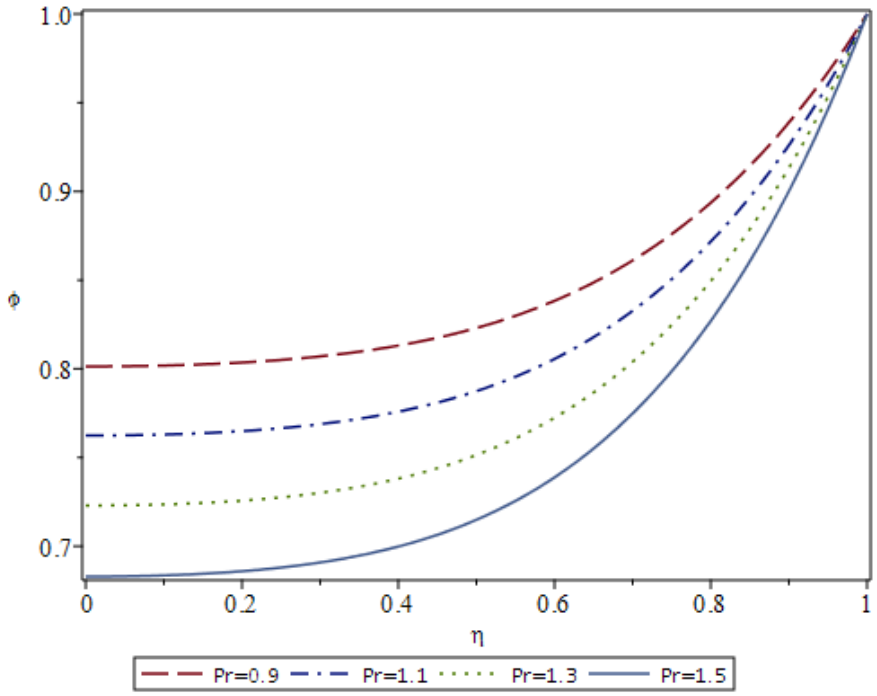

Figure 39: Influence of Pr on $\phi(\eta)$ at S=0.5, β=0.1, Du=0.5, Sr=0.5, Ha=0.5, Q=0.1, Kr=0.1, Sc=0.7, δ=0.1, R=0.1, Ec=0.1

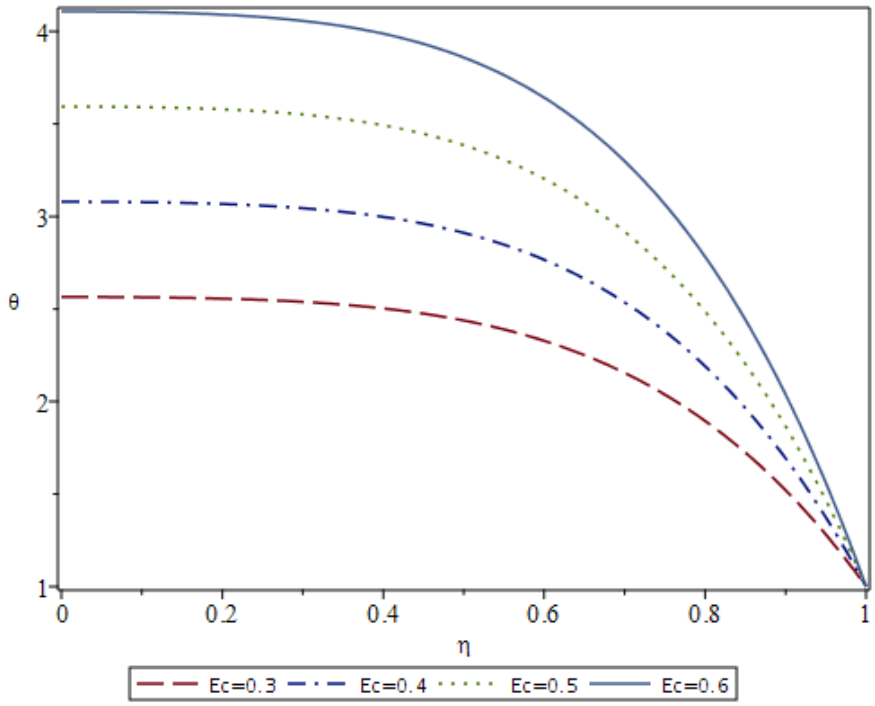

Figure 40: Influence of Ec on $\theta(\eta)$ at S=0.5, β =0.1, Du=0.5, Sr=0.5, Ha=0.5, Q=0.1, Kr=0.1, Pr=0.7, Sc=0.7, δ =0.1, R=0.1

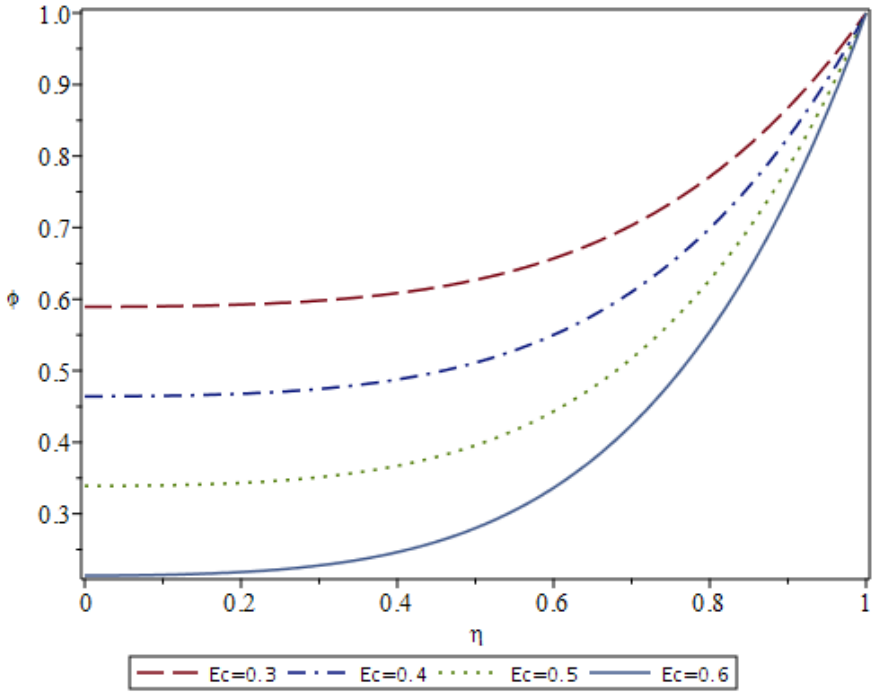

Figure 41: Influence of Ec on $\phi(\eta)$ at S=0.5, β =0.1, Du=0.5, Sr=0.5, Ha=0.5, Q=0.1, Kr=0.1, Pr=0.7, Sc=0.7, δ =0.1, R=0.1

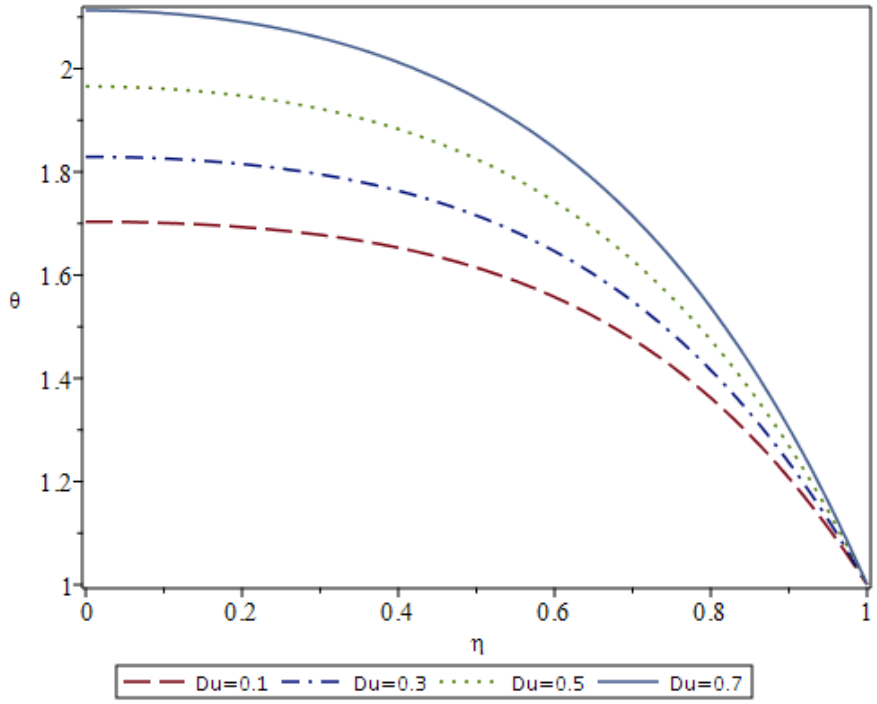

Figure 42: Influence of Du on $\theta(\eta)$ at S=0.4, β=0.2, Sr=0.5, Ha=0.5, Q=0.5, Kr=1.6, Sc=0.7, δ=0.01, R=0.1, Ec=0.1, Pr=1.2

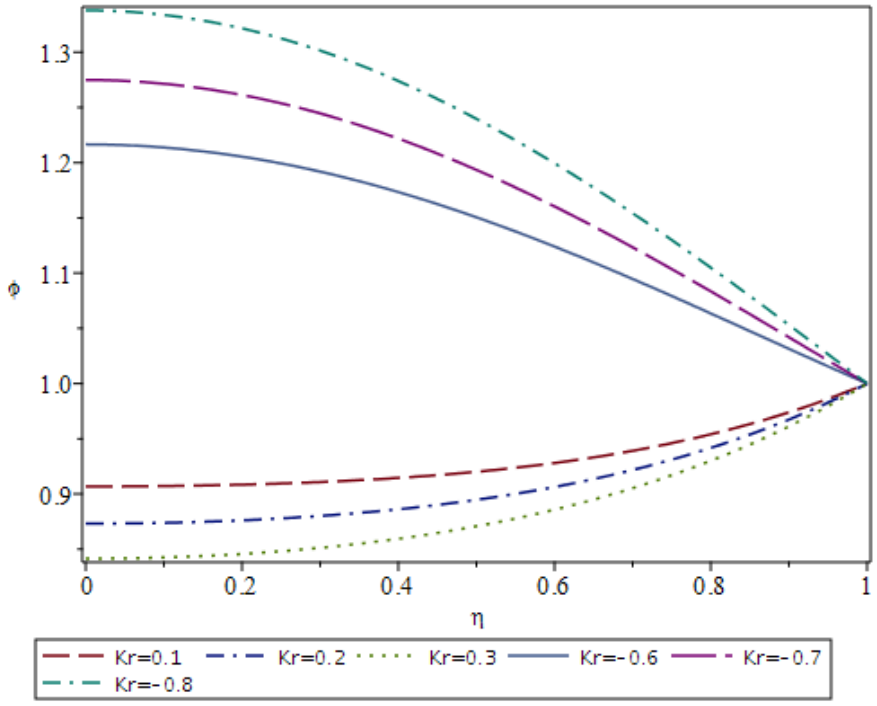

Figure 43: Influence of Kr on $\phi(\eta)$ at S=0.1, β=0.5, Du=0.5, Sr=0.5, Ha=0.1, Q=0.1, Sc=0.7, δ=0.1, R=0.1, Ec=0.1, Pr=0.7

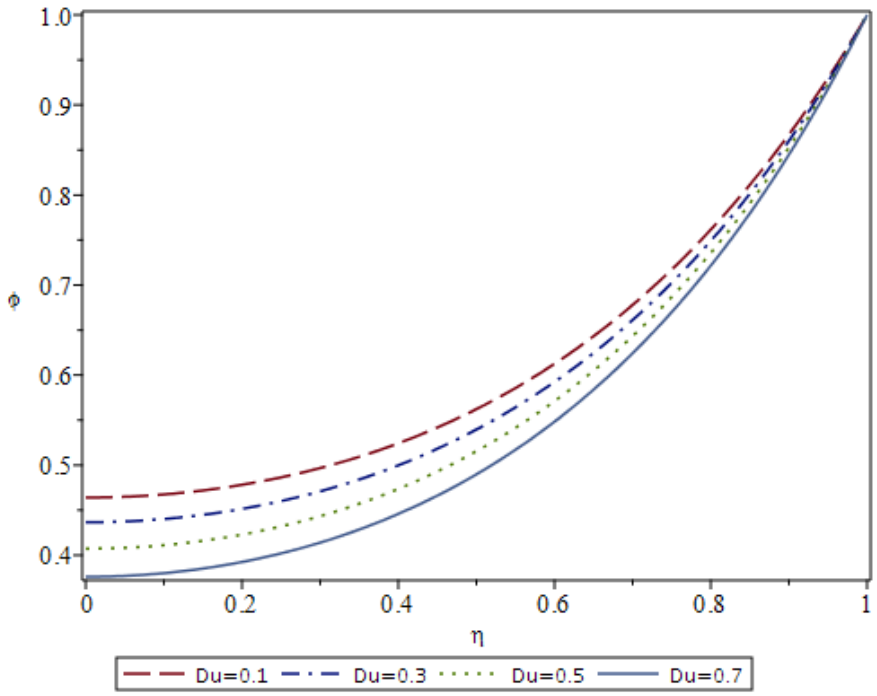

Figure 44: Influence of Du on $\phi(\eta)$ at S=0.4, β=0.2, Sr=0.5, Ha=0.5, Q=0.5, Kr=1.6, Sc=0.7, δ=0.01, R=0.1, Ec=0.1, Pr=1.2

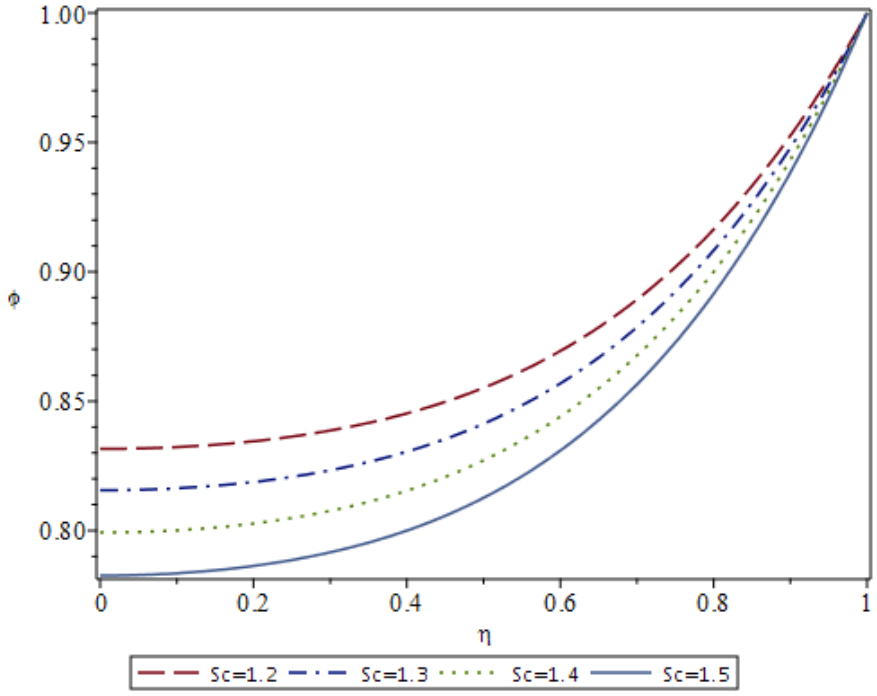

Figure 45: Influence of Sc on $\phi(\eta)$ at S=0.1, β=0.5, Du=0.5, Sr=0.5, Ha=0.1, Q=0.1, Kr=0.1, δ=0.1, R=0.1, Ec=0.1, Pr=0.7

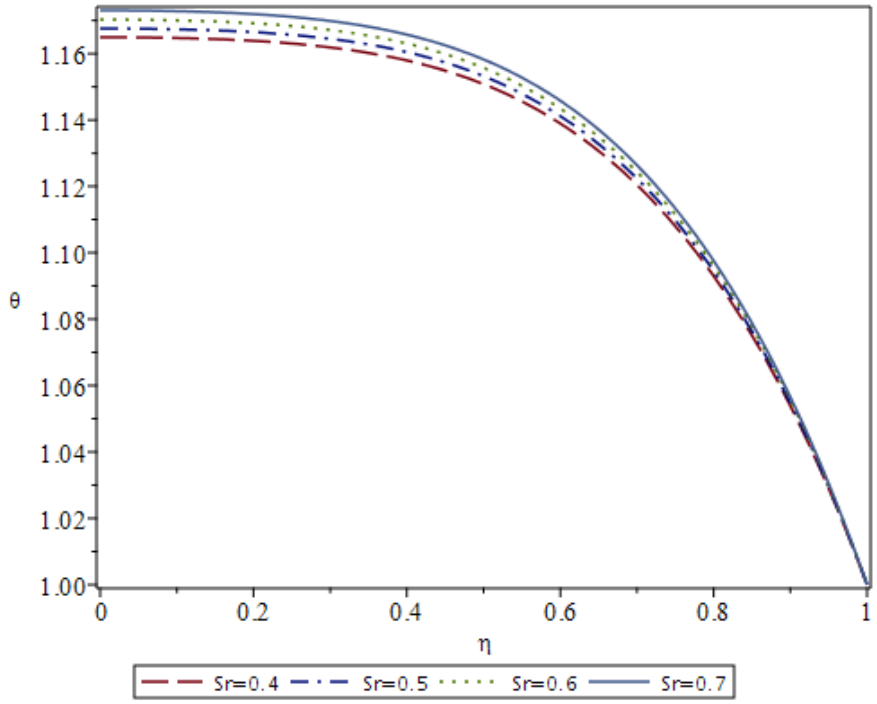

Figure 46: Influence of Sr on $\theta(\eta)$ at S=0.1, β=0.5, Du=0.5, Ha=0.1, Q=0.1, Kr=0.1, Sc=0.5, δ=0.1, R=0.1, Ec=0.1, Pr=0.7

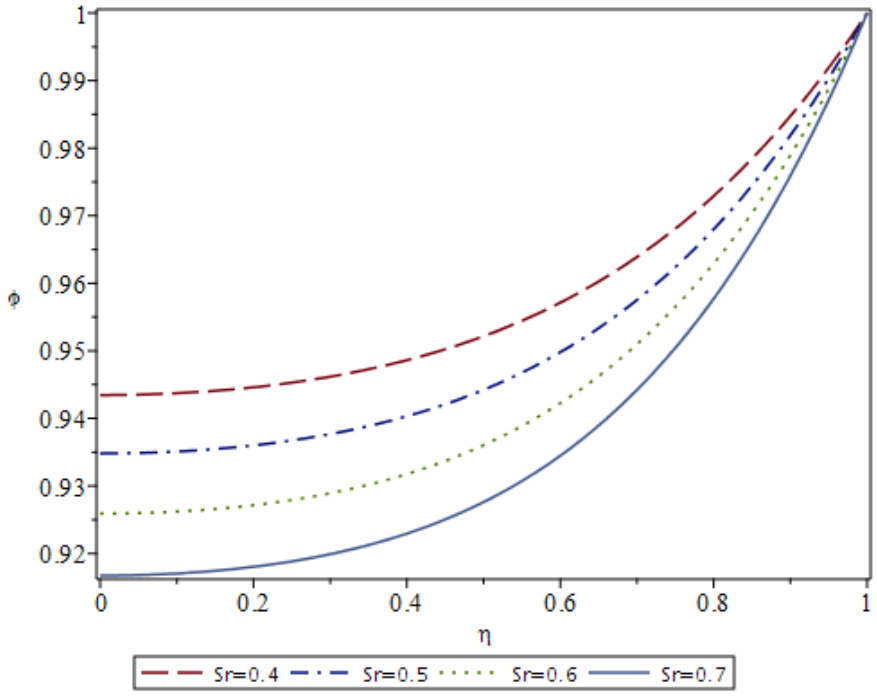

Figure 47: Influence of Sr on $\phi(\eta)$ at S=0.1, β=0.5, Du=0.5, Ha=0.1, Q=0.1, Kr=0.1, Sc=0.5, δ=0.1, R=0.1, Ec=0.1, Pr=0.7

4.2 PHYSICAL AND ENGINEERING ASPECTS:

In engineering sciences, the physical parameters like Skin-friction coefficients, Nusselt and Sherwood numbers are critical for momentum, heat transfer, and mass transfer coefficients. In this section, the behavior of Skin-friction coefficients, Nusselt and Sherwood numbers that are expressed as

$$\begin{aligned} C_f &= \frac{\tau_w}{\rho_f {v_w}^2}\ (Skin\ Friction\ Coefficient), \\ Nu &= \frac{lq_w}{\alpha_f(T_o - T_w)}(Nusselt\ Number), \\ Sh &= \frac{lq_s}{D_m(C_o - C_w)}\ \ (Sherwood\ Number), \end{aligned} \tag{3.1}$$

are evaluated and presented. In above equations τ_w, q_w and q_s are the skin friction, thermal and mass fluxes at surface of parallel plates and can be denoted by:

$$\begin{aligned} \tau_w &= \mu\left(1+\frac{1}{\beta}\right)\left[\frac{\partial u}{\partial y}\right]_{y=h(t)}, \\ q_w &= \alpha_f\left(\frac{\partial T}{\partial y} - \frac{16\sigma^* {T_w}^2}{3k^*}\frac{\partial T}{\partial y}\right)_{y=h(t)}, \\ q_s &= D_m\left(\frac{\partial C}{\partial y}\right)_{y=h(t)} \end{aligned} \tag{3.2}$$

Moreover, these physical parameters are converted to dimensionless form in order to incorporate them into the analytical solution and understand their behavior for the given application. In non-dimensionless form, these parameters can be expressed as:

$$\begin{aligned} \frac{l^2}{x^2(1-\alpha t)} Re_x C_f &= \left(1+\frac{1}{\beta}\right) f''(1), \\ \sqrt{(1-\alpha t)}\, Nu &= -\left(1+\frac{4}{3}R\right)\theta'(1), \\ \sqrt{(1-\alpha t)}\, Sh &= -\phi'(1) \end{aligned} \tag{3.3}$$

The effect of control parameters on $f''(1)$, $\theta'(1)$ and $\phi'(1)$ are illustrated in Figure 48 to Figure 50.In Figure 48,the effect of Squeezing number on momentum transport coefficient is shown in which it can be observed that $f''(1)$ increases with increase in S for S>0 resulting in reduction of momentum transport and this momentum transport is increasing for S<0. Figure 49 highlights the effect of Hartmann number Ha on momentum transport which shows that for Ha>0,

the momentum transport decreases, and this behavior is reversed for Ha<0. Similarly, the Casson fluid parameter β increase the momentum transport by reducing $f''(1)$ as shown in Figure 50. This reduction is accelerated for β<4 and decay gradually as β increases.

Figure 51 shows the heat transfer coefficient behavior by varying Dufour number Du and it is observed that Du increases the heat transfer coefficient. Similarly, the squeezing number S also increases the heat transfer coefficient as illustrated in Figure 52. However, the radiation parameter R decreases the heat transfer coefficient which is depicted in Figure 53. Furthermore, Figure 54 shows the behavior of increasing heat transfer in presence of heat source (Q>0) and decreases in presence of heat sink (Q<0).

Mass transfer coefficient holds direct relation with squeezing number, Chemical reaction parameter which can be observed in Figure 55, Figure 56 and Figure 57 respectively. But Mass transfer coefficient is decreasing with increasing Soret Number as depicted in Figure 56.

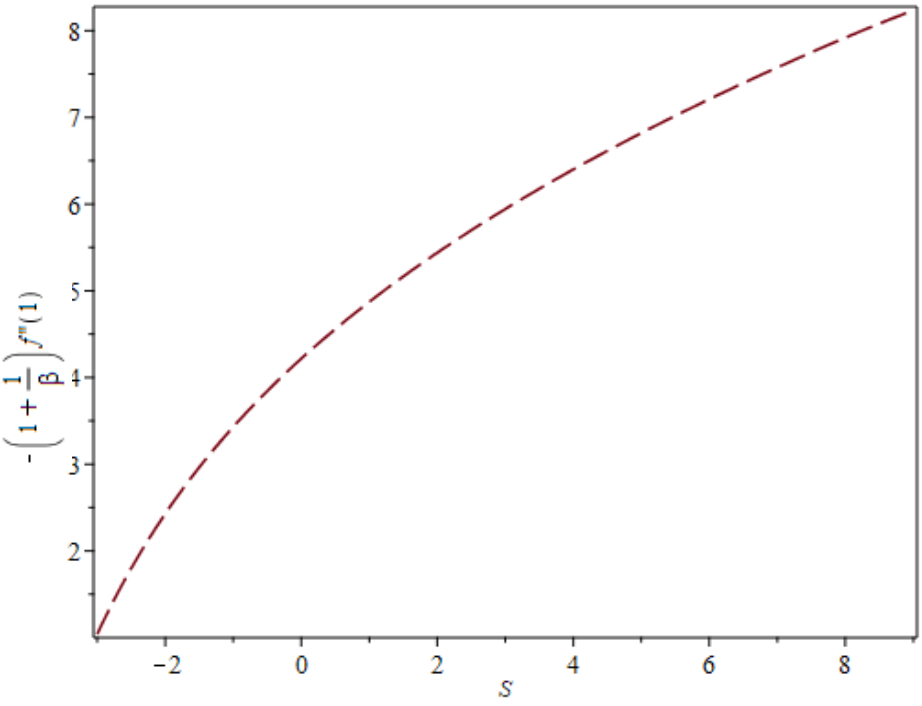

Figure 48: Effect of S on Momentum Transport Coefficient at β=2.5, Du=0.5, Sr=0.5, Ha=0.3, Q=0.2, Kr=0.2, Sc=0.7, δ=0.5, R=0.2, Ec=0.2, Pr=0.7

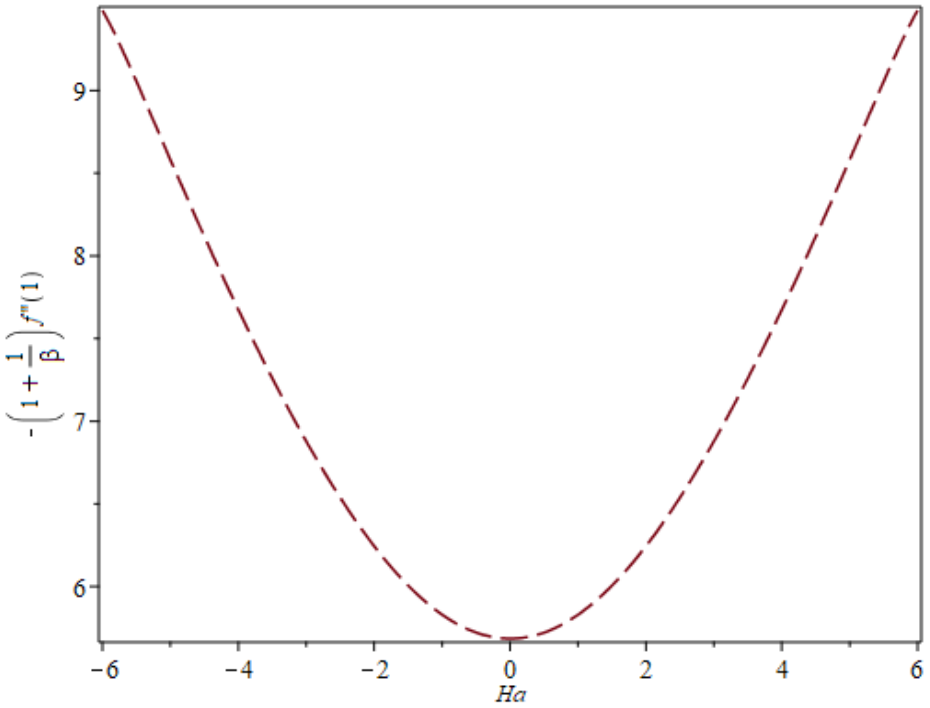

Figure 49: Effect of Ha on Momentum Transport Coefficient at β=2.5, Du=0.5, Sr=0.5, S=2.5, Q=0.2, Kr=0.2, Sc=0.7, δ=0.5, R=0.2, Ec=0.2, Pr=0.7

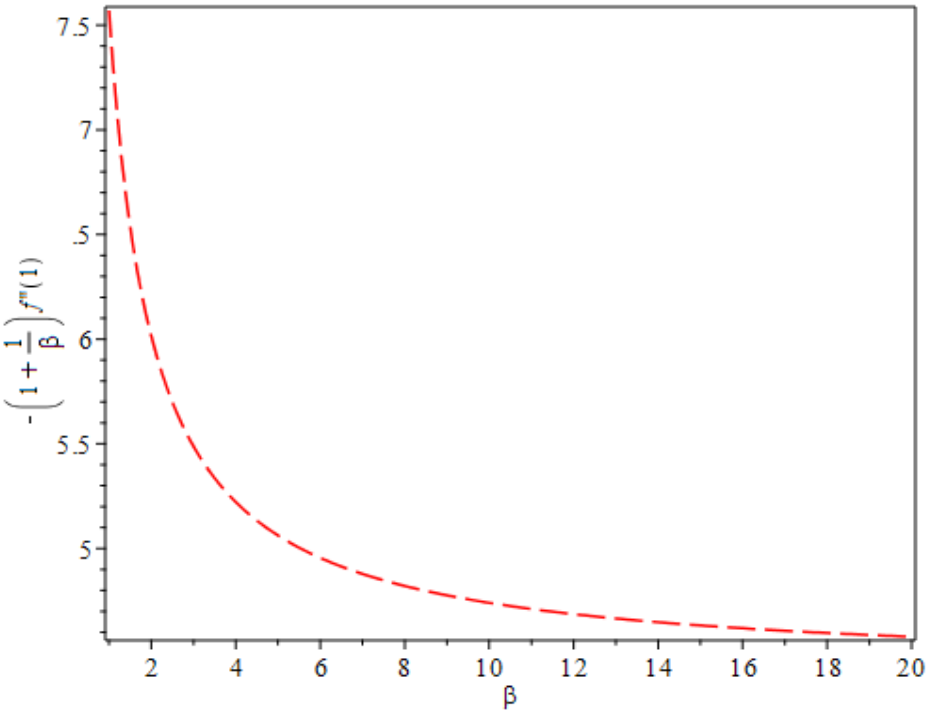

Figure 50: Effect of β on Momentum Transport Coefficient at β=2.5, Du=0.5, Sr=0.5, Ha=0.3, Q=0.2, Kr=0.2, Sc=0.7, δ=0.5, R=0.2, Ec=0.2, Pr=0.7

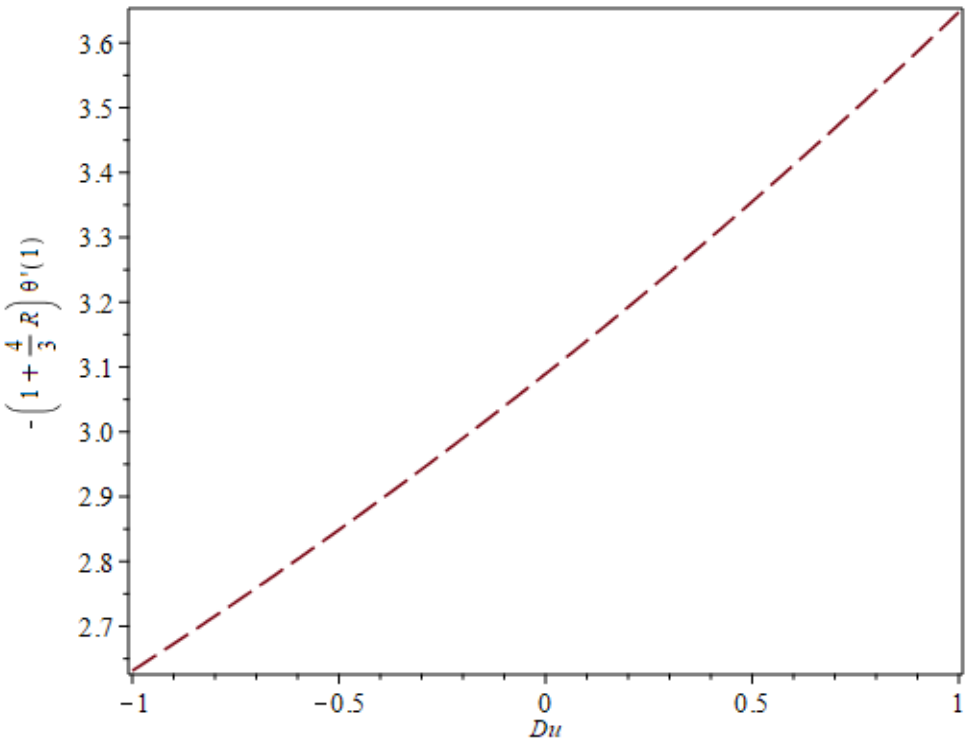

Figure 51: Effect of Du on Heat Transfer Coefficient at S=2.5, β=0.5, Sr=0.5, Ha=1.5, Q=0.6, Kr=0.2, δ=0.1, R=0.6, Ec=0.2, Pr=0.7, Sc=0.7

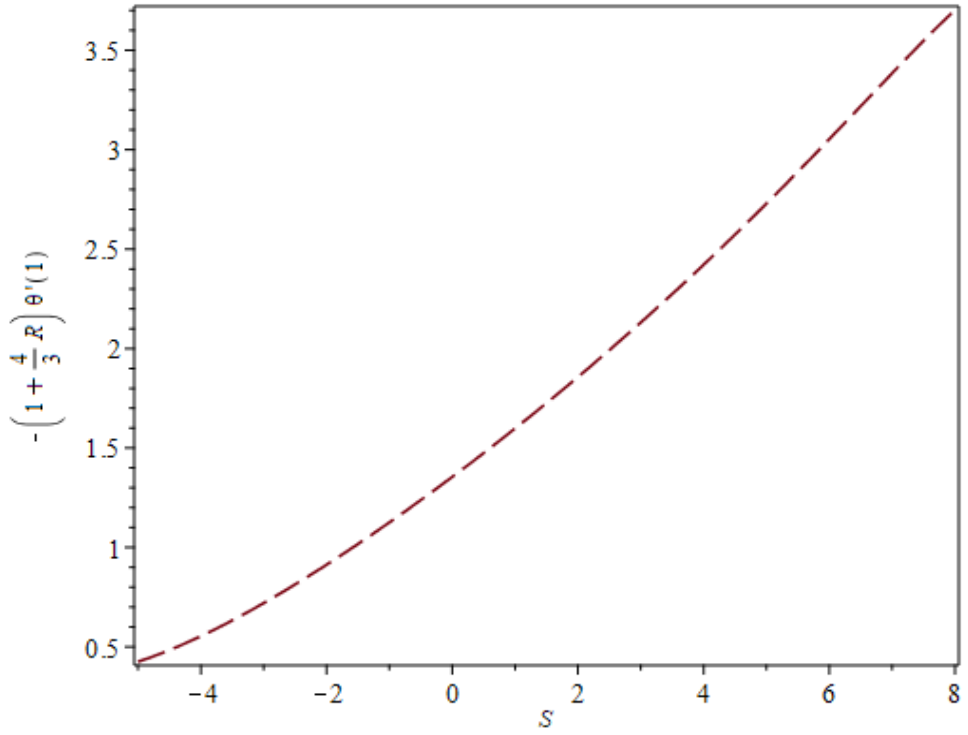

Figure 52: Effect of S on Heat Transfer Coefficient at Du=0.2, β=0.5, Sr=0.5, Ha=1.5, Q=0.3, Kr=0.2, δ=0.1, R=0.6, Ec=0.2, Pr=0.7, Sc=0.7

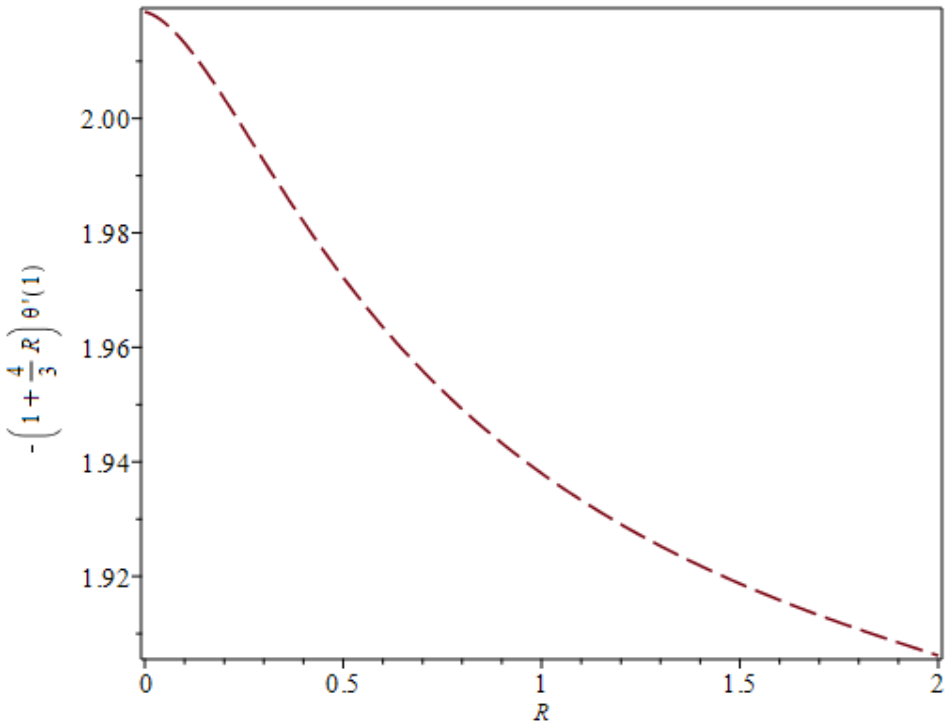

Figure 53: Effect of R on Heat Transfer Coefficient at S=2.5, β=0.5, Sr=0.5, Ha=1.5, Q=0.3, Kr=0.2, δ=0.1, Du=0.2, Ec=0.2, Pr=0.7, Sc=0.7

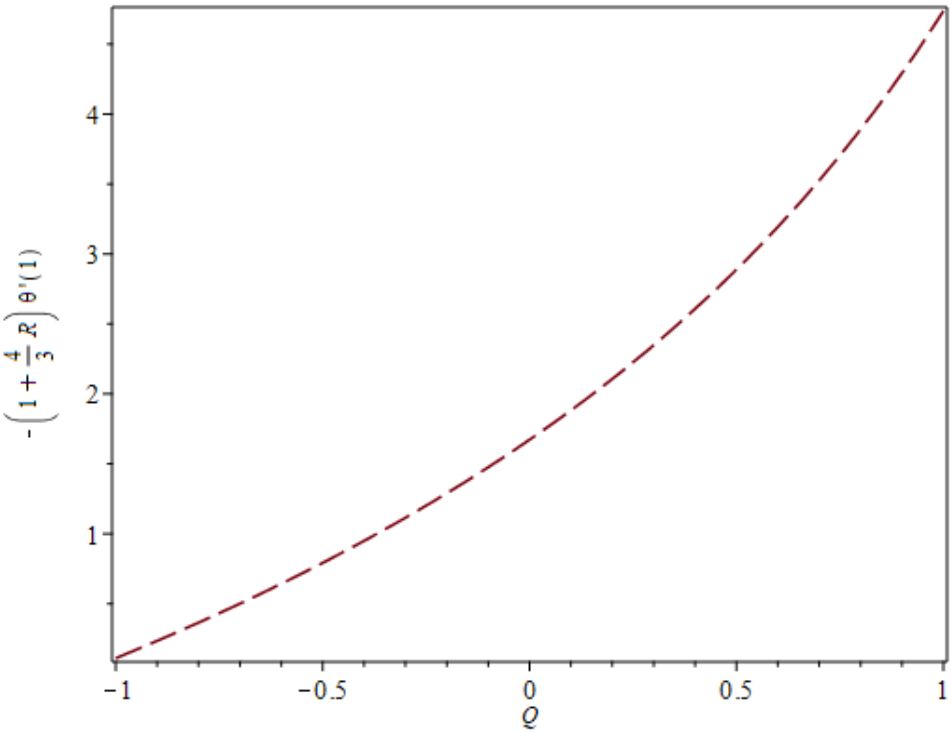

Figure 54: Effect of Q on Heat Transfer Coefficient at Du=0.2, β=0.5, Sr=0.5, Ha=1.5, S=2.5, Kr=0.2, δ=0.1, R=0.6, Ec=0.2, Pr=0.7, Sc=0.7

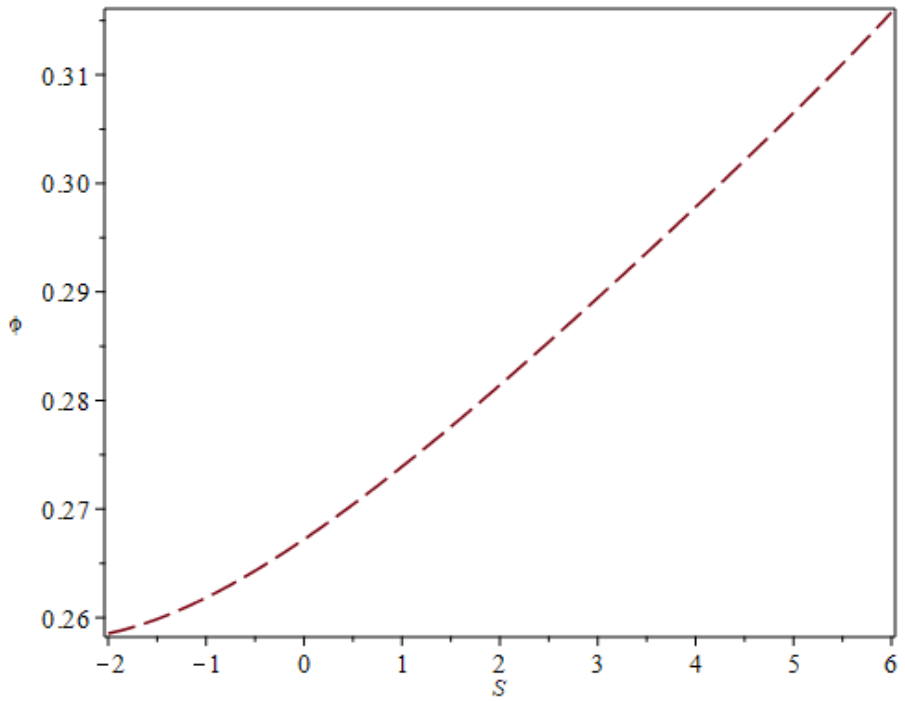

Figure 55: Effect of S on Mass Transfer Coefficient at Du=0.5, β=0.5, Sr=0.2, Ha=0.5, Kr=0.1, Sr=0.2, δ=0.5, R=0.2, Ec=0.2, Pr=0.7, Sc=0.7

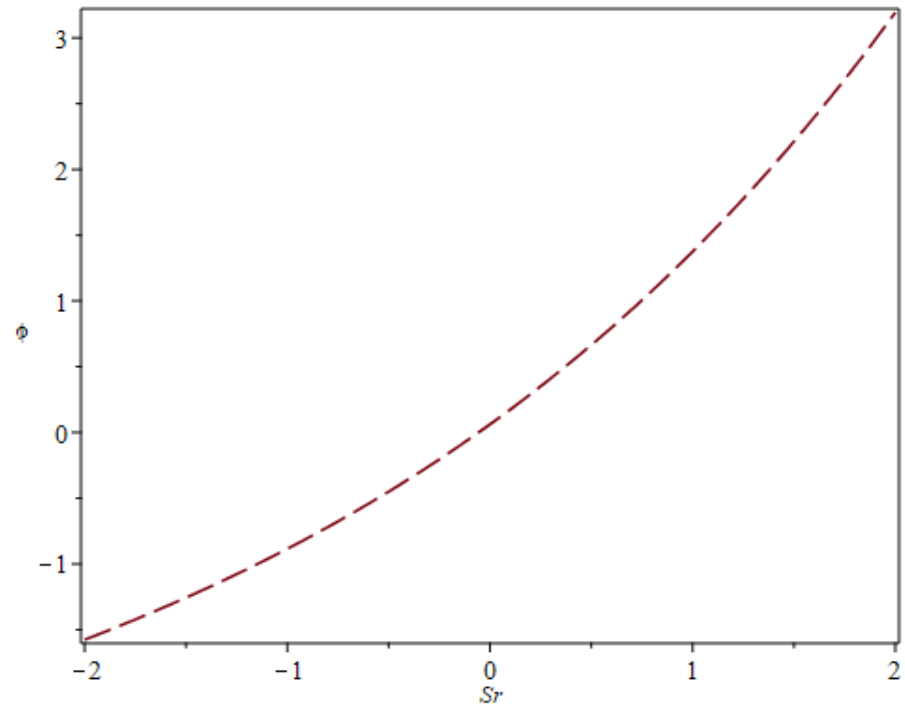

Figure 56: Effect of Sr on Mass Transfer Coefficient at Du=0.5, β=0.5, Sr=0.2, Ha=0.5, S=2.5, Kr=0.1, δ=0.5, R=0.2, Ec=0.2, Pr=0.7, Sc=0.7

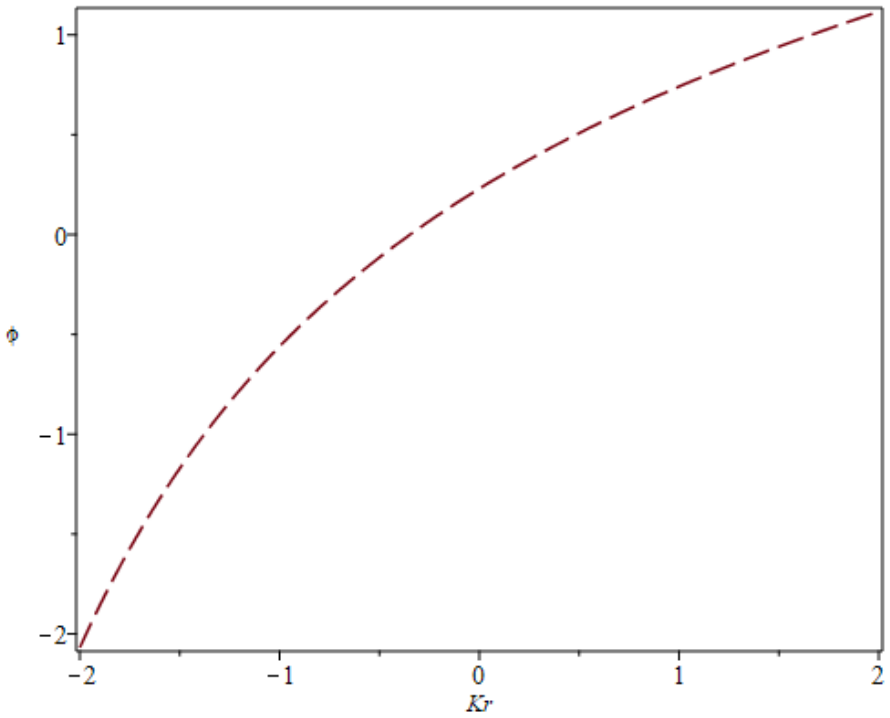

Figure 57: Effect of Kr on Mass Transfer Coefficient at Du=0.5, β=0.5, Sr=0.2, Ha=0.5, S=2.5, Sr=0.2, δ=0.5, R=0.2, Ec=0.2, Pr=0.7, Sc=0.7

CHAPTER 4: CONCLUSION

The behavior of Casson fluid between two parallel plates moving in transverse direction under the influence of electromagnetic, radiation and chemical reaction is investigated. The governing equation for Casson fluid is solved for given boundary conditions using similarity transformations, analytic (HAM) and approximate (FDM) solutions schemes. MAPLE is employed to deduce these solutions. Subsequently, these solutions are found in agreement with each other and with the existing results of Shooting method and bvp4c method.

HAM is shown to provide better results as compared to those deduced using shooting method, bvp4c and FDM not only in terms of accuracy indeed it performs better with regards to computational time and cost. All the findings of this work based upon the variation in the physical parameters $Ha, Kr, S, \delta, Ec, Q, R, Pr, Sc, \beta, Du$ and Sr are summarized in the following table.

Table 6: Effect of Flow Parameters on Velocities, Temperature and Concentration

S. No.	Parameter	Action	Axial velocity	Normal Velocity	Temperature	Concentration
1	Casson Fluid Parameter	Increasing	Increasing slightly above eta =0.4	Slope increasing slightly	decreasing	Increasing
2	Positive Squeezing Number	Increasing	No significant change	No significant change	Slightly decreasing	Slightly increasing
3	Negative Squeezing Number	decreasing to -∞	Reversing and increasing above eta =0.4	Slope is increasing	Increasing	decreasing
4	Hartmann Number	Increasing	Decreasing slightly above eta =0.4	Slope is decreasing slightly	Increasing	decreasing

5	Radiation parameter	Increasing	No change	No change	Decreasing	Increasing
6	Heat Source/sink Parameter	Increasing	No change	No change	Increasing	Decreasing
7	Prandtl Number	Increasing	No change	No change	Increasing	Decreasing
8	Eckert Number	Increasing	No change	No change	Increasing	Decreasing
9	Dufour Number	Increasing	No change	No change	Increasing	Decreasing slightly
10	Chemical reaction parameter	Increasing	No change	No change	-	Decrease
11	Schmidt Number	Increasing	No Change	No Change	-	Decreasing
12	Soret Number	Increasing	No Change	No Change	Increasing slightly	Decreasing

APPENDIX A: PROGRAMMING CODE

Programming of HAM on MAPLE:

```
>restart: with
(PDEtools):declare(f(eta),theta(eta),phi(eta));Du:=0.5;Sr:=0.5;R
:=0.2;Ec:=0.2;Kr:=0.2;Pr:=0.7;Sc:=0.7;delta:=0.5;h[1]:=-
0.6;h[2]:=-0.6;h[3]:=-0.6;Q:=0.2;

> for m from 1 to 15 do eq[m]:=(1+1/beta)*diff(f[m-
1](eta),eta,eta,eta,eta)-S*(eta*diff(f[m-
1](eta),eta,eta,eta)+3*diff(f[m-1](eta),eta,eta))-
sum(S*(diff(f[m-1-k](eta),eta)*diff(f[k](eta),eta,eta)-f[m-1-
k](eta)*diff(f[k](eta),eta,eta,eta)),k=0..m-1)-Ha^2*diff(f[m-
1](eta),eta,eta) end do:

> for m from 1 to 15 do eqt[m]:=(1+4/3*R)*diff(theta[m-
1](eta),eta,eta)+Pr*S*(-eta*diff(theta[m-1](eta),eta)+Q*theta[m-
1](eta))+Du*Pr*diff(phi[m-1](eta),eta,eta)+sum(Pr*S*f[m-1-
k](eta)*diff(theta[k](eta),eta)+Pr*Ec*((1+1/beta)*(diff(f[m-1-
k](eta),eta,eta)*diff(f[k](eta),eta,eta)+4*delta^2*diff(f[m-1-
k](eta),eta)*diff(f[k](eta),eta))+Ha^2*diff(f[m-1-
k](eta),eta)*diff(f[k](eta),eta)),k=0..m-1) end do:

> for m from 1 to 15 do eqp[m]: =diff(phi[m-1](eta),eta, eta)-
Sc*S*eta*diff(phi[m-1] (eta),eta)-Sc*Kr*phi[m-
1](eta)+Sr*Sc*diff(theta[m-1](eta),eta,eta)+sum(Sc*S*f[m-1-
k](eta)*diff(phi[k](eta),eta),k=0..m-1) end do:

> f[0](eta):=0.5*(3*eta-eta^3);theta[0](eta):=1;phi[0](eta):=1;
sys[1]:=h[1]*(int(int(int(int(eq[1],eta),eta),eta),eta))+C[1][1]
+C[2][1]*eta+C[3][1]*eta^(2)+C[4][1]*eta^(3);
f[0](eta):=0.5*(3*eta-eta^3);theta[0](eta):=1;phi[0](eta):=1;
syst[1]:=h[2]*(int(int(eqt[1],eta),eta))+C[5][1]+C[6][1]*eta;
f[0](eta):=0.5*(3*eta-eta^3);theta[0](eta):=1;
phi[0](eta):=1;sysp[1]:=h[3]*(int(int(eqp[1],eta),eta))+C[7][1]+
C[8][1]*eta;
subs(eta=0,sys[1])=0;C[1][1]:=rhs(%);
simplify(subs(eta=0,diff(sys[1],eta,eta)))=0;C[3][1]:=rhs(%);
ee1[1]:=simplify(subs(eta=1,sys[1]))=0;
ee2[1]:=simplify(subs(eta=1,diff(sys[1],eta)))=0;
3*ee1[1]-ee2[1]:simplify(%,size);solve(%,C[2][1]):C[2][1]:=(%);
solve(ee1[1],C[4][1]):C[4][1]:=(%);
subs(eta=0,diff(syst[1],eta))=0;C[6][1]:=solve(%,C[6][1]);
subs(eta=1,syst[1])=0;C[5][1]:=solve(%,C[5][1]);
subs(eta=0,diff(sysp[1],eta))=0;C[8][1]:=solve(%,C[8][1]);
subs(eta=1,sysp[1])=0;C[7][1]:=solve(%,C[7][1]);
```

```
f[1](eta):=simplify(sys[1]);theta[1](eta):=simplify(syst[1]);phi
[1](eta):=simplify(sysp[1]);

> for k from 2 to 10 do
f[0](eta):=0.5*(3*eta-eta^3);theta[0](eta):=1;phi[0](eta):=1;
sys[k]:=h[1]*(int(int(int(int(eq[k],eta),eta),eta),eta))+C[1][k]
+C[2][k]*eta+C[3][k]*eta^(2)+C[4][k]*eta^(3);
f[0](eta):=0.5*(3*eta-eta^3);theta[0](eta):=1;phi[0](eta):=1;
syst[k]:=h[2]*(int(int(eqt[k],eta),eta))+C[5][k]+C[6][k]*eta;
f[0](eta):=0.5*(3*eta-eta^3);theta[0](eta):=1;phi[0](eta):=1;
sysp[k]:=h[3]*(int(int(eqp[k],eta),eta))+C[7][k]+C[8][k]*eta;
subs(eta=0,sys[k])=0;C[1][k]:=rhs(%);
simplify(subs(eta=0,diff(sys[k],eta,eta)))=0;C[3][k]:=rhs(%);
ee1[k]:=simplify(subs(eta=1,sys[k]))=0;
ee2[k]:=simplify(subs(eta=1,diff(sys[k],eta)))=0;
3*ee1[k]-ee2[k]:simplify(%,size);solve(%,C[2][k]):C[2][k]:=(%);
solve(ee1[k],C[4][k]):C[4][k]:=(%);
subs(eta=0,diff(syst[k],eta))=0:C[6][k]:=solve(%,C[6][k]);
subs(eta=1,syst[k])=0:C[5][k]:=solve(%,C[5][k]);
subs(eta=0,diff(sysp[k],eta))=0:C[8][k]:=solve(%,C[8][k]);
subs(eta=1,sysp[k])=0:C[7][k]:=solve(%,C[7][k]);
f[k](eta):=simplify(sys[k])+f[k-
1](eta);theta[k](eta):=simplify(syst[k])+theta[k-
1](eta);phi[k](eta):=simplify(sysp[k])+phi[k-1](eta);
end do:

>n1:=f[0](eta)+f[1](eta)+f[2](eta)+f[3](eta)+f[4](eta)+f[5](eta)
+f[6](eta)+f[7](eta)+f[8](eta)+f[9](eta)+f[10](eta):
>n2:=theta[0](eta)+theta[1](eta)+theta[2](eta)+theta[3](eta)+the
ta[4](eta)+theta[5](eta)+theta[6](eta)+theta[7](eta)+theta[8](et
a)+theta[9](eta)+theta[10](eta):
>n3:=phi[0](eta)+phi[1](eta)+phi[2](eta)+phi[3](eta)+phi[4](eta)
+phi[5](eta)+phi[6](eta)+phi[7](eta)+phi[8](eta)+phi[9](eta)+phi
[10](eta):
```

Programming of FDM (Backward Scheme) on Maple:

```
> restart;
>S:=0.5;Ha:=0.5;beta:=0.3;Du:=0;R:=0.3;Q:=0.3;Pr:=1.5;Ec:=0.3;Kr
:=0.5;Sc:=1.5;Sr:=0;delta:=0.5;h:=1/100; i:=100; f[0]:=0;
f[99]:=1;
f[i]:=1;theta[i]:=1;phi[i]:=1;theta[1]:=theta[0];phi[1]:=phi[0];
```

$$S := 0.5$$

$$Ha := 0.5$$

$$\beta := 0.3$$

$$Du := 0$$

$$R := 0.3$$

$$Q := 0.3$$

$$Pr := 1.5$$

$$Ec := 0.3$$

$$Kr := 0.5$$

$$Sc := 1.5$$

$$Sr := 0$$

$$\delta := 0.5$$

$$h := \frac{1}{100}$$

$$i := 100$$

$$f_0 := 0$$

$$f_{99} := 1$$

$$f_{100} := 1$$

$$\theta_{100} := 1$$

$$\phi_{100} := 1$$

$$\theta_1 := \theta_0$$

$$\phi_1 := \phi_0$$

```
> for i from 100 by -1 to 4 do
eqn[i]:=(1+1/beta)*(f[i]-4*f[i-1]+6*f[i-2]-4*f[i-3]+f[i-4])/h^4-
S*i*h*(f[i]-3*f[i-1]+3*f[i-2]-f[i-3])/h^3-S*3*(f[i]-2*f[i-
1]+f[i-2])/h^2-S*(f[i]-2*f[i-1]+f[i-2])/h^2*(f[i]-f[i-
1])/h+S*(f[i]-3*f[i-1]+3*f[i-2]-f[i-3])/h^3*f[i]-Ha^2*(f[i]-
2*f[i-1]+f[i-2])/h^2:
end do;
> eqn[3]:=f[2]-2*f[1]+f[0]:
> sys:=[1-36]:
> Ans:=fsolve(sys);
> for i from 5 by 10 to 98 do
f[i]:=rhs(Ans[i]);
end do;
```

$$f_5 := 0.$$

$$f_{15} := 0.1483525801$$

$$f_{25} := 0.2940676810$$

$$f_{35} := 0.4341983244$$

$$f_{45} := 0.5657636174$$

$$f_{55} := 0.6857320442$$

$$f_{65} := 0.7910052689$$

$$f_{75} := 0.8784026388$$

$$f_{85} := 0.9446465916$$

$$f_{95} := 0.9863491859$$

```
> for i from 75 by -1 to 2 do
eqnt[i]:=(1+4/3*R)*(theta[i]-2*theta[i-1]+theta[i-
2])/h^2+Pr*S*(f[i]*(theta[i]-theta[i-1])/h-i*h*(theta[i]-
theta[i-1])/h+Q*theta[i])+Pr*Ec*((1+1/beta)*(((f[i]-2*f[i-
1]+f[i-2])/h^2)^2+4*delta^2*((f[i]-f[i-1])/h)^2)+Ha^2*((f[i]-
f[i-1])/h)^2)+Du*Pr*(phi[i]-2*phi[i-1]+phi[i-2])/h^2;
eqnp[i]:=(phi[i]-2*phi[i-1]+phi[i-2])/h^2+Sc*S*(f[i]*(phi[i]-
phi[i-1])/h-i*h*(phi[i]-phi[i-1])/h)-
Sc*Kr*phi[i]+Sr*Sc*(theta[i]-2*theta[i-1]+theta[i-2])/h^2;
end do:
> syst:={seq(eqnt[i],i=2..75),seq(eqnp[i],i=2..75)};
> Ans2:=fsolve(syst);
```

APPENDIX A: VELOCITY FIELD AND CONTOURS OF TEMPERATURE AND CONCENTRATION

Contours at value R =0.1 & 0.4

Temperature (R = 0.1)

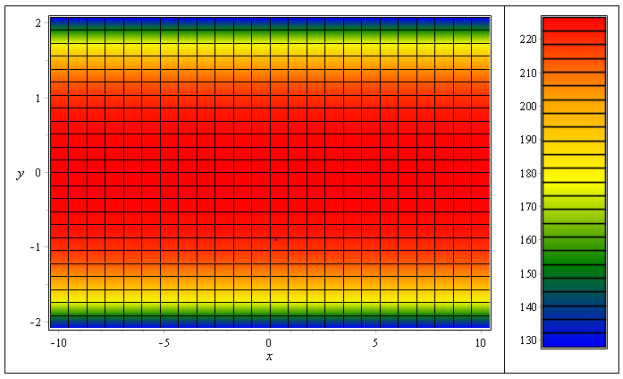

Temperature (R = 0.4)

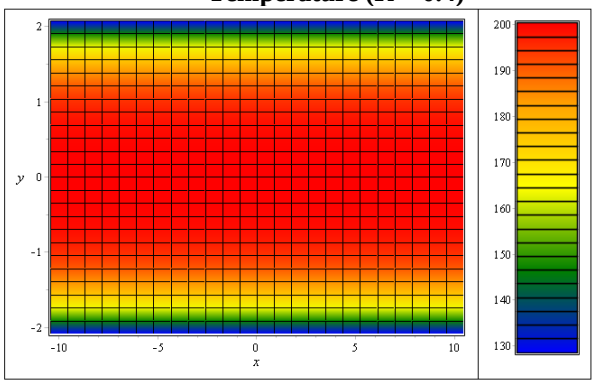

Concentration (R = 0.1)

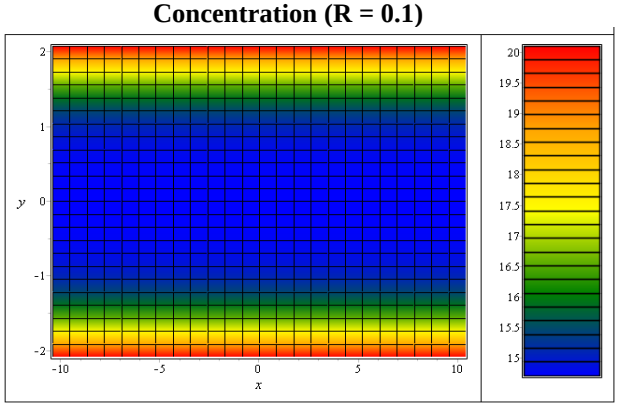

Concentration (R = 0.4)

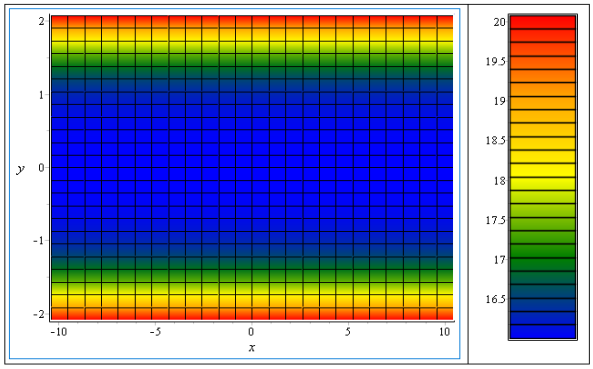

Contours at different Q= -2.5 & 2.5

Temperature (Q = -2.5)

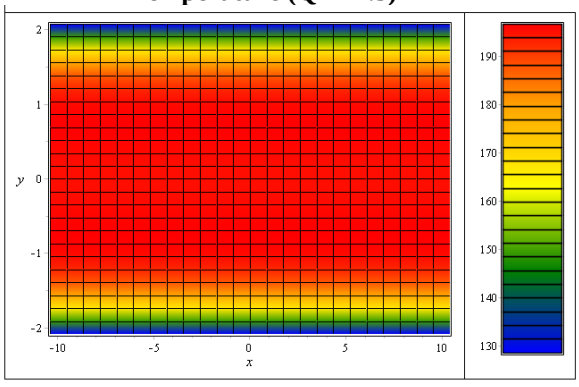

Temperature (Q = 2.5)

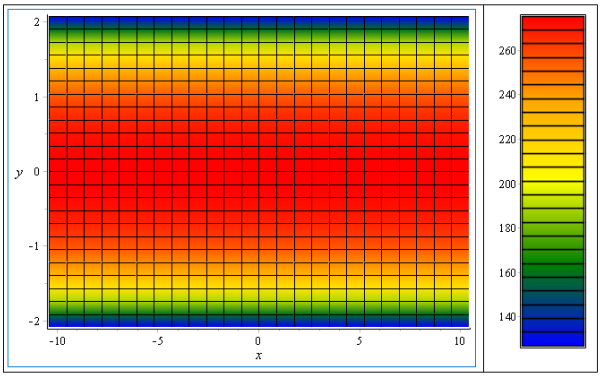

Concentration (Q = -2.5)

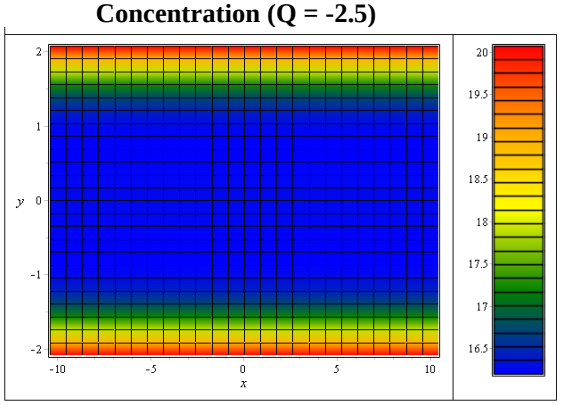

Concentration (Q = -2.5)

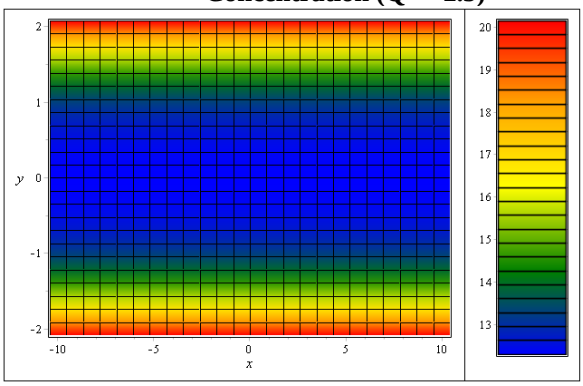

Contours at different Prandtl number Pr= 0.9 & 1.5

Temperature (Pr = 0.9)

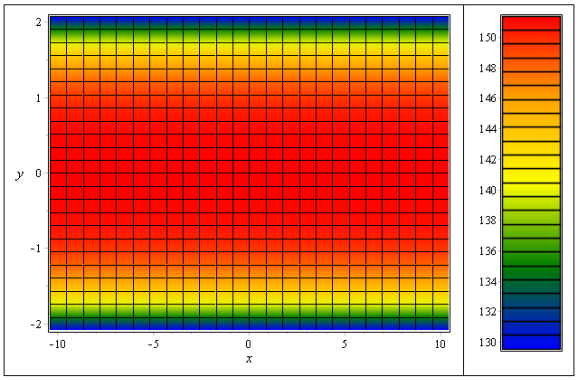

Temperature (Pr = 1.5)

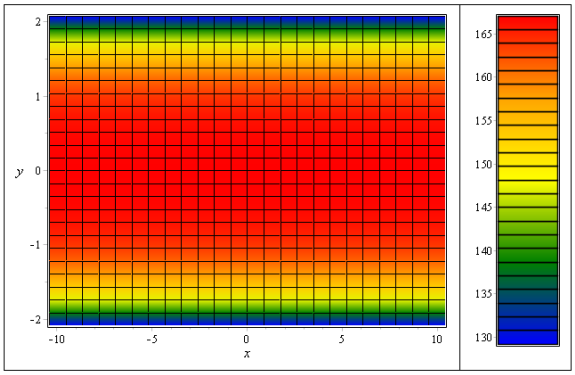

Concentration (Pr = 0.9)

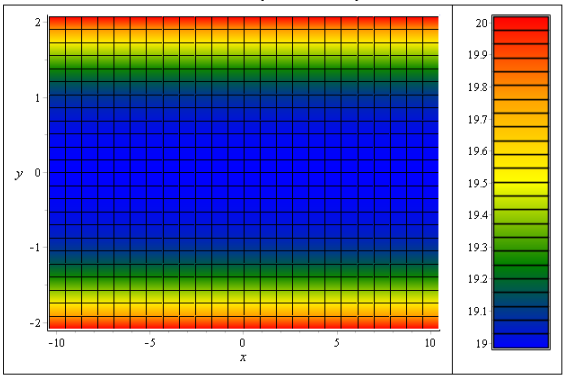

Concentration (Pr = 1.5)

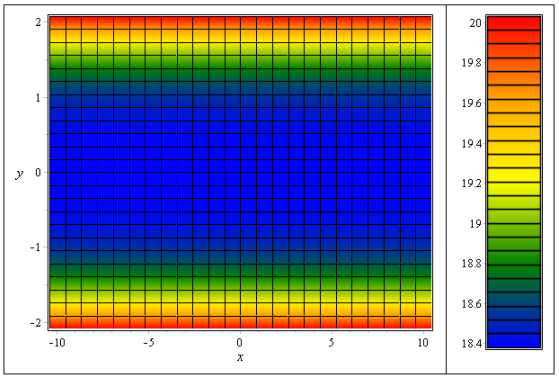

Contours at different Eckert Number Ec = 0.3 & 0.6

Temperature (Ec = 0.3)

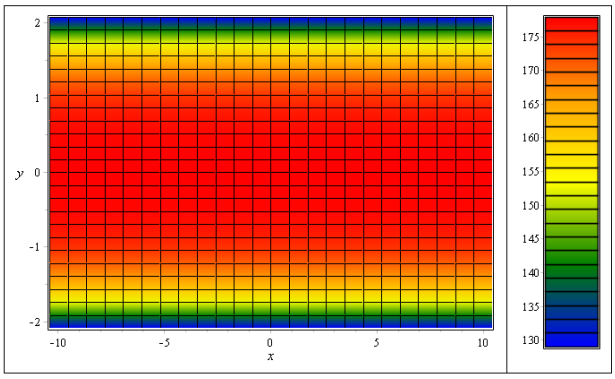

Temperature (Ec = 0.6)

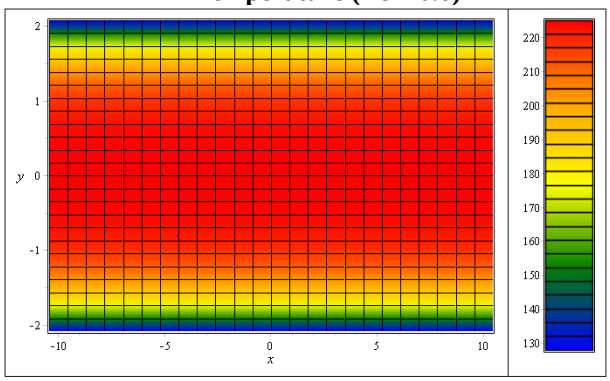

Concentration (Ec = 0.3)

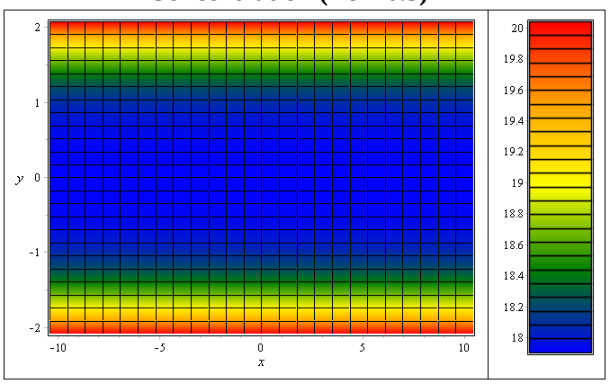

Concentration (Ec = 0.6)

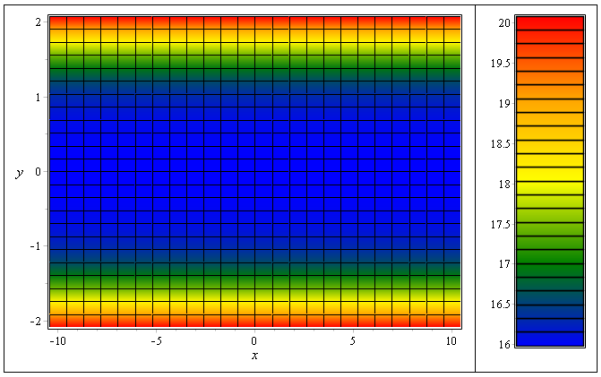

Contours at different Dufour Number Du = 0.1 & 0.7

Temperature (Du = 0.1)

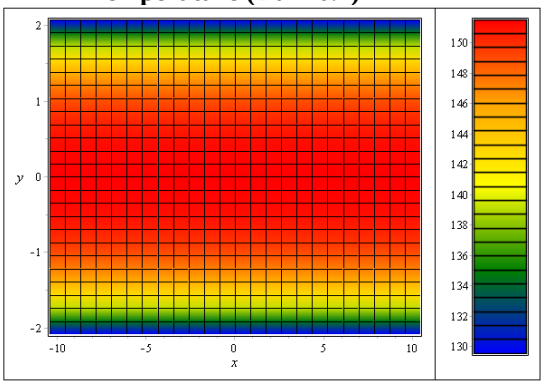

Temperature (Du = 0.7)

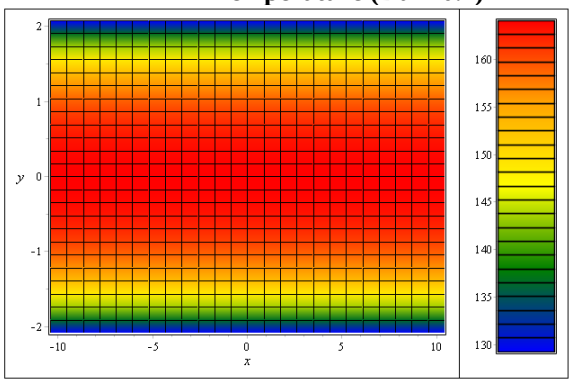

Concentration (Du = 0.1)

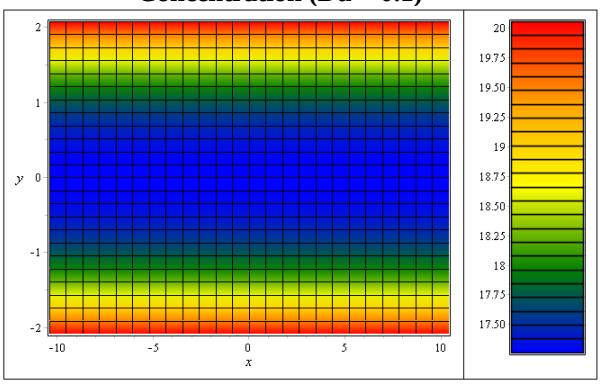

Concentration (Du = 0.7)

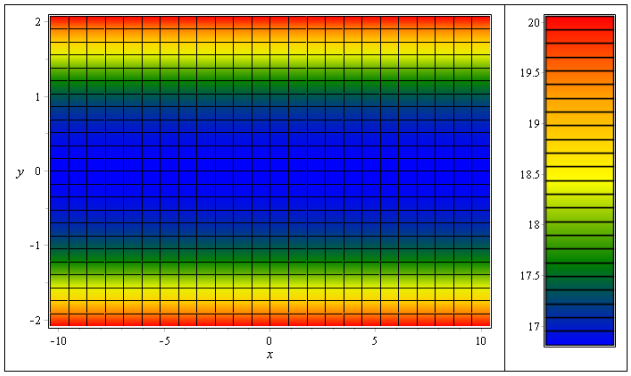

Contours at Kr =0.3 & -0.8

Temperature (Kr = 0.3)

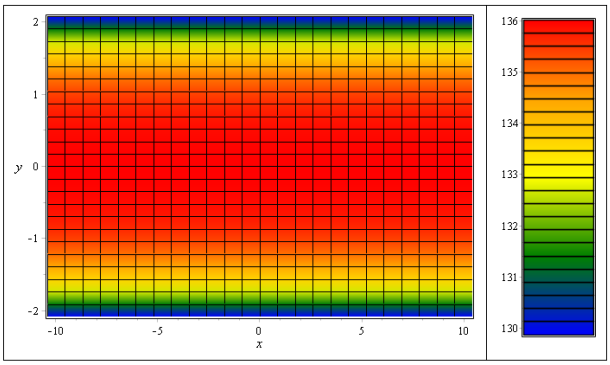

Temperature (Kr = -0.8)

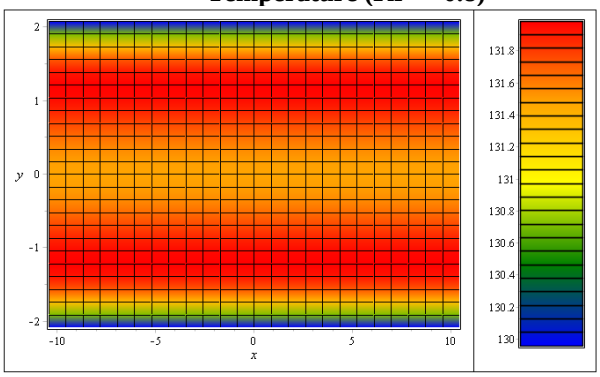

Concentration (Kr = 0.3)

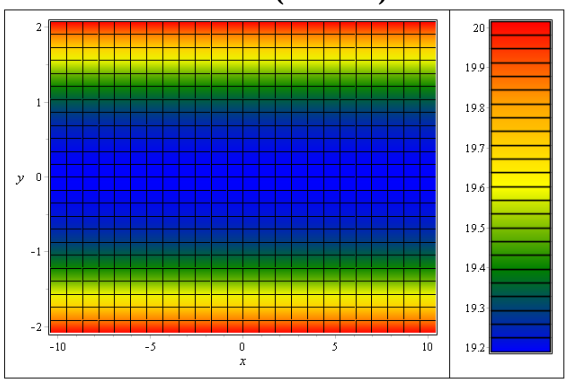

Concentration (Kr = -0.8)

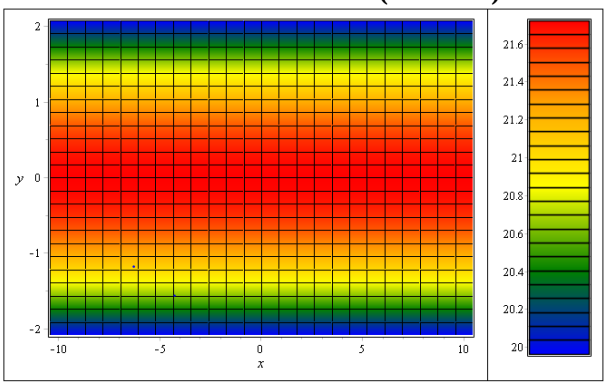

Contours at Sc = 1.2 & 1.5

Temperature (Sc=1.2)

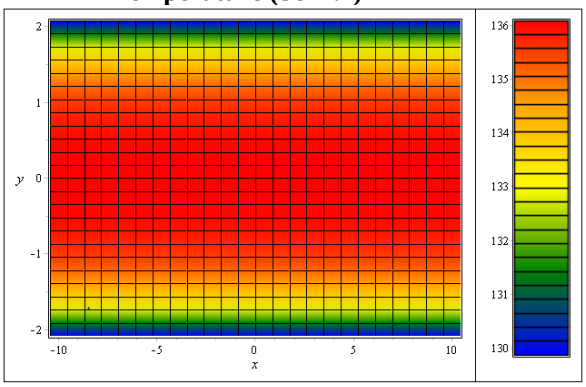

Temperature (Sc=1.5)

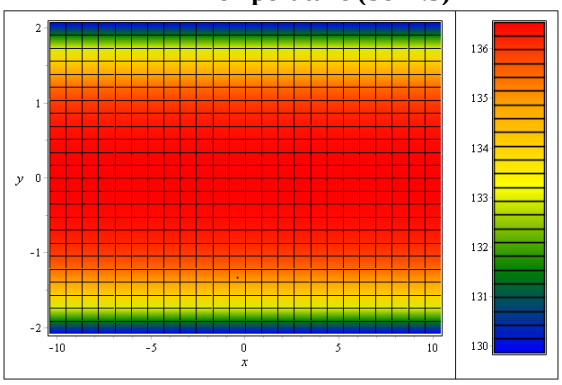

Concentration (Sc = 1.2)

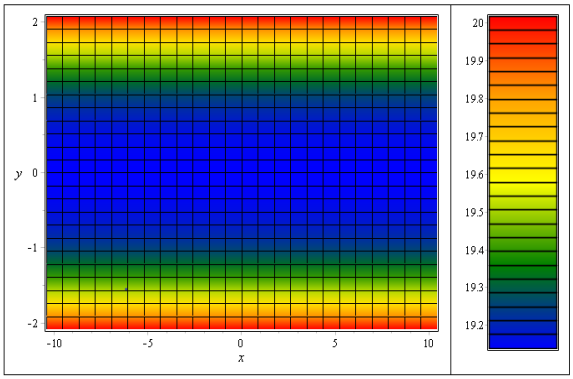

Concentration (Sc = 1.5)

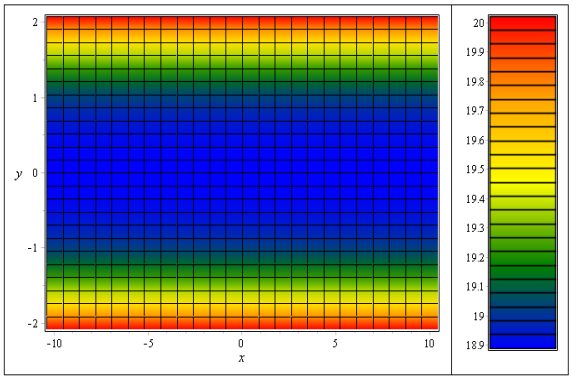

Contours at Sr = 0.4 & 0.7

Temperature (Sr = 0.4)

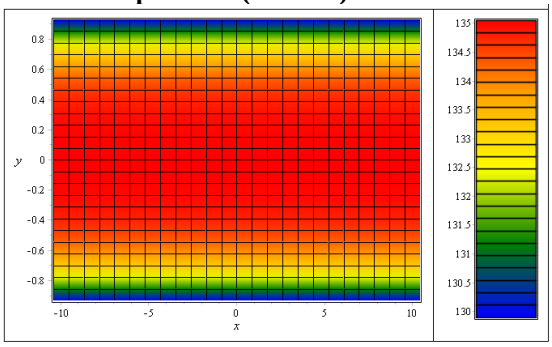

Temperature (Sr = 0.7)

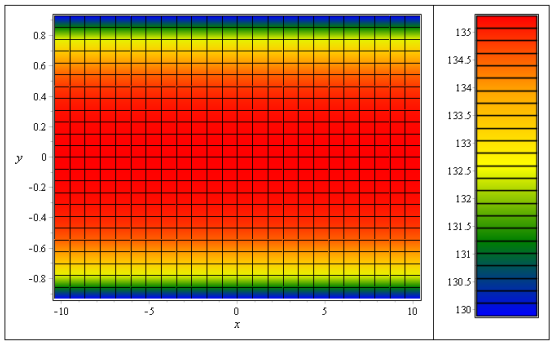

Concentration (Sr = 0.4)

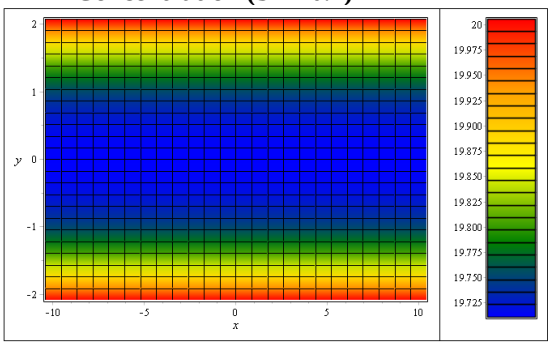

Concentration (Sr = 0.7)

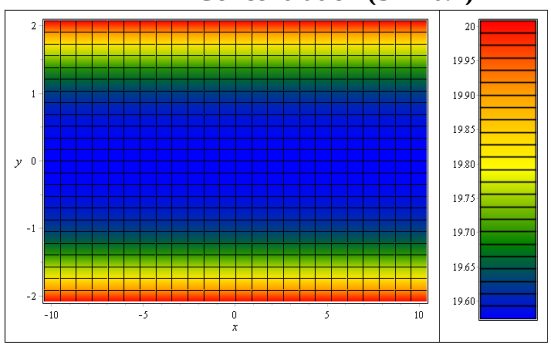

REFERENCES

[1] J. Stefan, "Versuche über die scheinbare Adhäsion," *Annalen der Physik,* h vol. 230, no. 2, pp. 316-318, 1875/01/01 1875,

[2] O. Reynolds, "On the Theory of Lubrication and Its Application to Mr. Beauchamp Tower's Experiments, Including an Experimental Determination of the Viscosity of Olive Oil," *Philosophical Transactions of the Royal Society of London Series I,* vol. 177, pp. 157-234, January 01, 1886 1886. [Online].

[3] F. R. Archibald, "Load Capacity and Time Relations for Squeeze Films," *Transactions of the American Society of Mechanical Engineers,* vol. 78, no. 1, pp. 29-35, 2022.

[4] G. Domairry and A. Aziz, "Approximate Analysis of MHD Squeeze Flow between Two Parallel Disks with Suction or Injection by Homotopy Perturbation Method," *Mathematical Problems in Engineering,* vol. 2009, p. 603916, 2009/06/14 2009.

[5] A. M. Siddiqui, S. Irum, and A. R. Ansari, "Unsteady Squeezing Flow of a Viscous MHD Fluid Between Parallel Plates, a Solution Using the Homotopy Perturbation Method," *Mathematical Modelling and Analysis,* vol. 13, no. 4, pp. 565-576, 2008/01/01 2008.

[6] M. Mustafa, T. Hayat, And S. Obaidat, "On Heat and Mass Transfer in the Unsteady Squeezing Flow Between Parallel Plates," *Meccanica,* vol. 47, no. 7, pp. 1581-1589, 2012.

[7] J. A. Weaver and R. Viskanta, "Natural Convection due to Horizontal Temperature And Concentration Gradients—2. Species Interdiffusion, Soret And Dufour Effects," *International Journal of Heat and Mass Transfer,* vol. 34, no. 12, pp. 3121-3133, 1991/12/01/ 1991.

[8] C. Sulochana, S. S. Payad, and N. Sandeep, "Non-Uniform Heat Source or Sink Effect on the Flow of 3D Casson Fluid in the Presence of Soret and Thermal Radiation," *International Journal of Engineering Research in Africa,* vol. 20, pp. 112-129, 2016.

[9] M. Nawaz, T. Hayat, and A. Alsaedi, "Dufour And Soret Effects On MHD Flow Of Viscous Fluid Between Radially Stretching Sheets In Porous Medium," *Applied Mathematics and Mechanics,* vol. 33, no. 11, pp. 1403-1418, 2012/11/01 2012.

[10] O. Ojjela and N. Naresh Kumar, "Unsteady MHD Mixed Convective Flow of Chemically Reacting and Radiating Couple Stress Fluid in a Porous Medium Between Parallel Plates with Soret and Dufour Effects," *Arabian Journal for Science and Engineering,* vol. 41, no. 5, pp. 1941-1953, 2016/05/01 2016.

[11] H. Khan, M. Qayyum, O. Khan, and M. Ali, "Unsteady Squeezing Flow of Casson Fluid with Magnetohydrodynamic Effect and Passing through Porous Medium," *Mathematical Problems in Engineering,* vol. 2016, p. 4293721, 2016/12/29 2016.

[12] S. I. Khan, S. T. Mohyud-Din, and B. Bin-Mohsin, "Thermo-Diffusion and Diffuso-Thermo Effects on MHD Squeezing Flow Between Parallel Disks," *Surface Review and Letters,* vol. 24, pp. 1750022-721, January 01, 2017 2017.

[13] N. B. Naduvinamani and U. Shankar, "Thermal-Diffusion and Diffusion-Thermo Effects on Squeezing Flow of Unsteady Magneto-Hydrodynamic Casson Fluid Between Two Parallel Plates with Thermal Radiation," *Sādhanā,* vol. 44, no. 8, p. 175, 2019/07/08 2019.

[14] N. Ahmed, U. Khan, S. I. Khan, S. Bano, and S. T. Mohyud-Din, "Effects on Magnetic Field in Squeezing Flow of a Casson Fluid Between Parallel Plates," *Journal of King Saud University - Science,* vol. 29, no. 1, pp. 119-125, 2017/01/01/ 2017.

[15] S. T. Mohyud-Din, M. Usman, W. Wang, and M. Hamid, "A Study of Heat Transfer Analysis for Squeezing Flow of a Casson Fluid via Differential Transform Method," *Neural Computing and Applications,* vol. 30, no. 10, pp. 3253-3264, 2018/11/01 2018.

[16] D. W. C. E. A.A. Collyer (Editor), *Rheological Measurement,* 2nd ed. London, UK: Chapman & Hali, 1998.

[17] A. R. Bahadir and T. Abbasov, "A Numerical Approach to Hydromagnetic Squeezed Flow and Heat Transfer between Two Parallel Disks," *Industrial Lubrication and Tribology,* vol. 63, pp. 63-71, 2011.

[18] B. Bin-Mohsin, N. Ahmed, Adnan, U. Khan, and S. Tauseef Mohyud-Din, "A Bioconvection Model for a Squeezing Flow of Nanofluid Between Parallel Plates in the Presence of Gyrotactic Microorganisms," *The European Physical Journal Plus,* vol. 132, no. 4, p. 187, 2017/04/26 2017.

[19] J. C. Butcher, *Numerical Methods for Ordinary Differential Equations*. UK: John Wiley & Sons, 2003.

[20] C. Dorier and J. Tichy, "Behavior of a Bingham-Like Viscous Fluid in Lubrication Flows," *Journal of Non-Newtonian Fluid Mechanics,* vol. 45, no. 3, pp. 291-310, 1992/12/01/ 1992.

[21] T. K. a. G. Dumas, "CFD Analysis of a Hydrokinetic Turbine Based on Oscillating Hydrofoils," *Journal of Fluids Engineering,* 2011.

[22] H. M. Duwairi, B. Tashtoush, and R. A. Damseh, "On Heat Transfer Effects of a Viscous Fluid Squeezed and Extruded Between Two Parallel Plates," *Heat and Mass Transfer,* vol. 41, pp. 112-117, December 01, 2004 2004.

[23] F. D. J. ERIK OBERG, . HOLBROOK L. HORTON, AND HENRY H. RYFFEL, *Machinery's Handbook 30th Edition*. New York: Industrial Press Inc., 2016.

[24] R. J. Grimm, "Squeezing Flows of Newtonian Liquid Films - An Analysis Including Fluid Inertia," *Applied Scientific Research,* vol. 32, pp. 149-166, July 01, 1976 1976. [Online].

[25] U. Khan, N. Ahmed, and S. Tauseef Mohyud-Din, "Thermo-Diffusion, Diffusion-Thermo and Chemical Reaction Effects on MHD Flow of Viscous Fluid in Divergent and Convergent Channels," *Chemical Engineering Science,* vol. 141, pp. 17-27, 2016/02/17/ 2016.

[26] D. C. Kuzma, "Fluid Inertia Effects in Squeeze Films," *Applied Scientific Research,* vol. 18, no. 1, pp. 15-20, 1968/01/01 1968, doi: 10.1007/BF00382330.

[27] A. Lawal and D. M. Kalyon, "Squeezing Flow of Viscoplastic Fluids Subject to Wall Slip," *Polymer Engineering and Science,* vol. 38, pp. 1793-1804, 1998.

[28] M. Mahmood, S. Asghar, and M. A. Hossain, "Squeezed Flow and Heat Transfer over a Porous Surface for Viscous Fluid," *Heat and Mass Transfer,* vol. 44, no. 2, pp. 165-173, 2007/12/01 2007.

[29] E. R. Maki, D. C. Kuzma, and R. J. Donnelly, "Magnetohydrodynamic Lubrication Flow Between Parallel Plates," *Journal of Fluid Mechanics,* vol. 26, pp. 537 - 543, 1966.

[30] Muhaimin, R. Kandasamy, and I. Hashim, "Effect of Chemical Reaction, Heat and Mass Transfer on Nonlinear Boundary Layer Past a Porous Shrinking Sheet in the Presence of Suction," *Nuclear Engineering and Design,* vol. 240, no. 5, pp. 933-939, 2010/05/01/ 2010.

[31] G. C. N M Crawford, and SW T Spence, "An Experimental Investigation into the Pressure Drop for Turbulent Flow in 90 Elbow Bends," *Proc. IMechE Vol. 221 Part E: J. Process Mechanical Engineering,* pp. 77-88, 2007.

[32] E. B. P.L. Spedding, G.M. Mcnally, "Fluid Flow through 90 Degree Bends," *Asia-Pacific Journal of Chemical Engineering 12(1-2),* pp. 107 - 128, 2004.

[33] C. S. K. Raju and N. Sandeep, "Heat and Mass Transfer in MHD Non-Newtonian Bio-Convection Flow over a Rotating Cone/Plate with Cross Diffusion," *Journal of Molecular Liquids,* vol. 215, pp. 115-126, 2016/03/01/ 2016.

[34] B. Tashtoush, M. Tahat, and D. Probert, "Heat Transfers and Radial Flows via a Viscous Fluid Squeezed Between Two Parallel Disks," *Applied Energy,* vol. 68, no. 3, pp. 275-288, 2001/03/01/ 2001.

[35] J. A. Tichy and W. O. Winer, "Inertial Considerations in Parallel Circular Squeeze Film Bearings," *Journal of Lubrication Technology,* vol. 92, no. 4, pp. 588-592, 1970.

[36] W. A. Wolfe, "Squeeze Film Pressures," *Applied Scientific Research, Section A,* vol. 14, no. 1, pp. 77-90, 1965/01/01 1965.

Hassan Ahmed (321077)Thesis

by Hassan Ahmed

Submission date: 23-Aug-2023 11:58AM (UTC-0700)
Submission ID: 2150097778
File name: Final_Draft.docx (1.94M)
Word count: 11281
Character count: 65306

Hassan Ahmed (321077)Thesis

ORIGINALITY REPORT

13%	8%	14%	3%
SIMILARITY INDEX	INTERNET SOURCES	PUBLICATIONS	STUDENT PAPERS

PRIMARY SOURCES

1	www.ias.ac.in Internet Source	3%
2	Submitted to Higher Education Commission Pakistan Student Paper	2%
3	www.degruyter.com Internet Source	2%
4	N B Naduvinamani, Usha Shankar. "Thermal-diffusion and diffusion-thermo effects on squeezing flow of unsteady magneto-hydrodynamic Casson fluid between two parallel plates with thermal radiation", Sādhanā, 2019 Publication	1%
5	Usha Shankar, N. B. Naduvinamani. "Magnetized impacts of Cattaneo-Christov double-diffusion models on the time-dependent squeezing flow of Casson fluid: A generalized perspective of Fourier and Fick's laws", The European Physical Journal Plus, 2019	1%

Publication

6	Saima Noreen, M. Saleem. "SORET AND DUFOUR EFFECTS ON THE MHD PERISTALTIC FLOW IN A POROUS MEDIUM WITH THERMAL RADIATION AND CHEMICAL REACTION", Heat Transfer Research, 2016 Publication	1 %
7	N. B. Naduvinamani, Usha Shankar. "两平行板间非稳态 Casson 磁流体的辐射挤压流动", Journal of Central South University, 2019 Publication	1 %
8	Hayat, T.. "Thermal-diffusion and diffusion-thermo effects on axisymmetric flow of a second grade fluid", International Journal of Heat and Mass Transfer, 201106 Publication	1 %
9	Sheikholeslami, Mohsen, and Davood Domairry Ganji. "New semianalytical methods: application for MHD nanofluid hydrothermal behavior", External Magnetic Field Effects on Hydrothermal Treatment of Nanofluid, 2016. Publication	1 %

Exclude quotes	On	Exclude matches	< 1%
Exclude bibliography	On		